ISOLATION AND CHARACTERIZATION OF NANOCRYSTALLINE CELLULOSE FROM OIL PALM BIOMASS VIA TRANSITION METAL SALT CATALYZED HYDROLYSIS PROCESS

CHEN YOU WEI

INSTITUTE OF GRADUATE STUDIES
UNIVERSITY OF MALAYA
KUALA LUMPUR

2017

ISOLATION AND CHARACTERIZATION OF NANOCRYSTALLINE CELLULOSE FROM OIL PALM BIOMASS VIA TRANSITION METAL SALT CATALYZED HYDROLYSIS PROCESS

CHEN YOU WEI

DISSERTATION SUBMITTED IN FULFILMENT OF THE REQUIREMENTS FOR THE DEGREE OF MASTER OF PHILOSOPHY

INSTITUTE OF GRADUATE STUDIES
UNIVERSITY OF MALAYA
KUALA LUMPUR

2017

UNIVERSITY OF MALAYA

ORIGINAL LITERARY WORK DECLARATION

Name of Candidate: Chen You Wei

Matric No: HGA140012

Name of Degree: Master of Philosophy

Title of Project Paper/Research Report/Dissertation/Thesis ("this Work"):

Isolation and Characterization of Nanocrystalline Cellulose from Oil Palm Biomass via Transition Metal Salt Catalyzed Hydrolysis Process

Field of Study: Chemistry (Nanotechnology)

I do solemnly and sincerely declare that:

(1) I am the sole author/writer of this Work;
(2) This Work is original;
(3) Any use of any work in which copyright exists was done by way of fair dealing and for permitted purposes and any excerpt or extract from, or reference to or reproduction of any copyright work has been disclosed expressly and sufficiently and the title of the Work and its authorship have been acknowledged in this Work;
(4) I do not have any actual knowledge nor do I ought reasonably to know that the making of this work constitutes an infringement of any copyright work;
(5) I hereby assign all and every rights in the copyright to this Work to the University of Malaya ("UM"), who henceforth shall be owner of the copyright in this Work and that any reproduction or use in any form or by any means whatsoever is prohibited without the written consent of UM having been first had and obtained;
(6) I am fully aware that if in the course of making this Work I have infringed any copyright whether intentionally or otherwise, I may be subject to legal action or any other action as may be determined by UM.

Candidate's Signature Date:

Subscribed and solemnly declared before,

Witness's Signature Date:

Name:

Designation:

ABSTRACT

Nanocellulose is an interesting and renewable material in the nanotechnology field. It can be prepared from natural cellulose via various chemical treatments. Because of its nano-scale dimensions, nanocellulose exhibits various outstanding and excellent physicochemical properties as compared with typical micro-sized dimension cellulose material, such as large surface area, high porosity, high aspect ratio, excellent tensile strength and modulus, and biodegradability. Conventionally, concentrated mineral acids (such as H_2SO_4, HCl, and HNO_3) have been used to prepare nanocellulose via hydrolysis of cellulose derived from lignocellulosic biomass. However, such treatment is highly corrosive and probably destroys the overall hierarchical structure of the cellulose with very poor yield. In this research, the focus is priority given to overcome these drawbacks by using transition metal based catalysts, namely Fe(III), Co(II), Ni(II), Cr(III), Mn(II) as a highly potential hydrolyzing catalyst assisted with dilute sulfuric acid by converting cellulose fiber into nanoscale structure. Previous studies have been widely reported that transition metal salts act as Lewis acid catalyst, which is less corrosive and effective in hydrolyzing the bonding systems of the cellulose structure into smaller dimensions. This project is divided into three main sections: (i) Catalytic screening for hydrolysis of cellulose to nanocellulose; (ii) Optimization study of nanocellulose production by using response surface methodology (RSM); and (iii) Facile production of nanocellulose from oil palm empty fruit bunch (OPEFB) via one-pot oxidative-hydrolysis isolation approach. The results demonstrated that the Cr(III)-transition metal based catalyst rendered better hydrolysis efficiency, which the yielded nanocellulose possessed of the highest crystallinity index (75.6%) among the other catalysts. In order to optimize operating conditions, a central composite design (RSM-CCD) system was conducted by manipulating the independent hydrolysis variables,

including reaction temperature (x_1), reaction time (x_2), $Cr(NO_3)_3$ concentration (x_3) and H_2SO_4 concentration (x_4). Responses were selected in terms of crystallinity index (y_1) and product yield (y_2) of nanocellulose. The hydrolysis efficiency of catalytic acid was greatly enhanced in the presence of catalyst, and the synergistic effect of H^+ (from H_2SO_4) and Cr^{3+} cations could further increase the nanocellulose crystallinity as compared with hydrolysis system that catalyzed by either dilute acid or metal salt alone. Under the RSM optimized operational conditions at 82 °C, 0.22 M Cr(III)-transition metal based catalyst and 0.80 M H_2SO_4 with 1 h of reaction, the yielded nanocellulose was observed in the form of interconnected spider-web-like network structure with the average diameter of 18.4 ± 7.3 nm. TGA results suggested that the thermal stability of the optimized nanocellulose was mainly affected by the active sulfate groups, which is form H_2SO_4 solution and shorter chain of hydrolyzed cellulose. In summary, it can conclude that the proposed hydrolysis approach, which is Cr(III)-transition metal based catalyst assisted with dilute sulfuric acid is highly efficient for hydrolysis of cellulose to nanocellulose with high yield of 82.9%. In addition, the one-pot oxidative-depolymerization process had been developed in order to isolate nanocellulose from oil palm empty fruit bunch. Results revealed that the one-pot isolated nanocellulose rendered higher crystallinity (80.3%) and better thermal stability (320 °C) as compared with conventional multistep purification process (75.4% and 307 °C). Besides that, the nanocellulose prepared via one-pot isolation had higher yield of 42% compared to the multistep process (~27.5%). In summary, Cr(III)-transition metal based catalyst is able to produce higher crystallinity nanocellulose with greater yield due to its high selectively towards cellulose hydrolysis under mild reaction conditions. Also, the trivalent state chromium transition metal based catalyst was capable of reacting with more electrons in glucose units and eventually resulted in the cleavage of bonding system.

ABSTRAK

Nanoselulosa merupakan bahan yang boleh diperbaharui dalam bidang nanoteknologi. Ia boleh disediakan daripada selulosa semulajadi melalui pelbagai kaedah rawatan kimia. Nanoselulosa mempunyai pelbagai sifat fizikal kimia berbanding dengan bahan selulosa yang mempunyai saiz berdimensi mikro, seperti luas permukaan yang besar, keliangan yang tinggi, nisbah aspek yang tinggi, kekuatan tegangan yang sangat baik, dan biopemerosotan. Secara konvensional, asid organik pekat (contohnya, H_2SO_4, HCl, dan HNO_3) selalu digunakan untuk menyediakan nanoselulosa melalui hidrolisis selulosa yang diperoleh daripada biojisim lignoselulosa. Walau bagaimanapun, rawatan ini adalah sangat mengakis dan mampu memusnahkan keseluruhan struktur selulosa dengan hasil produk yang rendah. Dalam kajian ini, keutamaan diberikan untuk mengatasi kelemahan asid organik dengan menggunakan mangkin berasaskan garam logam peralihan iaitu Fe(III), Co(II), Ni(II), Cr(III) dan Mn(II) bersama dengan sulfurik asid sebagai mangkin yang berpotensi untuk menukar selulosa ke struktur nano. Kajian terdahulu telah membuktikan bahawa garam logam peralihan bertindak sebagai mangkin asid Lewis yang kurang menghakis dan berkesan dalam menghidrolisis sistem ikatan struktur selulosa ke dimensi yang lebih kecil. Projek ini dibahagikan kepada tiga bahagian utama: (i) penilaian kesan penggunaan garam logam untuk hidrolisis selulosa kepada nanoselulosa; (ii) Proses pengoptimuman untuk menghasilkan nanoselulosa dengan menggunakan kaedah gerak balas permukaan *(RSM)*; dan (iii) pengeluaran nanoselulosa daripada biojisim kelapa sawit menggunakan o*ne-pot* oksidatif-hidrolisis. Keputusan menunjukkan bahawa mangkin ion metal berasaskan Cr(III) memberikan kecekapan hidrolisis yang lebih baik, iaitu menghasilkan nanosellulosa yang memiliki indeks penghabluran yang tertinggi (75.6%) berbanding mangkin lain. Untuk proses optimum, sistem reka bentuk komposit berpusat

(RSM-CCD) menggunakan pembolehubah hidrolisis yang tidak bersandar telah diaplikasikan, termasuk suhu tindak balas (x_1), masa (x_2), kepekatan mangkin ion metal berasaskan Cr(III) (x_3) dan kepekatan H_2SO_4 (x_4). Hasil eksperimen telah dipilih berdasarkan indeks penghabluran (y_1) dan hasil produk nanoselulosa (y_2). Kecekapan hidrolisis asid pemangkinan telah dipertingkatkan dengan kehadiran mangkin garam logam manakala kesan gabungan tenaga antara H^+ (dari H_2SO_4) dan kation Cr^{3+} mampu meningkatkan penghabluran nanoselulosa berbanding dengan sistem hidrolisis yang menggunakan sama ada asid cair atau garam logam sahaja. Melalui keadaan tindak balas yang telah dioptimumkan oleh RSM pada 82 °C, 0.22 M mangkin ion metal berasaskan Cr(III), 0.80 M H_2SO_4 dan 1 jam tindak balas, nanoselulosa yang diperolehi mempunyai struktur rangkaian seakan sarang labah-labah dengan diameter purata 18.4 ± 7.3 nm. Keputusan TGA membuktikan bahawa kestabilan haba bagi nanoselulosa yang telah dioptimumkan dipengaruhi oleh kumpulan sulfat aktif yang membentuk larutan H_2SO_4 dan rantaian selulosa yang lebih pendek. Kesimpulannya, pendekatan hidrolisis yang dicadangkan, iaitu proses dengan menggunakan mangkin ion metal-Cr(III) dibantu oleh asid sulfat cair adalah sangat berkesan untuk menghasilkan nanocellulosa dengan hasil produk yang tinggi (82.9%). Di samping itu, *one-pot* oksidatif-hidrolisis telah digunakan untuk mendapatkan nanoselulosa dari biojisim kelapa sawit. Hasil kajian menunjukkan bahawa nanoselulose daripada *one-pot* oksidatif-hidrolisis mempunyai penghabluran lebih tinggi (80.3%) dan kestabilan haba yang lebih tinggi (320 °C) berbanding daripada hasil proses penulenan multilangkah konvensional (75.4% dan 307 °C). Selain itu, nanoselulose yang disediakan melalui *one-pot* oksidatif-hidrolisis mempunyai hasil produk yang lebih tinggi (42%) berbanding dengan proses multilangkah (~27.5%). Kesimpulannya, mangkin berasaskan logam peralihan Cr(III) boleh menghasilkan nanoselulosa yang tinggi kehablurannya dengan hasil yang lebih banyak. Hal ini kerana, kepemilihannya tinggi terhadap proses

hidrolisis pada keadaan tindak balas yang sederhana. Selain itu, keadaan trivalensi membolehkan mangkin berasaskan logam peralihan kromium ini bertindak balas dengan lebih banyak elektron pada unit glukosa seterusnya membolehkan berlakunya pembelahan pada sistem ikatan.

ACKNOWLEDGEMENTS

I would like to convey my heartfelt gratitude and sincere appreciation to all people who have inspired and helped me during my master study. This thesis would not have been possible without those supports from many people.

First and foremost, I would like to express my sincerest gratitude to my supervisors; Dr. Lee Hwei Voon and Prof. Dr. Sharifah Bee who always support me throughout my research journey. Very special thanks also go to all the research officers and friends in NANOCAT for their helpful support and kind guidance. Besides that, I would also like to thank you Dr. Juan Joon Ching for his guidance.

Last but not least, my deepest gratitude goes to my family for their unflagging love and support throughout my life. I would like to express my deepest heartfelt appreciation to Jayson Chew for his excellent guidance and invaluable suggestion throughout my study.

TABLE OF CONTENTS

CHAPTER 2: LITERATURE REVIEW

CHAPTER 3: RESEARCH METHODOLOGY

CHAPTER 4: RESULTS AND DISCUSSION

LIST OF FIGURES

LIST OF TABLES

LIST OF SYMBOLS AND ABBREVIATIONS

α	:	Alpha
β	:	Beta
°C	:	Degree Celsius
°C/min	:	Degree Celsius per minutes
cm	:	Centimeter
CrI	:	Crystallinity index
3D	:	Three-dimensional
E_A	:	Elastic modulus in axial direction
E_T	:	Elastic modulus in transverse direction
g	:	Gram
g/cm^3	:	Gram per cubic centimeter
g/mol	:	Gram per mole
h	:	Hour
I_{200}	:	Intensity at plane 200
I_{am}	:	Intensity at amorphous region
kg	:	Kilogram
kHz	:	Kilohertz
kV	:	Kilovolt
kWh	:	Kilowatt hour
L/d	:	Length/diameter
M	:	Molarity
m	:	Meter
Ma	:	Milliampere
min	:	Minute

mm	:	Millimeter
Mm	:	Millimolar
Mpa	:	Megapascal
M_w	:	Molecular weight
M_{mono}	:	Molecular weight of the tricarbanilated cellulose monomer
nm	:	Nanometer
psi	:	Pounds per square inch
R^2	:	R-squared
rpm	:	Rotation per minute
s	:	Second
T_{max}	:	Maximum thermal decomposition temperature
T_{on}	:	Onset temperature
μm	:	Micrometer
v/v	:	Volume/volume
W	:	Watts
wt%	:	Weight percentage
w/v	:	Weight/volume
w/w	:	Weight/weight
θ	:	Theta
ρ	:	Density
σ	:	Tensile strength
AGU	:	Anhydroglucose unit
AFM	:	Atomic force microscopy
$AlCl_3$	:	Aluminum chloride
ANOVA	:	Analysis of variance
APS	:	Ammonium persulfate

ASTM	:	American society for testing and materials
[Bmim]Cl	:	1-butyl-3-methylimidazolium chloride
BNC	:	Bacterial nanocellulose
CCD	:	Central composite design
CH_3COOH	:	Glacial acetic acid
ClO_2	:	Chlorine dioxide
$CrCl_3$	:	Chromium(III) chloride
$Cr(OH)_3$	:	Chromium(III) hydroxide
$CuCl_2$	:	Copper(II) chloride
CV	:	Coefficient of variance
DI	:	Deionized
DMSO	:	Dimethyl sulfoxide
DOE	:	Design of experiment
DP	:	Degree of polymerization
DTG	:	Differential thermogravimetric
DP	:	Degree of polymerization
EFB	:	Empty fruit bunch
$FeCl_2$	:	Iron(II) chloride
$FeCl_3$	:	Iron(III) chloride
FESEM	:	Field emission scanning electron microscopy
$FeSO_4$	:	Iron(II) sulfate
$Fe_2(SO_4)_3$	:	Iron(III) sulfate
FTIR	:	Fourier transform infrared
GPa	:	Gigapascal
GPC	:	Gel permeation chromatography
HBr	:	Hydrobromic acid

HCl	:	Hydrochloric acid
HMF	:	5-hydroxymethylfurfural
HNO_3	:	Nitric acid
H_2O	:	Water molecules
H_2O_2	:	Hydrogen peroxide
H_2SO_4	:	Sulfuric acid
H_3O^+	:	Hydronium ion
H_3PO_4	:	Phosphoric acid
KBr	:	Potassium bromide
KOH	:	Potassium hydroxide
MCC	:	Microcrystalline cellulose
$MnCl_2$	:	Manganese(II) chloride
MS-NC	:	Multistep purification nanocellulose
$NaClO_2$	:	Sodium chlorite
NaOH	:	Sodium hydroxide
NCC	:	Nanocrystalline cellulose
NFC	:	Nanofibrillated cellulose
nm	:	Nanometer
NMR	:	Nuclear magnetic resonance
OPEFB	:	Oil palm empty fruit bunch
OPF	:	Oil palm fronds
OP-NC	:	One-pot isolation nanocellulose
OPT	:	Oil palm trunks
PTFE	:	Polytetrafluoroethylene
RSM	:	Response surface methodology
TEM	:	Transmission electron microscopy

TEMPO	:	2,2,6,6- tetramethylpiperidinyl-1-oxyl
TGA	:	Thermogravimetric analysis
THF	:	Tetrahydrofuran
WAXRD	:	Wide-angle X-ray diffraction
XPS	:	X-ray photoelectron spectroscopy
XRD	:	X-ray diffraction

CHAPTER 1: INTRODUCTION

1.1 Background of Research

Increasing demand of non-renewable fossil fuel has dramatically increased the price of crude oil resulted in the great challenge to global economic growth. The energy crisis has threatened the worldwide due to the excessive exploitation of the oil reserves by human population growth explosively. This has encouraged the scholar-researchers to search for alternative resource that can be used to replace the conventional fossil fuels and petroleum-based synthetic polymer that widely used in various industrial applications, such as filler in biocomposite materials, hybrid composites, reinforcing agent (Morais et al., 2013) and automotive applications (W. Li, Yue, & Liu, 2012). In this case, lignocellulosic biomass has been well reported as the most promising resource to the functioning of modern industrial societies (Dutta, De, & Saha, 2013; Mohamad Haafiz et al., 2013) due to their abundance, renewable, inexpensive and able to provide a unique natural resource for cost-effective and large-scale bio-energy collection (Anwar, Gulfraz, & Irshad, 2014).

As an agricultural plant, oil palm tree (*Elaeis guineensis*) has become one of the major and most profitable crops that significantly contribute to the economics of our country. A total of 95 million tons of this lignocellulosic material is produced annually and provides a continuous supply for the oil palm biomass related industries (Lamaming et al., 2015). These industries mainly involved in palm oil production, where the crude oil is extracted from the fresh palm fruits and further process into other valuable products, leaving large amount of solid waste/residue such as empty fruit bunch (EFB) from the palm oil mills. Normally, accompanying the production of 1 kg of palm oil, almost 4 kg of dry biomass is generated (Chin et al., 2015). In addition to that, the oil

palm biomass such as oil palm fronds (OPF), oil palm trunks (OPT), palm kernel shells, mesocarp fiber and mill effluent, may also come from plantation harvesting and replanting activity. In fact, around 30 million tons of oil palm biomass residues is contributed by oil palm industries in Malaysia every year, and most of them exist in the form of empty fruit bunch, oil palm trunks, and oil palm fronds (Rafatullah et al., 2013).

However, due to the poor practice of waste management in many local plantations, these plentiful lignocellulosic-rich solid residues have eventually caused the negative impacts to environmental and ecology systems, rather than converted into high-profit usage or value-added products. In normal practice, open burning is one of the most popular ways to manage this waste but resulted in uncontrollable environmental apprehensions such as greenhouse gas emission and severe air pollution (Singh et al., 2013). The second approach is that the biomass solid wastes are left to completely dry in the cultivated area and biodegrade on their own to become fertilizer; however, this may lead to the grow of microorganisms and ultimately become a threat to the original habitat of the community (Mohaiyiddin et al., 2016).

Basically, the oil palm biomass residues are the most promising lignocellulosic materials to be converted to a wide range of value-added products that can be grouped into nanomaterial, biofuel and bio-based chemical, which are great potential in many important fields, such as packaging, building, optoelectronic devices and pharmaceutical industry (Missoum et al., 2013). Thus, research and development for sustainable technology are necessary in order to discover an ideal and wise route for a greener and nature-friendly biomass biorefinery process. Through this process, the biomass will be fractionated into different by-products (*i.e.* fuel, chemicals, and biomaterials), which can further transform into marketable value-added end products

(reducing sugar, gasoline, diesel, hydrocarbons, liquefaction-derived bio-oil, nanocellulose) (Ng et al., 2012).

1.2 Physicochemical Properties of Oil Palm Biomass

Palm-based lignocellulosic biomass consists of a defensive inner framework which functions as the structural robustness of cell wall, hydrolytic stability and provide the resistance against microbial. Basically, oil palm industries generate massive quantities of biomass residues which can be categorized into three main clusters: Oil palm frond (OPF), oil palm trunk (OPT) and oil palm empty fruit bunch (OPEFB). It is well known that the physical and chemical constituents of oil palm biomass highly depends on its origin, species, growing conditions, humidity, stress, temperature, soil conditions, weather effect, plant age and maturity of fibers (Jawaid & Khalil, 2011). However, the major components of these lignocellulosic fibers consists of three primarily biopolymers, *i.e.* carbohydrate polymers (cellulose, hemicellulose) and an aromatic polymer (lignin). **Table 1.1** summarizes the proportions of the each component in typical palm-based lignocellulosic biomass residues.

Table 1.1: Composition of typical oil palm based biomass (Khalil et al., 2012).

Components	Chemical composition (wt%)		
	OPT	OPF	OPEFB
Lignin	18–23	20–21	13–37
Holocellulose	42–45	80–83	68–86
Hemicellulose	12–17	34–38	17–33
Cellulose	29–37	40–50	43–65
Ash	2–3	2–3	1–6

The complex hierarchy configuration of lignocellulosic biomass is the main challenge for the fractionation process, where lignin, hemicellulose, and cellulose components are well-hindered by structural, physicochemical and compositional factors.

In fact, the inner structure of biomass is self-protected to give the structural robustness and hydrolytic stability of the cell walls as well as against the microbial attack (Lee, Hamid, & Zain, 2014). Besides that, the cellulose is normally embedded by the lignin and hemicellulose matrix via physically and chemically linkages (such as ester and ether bonds) to form a cellulose-hemicellulose-lignin complex leads to the complicated biomass recalcitrance.

1.2.1 Cellulose

The macromolecule of cellulose is the most important natural biopolymer available on Earth. It is also considered as the most abundant and renewable polymer in the biosphere. The production of cellulose is expected to be over 7.5×10^{10} tons annually (Habibi, Lucia, & Rojas, 2010). Cellulose is the main structural component of typical plant cell wall homo-polysaccharides and widely distributed in higher plants (*i.e.* woody biomass) which consisting of up to 50%. However, cellulosic material can be also obtained from variety of resources, such as annual crops, algae (*Valonia*, *Oocystis apiculate*), bacteria (*Gluconacetobacter xylinus*), fungi, invertebrates, and even in several marine animals (*e.g.* tunicates, amoeba) (Abdul Khalil, Bhat, & Ireana Yusra, 2012; Klemm et al., 2011).

Generally, cellulose is a linear polymer chain that composed of unbranched *β*-(1,4)-linked *β*-D-glucopyranosyl units (anhydroglucose unit, AGU). Cellobiose is the dimer unit of glucose monomer. The surface of cellulose macromolecules is predominated by hydroxyl groups. In each glucose repeating unit, it has the chair conformation and consists of three different hydroxyl groups, which located at positions of C_2, C_3 (secondary hydroxyl) and C_6 (primary hydroxyl). The presence of these hydroxyl groups can lead to the formation of inter- and intramolecular hydrogen bonds and

allows the creation of three-dimensional, highly ordered crystal structures that are responsible for its highly rigidity, highly insoluble and resistant to most organic solvents (Abdul Khalil et al., 2012; Habibi et al., 2010).

At the supramolecular level, the polymeric cellulose chain is laterally interconnected with each other via hydrogen linkage among the –OH groups and the oxygen atom of adjacent molecules, which let them be packed into planar sheet structure. This allows the cellulose able to assemblies together to form individual cellulose chain-forming fibers and the morphological hierarchy is defined by elementary fibrils. In fact, these individual fibrils are connected through covalent bonds, hydrogen bonds and van der Waals forces into the larger units called microfibrils (George & Sabapathi, 2015). Eventually, the microfibrils are tended to be bundled and merged into fiber which consists of two different regions: highly ordered structure (crystallites form) as well as unorganized and disordered domains with a lower degree of order (amorphous cellulose) (Adewuyi & Deshmane, 2015; Van de Vyver et al., 2011). Recently, some studies (Ioelovich, Leykin, & Figovsky, 2010; Kulasinski et al., 2014) have been reported that there are another two possible states of order in cellulose fibers, namely intermediate and para-crystalline structure, many details have not been completely elucidated yet.

For cellulose macromolecules, hydrogen bonding plays a noteworthy role in directing the crystalline packing as well as governing the physical properties (structural stability, strength) of cellulose structure. It is known that nature cellulosic fibers are hydrophobic and highly crystalline than lignin and hemicellulose, which further enhances the recalcitrance of the plant biomass (Davison et al., 2013). Due to this reason, cellulose can withstand higher degradation temperature than that of the other

two biopolymers which normally occurs at the temperature of around 320–356 °C (Pang et al., 2014). The empirical formula of native cellulose is $(C_6H_{10}O_6)_n$ and the backbone of cellulose chain contain the several hundred to more than ten thousand of AGU repeating blocks (Chirayil et al., 2014). The number of glucose units or also known as the degree of depolymerization (DP) of cellulose varies among a wide range, depending on its origin. For instance, the DP value of cotton cellulose is estimated to be 15000 and 10000 in wood pulp (Habibi, 2014). In addition to that, each cellulose chain possesses of dissimilar end groups at glucose unit with respect to the both terminals of its molecular axis: One end has chemically reducing functionality (hemiacetal group at C_1 position), and the other holds a pendant hydroxyl group at C_4 position, which also known as nominal non-reducing end group. **Figure 1.1** demonstrates the typical chemical structure of cellulose bio-macromolecule.

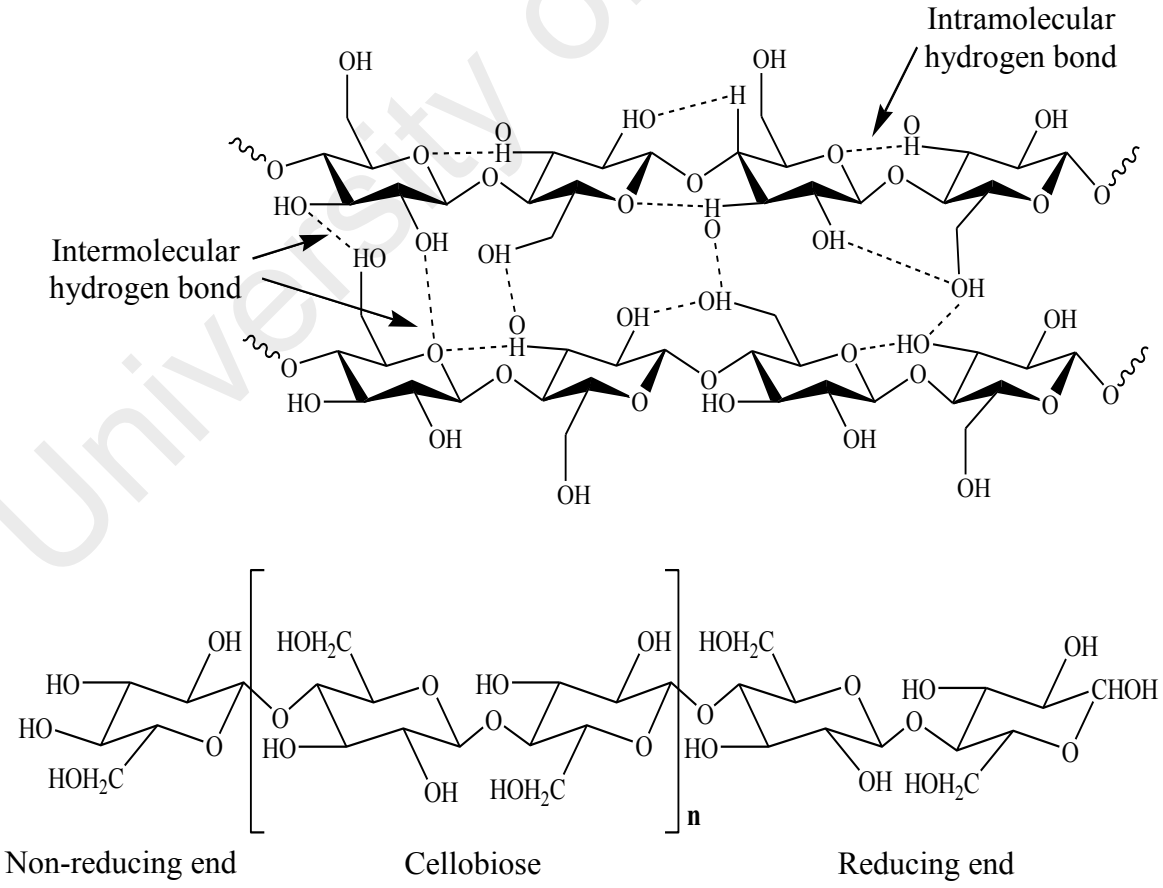

Figure 1.1: Chemical structure of cellulose chains at molecular level.

1.2.2 Hemicellulose

Hemicellulose is the second most abundant biopolymer after cellulose, with the estimated yearly production of 60 billion tons (Kotarska, Świerczyńska, & Dziemianowicz, 2015). Unlike cellulose, hemicellulose is the hetero-polysaccharide with amorphous and random nature, which composed of several heterogeneous classes of C_5 and C_6 sugar polymers. In nature, hemicellulose has branches with short lateral chains comprises of different monomeric sugar components, including pentoses (five carbon sugars: D-xylose, L-arabinose, rhamnose), hexoses (six carbon sugars: D-glucose, D-mannose, D-galactose) and uronic acids (*e.g.* D-glucuronic, D-galacturonic, 4-*o*-methyl glucuronic acids) (Scheller & Ulvskov, 2010). The backbone of hemicellulose is either hetero- or homopolymer with short branches that mostly connected by *β*-(1,4)-glycosidic linkages and rarely *β*-(1,3)-glycosidic bonds. Basically, hemicellulose components are categorized with sugar as a backbone, such as xylan, glucuronoxylan, galactomannan, glucomannan, arabinoxylan and xyloglucan (Dutta et al., 2012). The structure and arrangement of hemicellulose in softwood differ in a distinctive way as compared with those found in hardwoods and grasses (Gírio et al., 2012). In hardwood and annual plant, the most predominant sugar component is glucuronoxylan (15–30%) or xylan, while softwood hemicellulose contains mostly galactoglucomannan (10–20%) and arabinoglucuronoxylan (7–10%) (Dutta et al., 2012; Matsagar & Dhepe, 2015).

Lignocellulosic biomass consists of 25–35% of hemicellulose with the average molecular weight of less than 30 000. Cellulose is tightly coated with hemicellulose via non-covalent crosslinking to the surface of each microfibril. Due to its amorphous properties and single chain polysaccharides structure, hemicellulose is not that recalcitrant to bioconversion to monomeric sugars compared to lignin and cellulose (Davison et al., 2013; Kotarska et al., 2015). Therefore, hydrolysis process is more

preferred to occur in hemicellulose than cellulose and lignin is. Comparing to cellulose, hemicellulose is more thermochemical sensitivity and relatively easy hydrolyzed into its constituent sugars under mild conditions (Lee, Hamid, & Zain, 2014). When hydrolyzed, hemicellulose is a potential candidate to be converted into rare sugars; highly value-added compounds in biorefinery process. A comparison of the principal differences between hemicellulose and cellulose is given in **Table 1.2**.

Table 1.2: Characteristics of hemicellulose and cellulose in typical lignocellulosic biomass (Chen, 2014).

	Cellulose	Hemicellulose
Molecular weight	High (10 000 units)	Low (hundred units)
Subunits	Glucose units	Mixed sugars
Polymer topology	Linear	Branched
Degree of polymerization	Several hundred to thousands	< 200
Side groups substitution	No substitution	On C_2, C_3, and C_6
Composition	Crystalline + amorphous	Amorphous
Solubility	Low	High
Reactivity	Less reactive	More reactive
Hydrolysis[#]	Partial	Readily (susceptible)

Hydrolyzed by dilute acid, alkali or enzymes (hemicellulase); Reference: (Lee, Hamid, & Zain, 2014)

1.2.3 Lignin

Lignin is a complex, three-dimensional network and large molecular of polyphenolic polymer that consists of various crosslinked phenolic monomers. It is considered as the most complicated lignocellulosic component and smallest fraction (10–25%) in biomass. Naturally, lignin is a heterogeneous polymer that exists in a long chain, comprising largely of phenylpropane units (3 carbons attached with 6 carbon rings) mostly nonlinearly and randomly linked by ether bonds. It acts like adhesive by filling up the gap between cellulose and hemicellulose complexion with the polymers and binding cell walls component together (Anwar et al., 2014). Therefore, it is found in the primary cell wall of plant biomass, and plays the significant roles in imparting

structural support, mechanical strength, impermeability, water transport and resistance against the microbial/pathogens attack (Pang et al., 2014). Due to these properties, lignin has functioned as the protective barrier of plants to water penetration and restricts the chemical degradation of cellulose and hemicellulose into smaller monomers (Kotarska et al., 2015; Manavalan, Manavalan, & Heese, 2015). However, the recalcitrant nature of lignin in the cell wall may create a remarkable resistance towards the decomposition process of polysaccharides, and thus significantly affects the efficiency of hydrolysis treatment during biorefinery process (Hadar, 2013).

Lignin is existed in amorphous nature with the oxidative coupling of three main phenyl propionic alcohols primary units (monolignols), namely coniferyl alcohol (guaiacyl propanol; G unit), sinapyl alcohol (syringyl alcohol; S unit) and coumaryl alcohol (*p*-hydroxyphenyl propanol; H unit), as shown in **Figure 1.2**. Depending on the biomass origin, the lignin varies in monolignol compositions. In general, herbaceous plants have exhibited the lowest lignin content, whereas softwoods have the highest content of lignin. The major linkages formed between these phenolic monomers during the radical polymerization process of lignin biosynthesis are ether and C–C linkages (Li et al., 2015). The monomer compositions affect the molecular structure in terms of the extent of crosslinking with polysaccharides fraction and branching of the polymer. Until now, the exact structure of untreated lignin macromolecules found in plants (also termed as native lignin), is still unknown and uncertain. The formation of lignin vascular in the plant is via the polymerization process of phenol radical-radical coupling reactions (Achyuthan et al., 2010). However, the random nature of the coupling reactions causes the generated lignin polymers have no unique or fixed sequence of the phenylpropanoid units. This type of polymerization resulted in the wide-ranging structural diversity of natural lignin polymers as well as its racemic nature. Therefore,

the structure of lignin is always presented by using the contemporary structural model. In fact, the sterically chemical structure of lignin reveals the difficulties of the complete removal from lignocellulosic resources (Li et al., 2015).

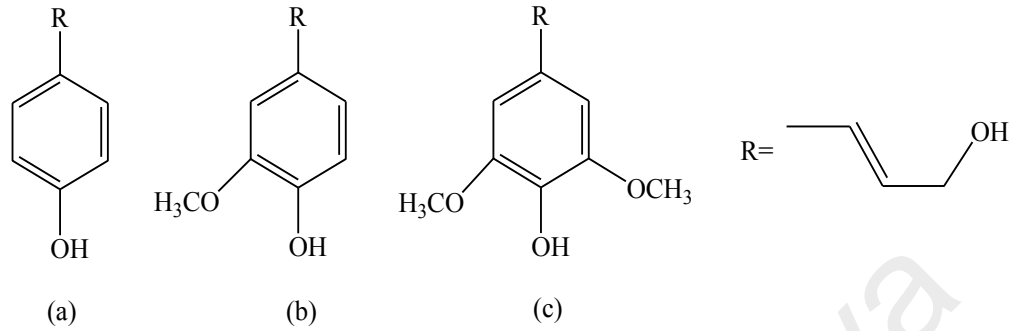

Figure 1.2: Structural units of monolignols, the dominant building blocks of lignin; (a) *p*-hydroxyphenyl, (b) guaiacyl, and (c) syringyl group.

In summary, cellulose provides the mechanical strength and rigidity for cell walls of plants, while the hemicellulose functions as the wire mesh that embedded around the cellulose bundles and providing the further reinforcement to the strength and linkage of plant structure. Lignin is less hydrophilic nature than hemicellulose and cellulose. In addition to this, lignin will fill the remaining space in the plant matrix and excludes water from the highly compact polysaccharide surrounding environment. This unique combination of these three biopolymers resulted in the high resistance and hydrophobicity nature of lignocellulosic biomass to mechanical, chemical and biological degradation (Davison et al., 2013).

1.3 Advantages of Nanocellulose and Its Applications

Nanocellulose is usually defined as the cellulosic material that precisely having at least one dimension in the range of 1 to 100 nm. However, it is worth mentioning that there is still a significant incongruity in the terminology and classification of these nano-dimensional cellulose products dictated by the large variability of starting lignocellulosic biomass (origin) and extraction procedures (preparation methodologies

and conditions). The unstandardized nomenclature presents in the literature results in some ambiguity and misunderstanding. In general, there are three main structures of nanocellulose, namely nanocrystalline cellulose (NCC), nanofibrillated cellulose (NFC) and bacterial nanocellulose (BNC). They have essentially different in term of morphology, regardless of its nanoscale dimensions (discussed in detail in **Section 2.3**).

Because of its nano-scale dimensions, nanocellulose exhibits various outstanding and excellent physicochemical properties compared with typical cellulose material, such as large specific surface area, high porosity, high aspect ratio, excellent tensile strength and modulus, and biodegradability (Cao et al., 2015). Recent years, many studies have been carried out on the synthesis of nanocellulose fibers as reinforcement agents in polymer nanocomposites. Compared with inorganic reinforcements, the main advantages of this naturally-derived nanostructured cellulosic material are: (i) a wide variety worldwide; (ii) renewable and economic feasible; (iii) low density, light material and less energy consumption during processing; and (iv) high specific strength, modifiable surface and reactive surface that can be graft with others polymers easily (Jonoobi et al., 2015). Also, the extraordinary Young's modulus of nanocellulose is relatively close to the derived from theoretical chemistry, and even stronger than Kevlar and glass material. This leads to the extensive development of this eco-friendly green material. **Table 1.3** summarizes the mechanical properties of some reinforcing agents.

Table 1.3: Mechanical properties of nanocellulose and several reinforcement materials available in market (Moon et al., 2011).

Material	ρ (g cm^{-3})	σ (GPa)	E_A (GPa)	E_T (GPa)
Carbon fiber	1.8	1.5–5.5	150–550	–
Crystalline cellulose	1.6	7.5–7.7	110–220	2.5
Boron nanowhiskers	–	2–8	250–360	–
Kevlar-49 fiber	1.4	3.5	124–130	2.5

Remark: ρ = density; σ = tensile strength; E_A, E_T = elastic modulus in axial and transverse direction, respectively.

Some potential applications of nanocellulose are listed below (Klemm et al., 2011):

- *Packaging, paperboard, and paper*: Nanocellulose is able to enhance the fiber-fiber bond strength and thus it has a significant reinforcement effect on paper materials.
- *Composite materials*: Nanocellulose has many unique properties and is commonly used as reinforcement or filler in bio-nanocomposites.
- *Food industry*: Nanocellulose can form dispersions and emulsions which suitable to be used as stabilizers and thickeners in food applications.
- *Medical and hygiene products*: Nanocellulose has good absorption properties and widely used in non-woven products, tissues, or diapers.
- *Other applications*: Cosmetics, films, painting, automotive, textile and so on.

1.4 Application and Conversion of Oil Palm Biomass to Value Added Products

At present, most of the oil palm biomass are disposed of at the oil palm plantation or burned at the mills/plantation sides to produce oil palm ash. Therefore, finding useful utilization of the oil palm biomass in fabrication of natural fiber based composites/hybrid composites will certainly improve the environmental problems which related to the disposal of oil palm wastes. To date, palm tree biomass has contributed a lot to our nation through its diverse usage in different industrial applications. The attention of researchers has been focused in developing the isolation of high novel nanocellulose through biomass utilization. Isolation and application of nanocellulose has been rapidly expanding in different way for supporting scientific, economic, industrial communities and environmental motivations. The common applications of oil palm biomass in different sector have been listed in **Table 1.4**.

Table 1.4: Industrial/product applications of oil palm fibers (Khalil et al., 2012).

Oil palm biomass	Industry/product
Oil palm empty fruit bunch	Biofuel
	Particle boards
	Hybrid composite
	Polymer biocomposite
	Medium-density fiberboard
	Plywood
Oil palm frond fibers	Downdraft gasifier
	Animal feed
	Biodegradable film
	Fiberboard
	Nutrient recycling
	Pulp, paper
Oil palm trunk fibers	Lignin
	Plywood, furniture

1.5 Heterogeneous Catalyst

The first step for cellulose utilization is to depolymerize it into the smaller molecular structure such as soluble glucose, oligosaccharides, and nanocellulose. However, the natural cellulose polymer forms a robust crystal structure with high chemical resistance, thus making the cellulose depolymerization processes more difficult. The most established methods for cellulose hydrolysis are known to be catalyzed by concentrated mineral acids. So far, H_2SO_4 is known as a typical acid for this process. However, the large-scale use of mineral acid suffers from several limitations such as catalyst recovery, reactor corrosion and requires treatment of the acid residue as lots of waste is produced (Hamid et al., 2015). From the industrial point of view, the above limitations must be taken into account when designing production processes. Moreover, several aspects also need to be concerned such as simplicity, economy, efficiency and environmental friendliness.

The utilization of heterogeneous acids has the potential to overcome some of the above limitations due to the ease of separation of catalysts from the final production. A significant development of this transformation has been made by using different types of solid acid catalysts which possess of strong acid strength and large pore size (Huang & Fu, 2013). Associated with these solid acid catalysts, many pretreatment technologies have been developed in order to increase the surface area of cellulose and reduce its crystallinity in order to improve the reaction efficiency and selectivity, such as ball milling, ionic liquids, etc. Apart from that, microwave irradiation induced assistance of the cellulose hydrolysis is an effective heating method compared to that of conventional oil heating (Xu et al., 2011). Due to these reasons, much effort has been done in the field of heterogeneous catalysts for the chemical industry.

1.5.1 Basic Principle

Although the heterogeneous catalyst is widely used for cellulose conversion, the fact that transfer resistance between solid acid and insoluble (or partially soluble) cellulose will eventually restrict the catalytic activity should be taken into account (Cabiac et al., 2011). Thus, it is important to promote the mass and heat transfer for enhancing the activity of solid acid catalysts for the cleavage of glycosidic linkage in cellulose. Among these, hydrothermal condition (H_2O as reaction medium) is a good choice for enhancing the accessibility of solid catalyst to cellulose matrix. Other than acting as the mass transfer medium, H_2O can also play a significant role as the catalyst for auto-hydrolysis process. The hydronium ions (H_3O^+) formed on the surface of catalyst could further promote the cellulose hydrolysis process. However, the development of this field is still in progress. The details principle of each heterogeneous catalyst will be discussed in **Section 1.5.2**.

Several critical features for an ideal acid catalyst for cellulose hydrolysis are as follows:

(i) Possesses of strong acidity and high accessibility of active sites for hydrolysis reaction;

(ii) Water-tolerant acid catalyst;

(iii) Ease in separation between the solid catalyst and the final product (nanocellulose) either in the gel or powder form;

(iv) Tunable pore size to improve the accessibility of reactant.

1.5.2 Categories of Heterogeneous Catalyst

Based on ideal criteria mentioned earlier, several possible green acid catalysts are highly potential to be designed as heterogeneous catalyst for cellulose hydrolysis:

(1) Metal oxides

Metal oxides are a type of solid catalyst with many Lewis acid sites. Metal oxides possess of high pore sizes and specific surface which are easy for the cellulose to access and contact with its active sites inside the metal oxide pores. These metal oxides can be used for the hydrolysis of cellulose, cellobiose and sucrose. As a type of strong solid acid catalyst, mesoporous transition-metal oxides have been prepared and widely used in organic chemical transformations reaction (Tagusagawa et al., 2010). The catalytic performance of cellulose hydrolysis reaction can be further improved when the nanoscale metal oxide catalysts are applied in the system.

(2) Polymer based acids

Polymer based acids with Brønsted acid sites can be used as effective solid catalysts mainly for organic reactions such as hydrolysis process. One of the polymer based acid is macroreticulate styrene-divinylbenzene resins with sulfonic groups (–

SO_3H). These catalysts are inexpensive, stable in most solvents and commercially available. The macroporous structures of these catalysts allow the entering of small molecules and thus interact with more active acid sites (Huang & Fu, 2013).

(3) Sulfonated carbonaceous based acids

Amongst the various types of solid acid catalyst, carbonaceous solid acids rendered the superior catalytic activities in cellulose hydrolysis process. The properties of these catalysts are good recyclability and low-cost, making them become better candidates for the production of biofuel precursors. Generally, carbon-based solid acids were prepared via the sulfonation process of incompletely carbonized natural polymers, such as cellulose, sugars and starch or by incomplete carbonization of sulfopolycyclic aromatic compounds with the presence of concentrated H_2SO_4 (Chang et al., 2013).

(4) Heteropoly acids

Heteropoly acids (HPAs) are a type of solid acid that consists of early transition metal–oxygen anion clusters. They are usually used as a recyclable acid in most of the chemical transformations (Huang & Fu, 2013). The most widely and common used HPAs are Keggin type acids. The HPAs are fascinating architectures and excellent physicochemical properties with the advantages of high proton mobility, Brønsted acidity and good stability (Klein et al., 2015). Basically, they dissolve in polar solvents and release H_3O^+, thus its acidic strength is stronger than typical mineral acids.

(5) Ion-exchange resin

Ion-exchange resin is a novel, environmental-friendly catalyst for the isolation of nanocellulose. Generally, the ion-exchange resin has been commercially used as solid acid catalysts in various reactions such as hydrolysis, isomerization, nitration and

transalkylation. Compared with homogeneous liquid, ion-exchange resin is ease of separation after reaction with less water washing, high reusability, low equipment corrosion and recyclable of the catalyst. Most importantly, ion-exchange resin is less aggressive to the cellulose depolymerization process than liquid mineral acids, and it is possible to terminate the hydrolysis reaction at any stage. During the ion-exchange resin hydrolysis, only the disordered region of cellulose is removed while the ordered region has remained unaltered. This can ensure that the degradation of crystalline cellulose is greatly reduced as the catalysts only attack the surface of crystalline cellulose. Therefore, nanocellulose obtained by ion-exchange resin hydrolysis rendered the higher crystallinity (Tang et al., 2011).

1.5.3 Reaction/Mechanism of Heterogeneous Catalyst in Hydrolysis Process

In this section, the reaction mechanism (**Figure 1.3–1.4**) of the solid acid catalysts for cellulose depolymerization process is included in the following part and their catalytic performance is summarized in **Table 1.5**. **Figure 1.3** illustrates the proposed mechanism of cellulose hydrolysis conducted by polymer based acids (*i.e.* cellulase-mimetic solid catalyst). Generally, the catalyst support (such as chloromethyl polystyrene resin) consists of the chlorine group (–Cl) which responsible in binding the cellulose by forming hydrogen bonds, while the sulfonic acid groups ($–SO_3H$) functioning as the hydrolytic domains. The $–SO_3H$ groups are introduced by partially substituting –Cl groups with sulfanilic acid (Shuai & Pan, 2012). In addition, later work carried out by Komanoya et al. proposed that the active Ru species (such as $RuO_2 \cdot H_2O$) was able to desorb the hydrated water in order to provide a Lewis acid site for the depolymerization process of cellulose into glucose on sulphonated mesoporous carbon (CMK-3), as schematically shown in **Figure 1.4** (Komanoya et al., 2011).

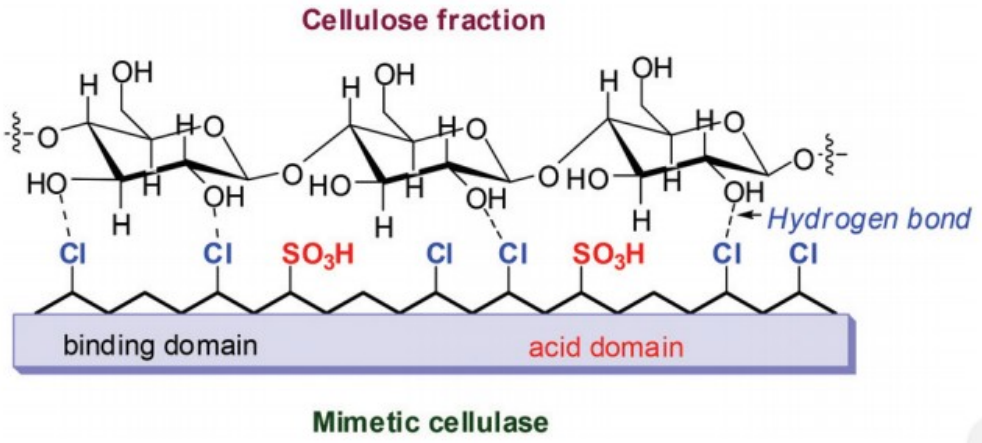

Figure 1.3: Hydrolysis mechanism of a cellulase-mimetic solid catalyst (Shuai & Pan, 2012).

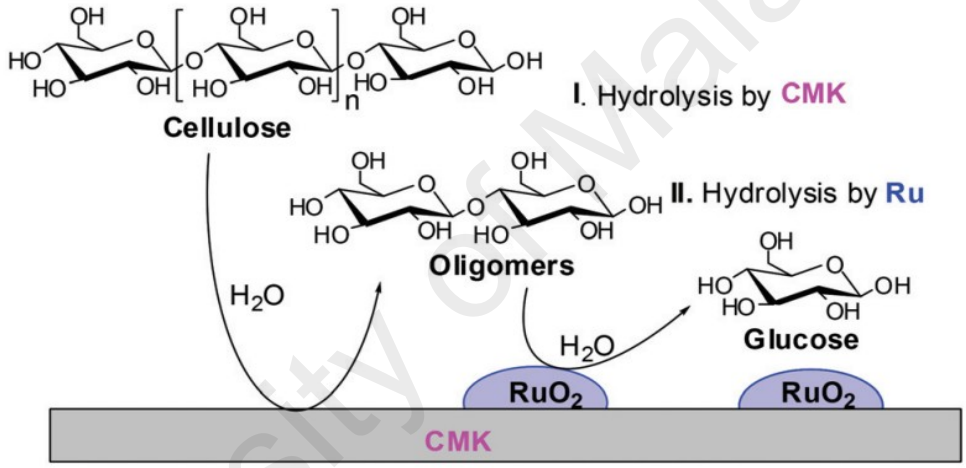

Figure 1.4: Hydrolysis of cellulose by Ru/CMK-3 (Komanoya et al., 2011).

Table 1.5: Different performances of solid acid catalysts in the hydrolysis of cellulose (Wang et al., 2014).

Catalyst	Cellulose	Conversion (%)	Yield of glucose (%)
Silica/carbon nanocomposites	Avicel	60.7	50.4
Tungstated zirconia	Avicel	42	19
Dowex 50WX8	Avicel	–	17.2
Nafion SAC 13	Cellobiose	11	9
$Cs_2HPW_{12}O_{40}$	Avicel	31.5	5

1.6 Problem Statement

The extraordinary features of nanocellulose have increased its demands in industrial applications, especially nanotechnology, and bio-nanocomposite processing fields. Conventionally, the isolation procedures for producing nanocellulose involve two stages:

1. Biomass pretreatments: multiple isolation procedures, namely dewaxing, alkalization and bleaching process, to extract the highly purified cellulosic material;
2. Catalytic hydrolysis: removal of amorphous domains in the cellulose matrix, yielding high crystalline segment cellulose nanoparticles.

In general, several promising hydrolysis techniques have been established and widely used for isolating nanocellulose from various cellulosic materials, including mechanical disintegration (J. Li et al., 2012), acid hydrolysis (Y. W. Chen et al., 2016) and enzyme-assisted hydrolysis (Cui et al., 2016). Compared to acid hydrolysis, biological treatment (enzyme-assisted hydrolysis) is considered as an eco-friendly and greener process to the environment, as only microorganisms are involved for cellulose hydrolysis process (Wan & Li, 2012). However, due to the strong inter-fibrillar hydrogen bonding and complicated multilayered structure of plant fibers, the complete conversion of cellulose catalyzed by enzymes such as cellulase is usually suffers from low efficiency (takes a longer period) and the process is not cost-effective (enzymes are expensive and hard to be recycled) (Mora-Pale et al., 2011). On the other hand, it is understandable that the mechanical treatment including cryocrushing, grinding, high-pressure homogenization, microfluidization, and high-intensity ultrasonication for producing nanocellulose is normally consuming a large amount of energy, repeated processing, or complex equipment for obtaining desired fiber dimensions (Lee, Hamid, & Zain, 2014). Thus, these are the main limiting factors to restrict the application of mechanical disintegration in nanocellulose processing industry, as it might increase the

capital costs of the production line and not economically feasible (Maurya, Singla, & Negi, 2015).

To address these problems, some new hydrolysis approaches have been developed by research scholars for preparing nanocellulose, such as solid acid hydrolysis (Liu et al., 2014), sono-chemical assisted hydrolysis (Rohaizu & Wanrosli, 2017), ammonium persulfate (APS) oxidative degradation (Cheng et al., 2014), ionic liquid (Tan, Abd Hamid, & Lai, 2015) and TEMPO-mediated oxidation (B. Li et al., 2015). But, APS oxidative degradation and solid acid hydrolysis approaches are usually time-consuming (approximately 16 h) (Goh et al., 2016). Sono-chemical assisted hydrolysis technique is highly energy demand because of high power (~1500 W) ultrasonicator probe is required throughout the process (Satyamurthy et al., 2011). Likewise, the oxidation hydrolysis system for the TEMPO-mediated method is rather complicated and typically assisted by other mechanical treatments (*i.e.* high power ultrasonication) (Rohaizu & Wanrosli, 2017). The limited contact between the solid phase catalyst active sites and cellulose macromolecule is the main obstacle of this technique, and lead to low hydrolysis efficiency, while the ionic liquid hydrolysis process is not economic feasibility due to high energy consuming for recovery process and costly chemicals (Hamid et al., 2016).

For these reasons, strong acid hydrolysis is still considered as the most effective isolation method to be used for preparing nanocellulose by selectivity dissolution the amorphous regions of the cellulose. The use of different acids such as phosphoric (Tang et al., 2015), hydrochloric (Boujemaoui et al., 2015), nitric acid (Y. Cao et al., 2015), formic (B. Li et al., 2015) or their mixtures is quoted in the literature, but mostly aqueous sulfuric acid (H_2SO_4) has been used (Liu et al., 2016). Acid hydrolysis has the

benefits of simple, convenience, highly efficient and moderate operation conditions in removal of cellulose defective regions, however, some issues have to be addressed such as costly procedures for recycling of acid waste effluents, highly corrosive of reactor vessel (or expensive corrosion-resistant coatings required), formation of large volumes of salts during neutralization of solution (Hamid et al., 2015). Also, under strongly acidic conditions, different types of undesirable by-products, principally water-soluble simple sugar instead of solid crystalline nanoparticles are obtained due to the excessive hydrolysis activity (over-degradation) of cellulose (Goh et al., 2016). Normally, the maximum yield of concentrated acid treated nanocellulose is usually lower than 50% (Hamid et al., 2016; Y. Li et al., 2014) as the hydrolysis process easily went too far. This may lower the quality as well as reduce the final yield of nanocellulose, which causes difficulty in scaling up the industrial production.

Considering the drawbacks of the typical pretreatment approaches mentioned above, dilute acid hydrolysis is being introduced as an alternative cellulose depolymerization strategy under milder reaction conditions. Dilute acid treatment benefits from the environment point of view on comparing with concentrated acid treatment due to limited equipment corrosive issues and relatively low acid consumptions (less than 10%) (Ji, Shen, & Wen, 2015). For these reasons, dilute acid pretreatment appeared to the most practicable and preferable for industrial scale. However, such treatment is found to be less effective in reacting to the hierarchical structure of plants (Yahya, Lee, & Hamid, 2015), especially towards the recalcitrance nature of cellulose due to its high ordered and compact structure, resulting in the low yield of nanocellulose product. There are two common types of reaction severities has been widely reported, including lower temperature (120 °C) for long period of time (30–90 min) or high temperature (180 °C) over a short retention time (Maurya et al., 2015). From an economic viewpoint, the

hydrolysis process conducted under extreme reaction conditions (*i.e.* long retention time or high temperature) is unfavorable for industrial practice due to not economic viability for long-term production, and this eventually will increase the capital and operating cost.

The weakness of dilute acid treatment can be overcome by introducing a suitable co-catalyst during the treatment that can help in increasing the hydrolysis selectivity of cellulose by producing tailor-made properties nanocellulose. In recent years, it has been proved that combining the metal ion catalyst with dilute acid treatment strategies can initiate the synergistic effect of reaction, which potentially reduce the treatment time and energy consumption for cellulose degradation process (Wang, Yuan, & Cui, 2013). Furthermore, the combined treatment not only able to minimize the quantity of chemicals required, but also tend to enhance the efficiency of cellulose hydrolysis, and thus, it is more economically attractive (Y. Zhang et al., 2015). Previously, inorganic metal salt catalyst has been proved to be effective in solubilizing the hemicellulose into oligomeric and monomeric sugars via hydrolysis stage (Shen et al., 2014). Interestingly, latest breakthroughs have shown that metal salt can effectively catalyze cellulose hydrolysis as it can induce the degradation of cellulose polymeric chains as well as disrupt the hydrogen bonding systems effectively (X. Cao et al., 2015; Wang et al., 2013). Several studies conducted by Li and his coworkers (Li et al., 2013; J. Li et al., 2015) found that the selectivity of acid hydrolysis assisted by metal ions can be greatly improved in cellulose amorphous regions and yield a high crystallinity of microcrystalline cellulose or nanocellulose. This is due to the activation energy of cellulose hydrolysis reaction can be significantly reduced with the presence of metal ion and H_3O^+ dissociated from acid (Hamid, Chowdhury, & Karim, 2014). It is expected that the synergy effect between the two hydrolyzing catalysts will be useful in fabricating high quality of nanocellulose with higher yield.

For the conventional biomass pretreatment, it is normally involved the multiple isolation procedures, including dewaxing, alkalization and bleaching process in order to isolate the purified cellulosic material from the complicated lignocellulosic biomass. These processes are mainly aimed for eliminating the non-cellulosic constituents before the hydrolysis process implied for nanocellulose production. With this technique, tedious and time-consuming preparation steps are required (Goh et al., 2016). In addition to that, several washing steps are required to purify the treated product obtained from each stage before proceeding to subsequent treatment. This not only resulted in more wastewater discharged, a large amount of treated product maybe loss during the washing steps. This eventually reduces the final product yield. Therefore, it is necessary to develop a simple and versatile biomass pretreatment for better and more practicable route for large-scale production of nanocellulose.

1.7 Objectives of Research

In the present research, we demonstrated a novel and sustainable hydrolysis technique to produce nanocellulose from α-cellulose model compound. The strategy was constructed in order to explore the potential of Lewis acid based catalysts, namely Fe(III), Co(II), Ni(II), Cr(III) and Ni(II)-based transition metal assisted by dilute H_2SO_4 acid catalyzed hydrolysis of cellulose. Later development of nanocellulose production included optimization study of hydrolysis parameters in order to obtain the maximum crystallinity index and nanocellulose product yield. Thus, the main objectives addressed in this work are as follows:

1. To study catalytic screening of transition metal-based catalysts for nanocellulose production via catalytic hydrolysis of cellulose materials;

2. To optimize the hydrolysis parameters for nanocellulose crystallinity index and product yield by using a central composite design (CCD) coupled with response surface methodology (RSM) modeling system;
3. To investigate physicochemical properties of nanocellulose products, in term of crystallinity index, morphological structure, particle size distribution, surface chemistry and thermal stability profile.
4. To develop one-pot oxidative-hydrolysis process for isolating nanocellulose from lignocellulosic biomass.

1.8 Scope of Research Work

In order to accomplish the project objectives, this thesis is organized into five chapters. Chapter 1 basically discusses the background of research, problem statements, research objectives and scope of work conducted on this project. It briefly highlights the importance of study, summarizes the major issues of the existing isolation techniques for nanocellulose production and the significance of our developed approach to solve the limitations of current hydrolysis technologies. Chapter 2 covers a summary of the literature related to the relevant past works, categories of nanocellulose products, current biomass pretreatment techniques, as well as the conventional isolation approaches together with their process details, advantages, and limitations.

Chapter 3 provides an outline of the materials selection, procedures of nanocellulose synthesis including: (i) Catalysts preliminary screening; (ii) Optimization study conducted by using response surface methodology (RSM); and (iii) One-pot oxidative-depolymerization isolation approach for the production of nanocellulose from oil palm biomass. All the results obtained will be discussed in Chapter 4. Chapter 5

summarizes the conclusions of the overall studies and several recommendations are suggested for further works that could be conducted in relevant fields.

1.9 Rationale and Significance

Based on the research scopes above mentioned, the following rationale and significance of this work are outlined as follows:

- Production of nanocellulose biomaterial from low-cost lignocellulosic biomass (such as oil palm biomass) for wide field of industrial application.
- Enhancement of hydrolysis efficiency and nanocellulose depolymerization selectivity by using transition metal-based catalyst assisted dilute acid catalyzed hydrolysis.
- Facile one-pot oxidative-hydrolysis preparation of nanocellulose from complex oil palm biomass with high quality of nanocellulose features (high crystallinity index, narrower particle size and higher aspect ratio).

CHAPTER 2: LITERATURE REVIEW

2.1 The Source of Cellulose: A Classification

Lignocellulosic biomass is mainly composed of three biopolymers: lignin, hemicellulose, and cellulose. Depending on the type of biomass, these polymers are organized into a complex and non-uniform structures in which cellulose fibers are embedded by lignin and hemicellulose sheath. It mainly can be categorized into several areas (Lee, Hamid, & Zain, 2014; Loow et al., 2015), including:

i. Forestry residues: obtained from forest logging places and management operations;
ii. Agricultural wastes: collected from various farming and agricultural activities;
iii. Municipal solid waste: produced from industrial and human activities; and
iv. Energy crops: grown for electricity or biofuel production.

Basically, Lignocellulose biomass consists of three main biopolymers: lignin (15–35%), hemicellulose (19–45%) and cellulose (30–50%) (Mood et al., 2013). These three major components of the plant consist of approximately 90% of its dry biomass. However, it is commonly assumed that the ratio between these biopolymers constituents within each biomass vary with type, origin, species, genetic, and environmental factors of the plant (**Table 2.1)**. In addition to that, a small amount of extractives, protein, and pectin can also be found on the plant. These materials such as waxes, nitrogenous materials, chlorophyll and nonstructural sugars can be easily removed using soxhlet treatment with different solvents such as ethanol, benzene, and toluene (Segneanu et al., 2013). The relative abundance of biopolymers in lignocellulosic biomass is a key factor in determining the suitability of the feedstock, as well as affecting the fractionation efficiency for biochemical, fuels and nanocellulose production during the conversion process (Dixon, 2013; Jordan et al., 2012).

Table 2.1: Chemical composition of lignocellulosic substrates in different biomass residues and generated wastes (Jonoobi et al., 2015; Loow et al., 2015).

Classification	Sources	Composition (%)		
		Cellulose	Hemicellulose	Lignin
Agriculture waste	Corncobs	45	35	15
	Sugarcane bagasse	38	27	21
	Corn stover	39–42	22–28	18–22
	Wheat straw	30	50	15
	Nut shells	25–30	25–30	30–40
	Rice straw	34	25	12
	Wheat shorts	66.8	11.5	21.7
	Cotton seed hairs	80–95	5–20	ns
	Pine	42–50	24–27	20
	Barley straw	33–40	20–35	8–17
	Rice husk	35	33	23
Forestry waste	Hardwood stems	45–55	24–40	18–25
	Oak	41	36	24
	Softwood stems	45–50	25–35	25–35
	Grasses	25–40	25–50	10–30
	Leaves	15–20	80–85	ns
	Hemp	75.56	10.66	6.61
Energy crops	Empty fruit bunch	41	24	21.2
	Poplar	50	25	18
	Miscanthus Giganteus	31	42	27
	Coastal Bermuda grass	25	35.7	6.4
	Distiller dried grains	78	1.8	20.5
	Solid cattle manure	2–5	1–3	3–6
	Switchgrass	45	31.4	12
Municipal solid waste	Waste paper	60–70	10–20	5–10
	Newspaper	40–55	25–40	18–30
	Swine waste	6	28	ns
	Industrial sludge	95	4.75	Very low

2.1.1 Agricultural Crops and Bio-Residues

Agriculture residues are considered as an effective source of cellulose for replacing the native wood material. It has great potential for use as a cost-effective and suitable source for producing the nanocellulose. If comparing with wood, these non-wood crop residues render positive characteristics such as low contents of hemicellulose and lignin,

and thus less bleaching processes are required for removing non-cellulosic components. On the other hand, the bio-residues contributed by agriculture or industrial activities have an excellent advantage as compared with other feedstocks by having low or even negative costs. Today, these plant residues are either burned or used for low-value products such as animal feed. Thus, the development of new value-added products such as nanocellulose is a potential route for improving the value of agricultural resources, at the meantime can contribute to solving disposal problems for industries. In fact, it should be noted that the cellulose microfibrils in agricultural fibers are less tightly bound in the primary cell wall compared to in the secondary wall in wood, therefore less energy is demanding to produce nanocellulose (Siró & Plackett, 2010).

In the literature, numerous studies have reported on the extraction of nanocellulose from diverse non-wood residues including algae (Chen et al., 2016), Nopal cactus (Vieyra et al., 2015), coconut hunks (Fahma et al., 2011), kenaf stem (Jonoobi, Harun, et al., 2011), rice straw (Hassan et al., 2012), industrial bio-residue (Jonoobi, Mathew, & Oksman, 2012), bamboo (Nguyen et al., 2013), *Posidonia oceanica* (Bettaieb et al., 2015), cotton, sisal, flax and agriculture byproduct (Ludueña et al., 2013). These studies indicate that most of the agricultural byproduct can be converted into high value-added nanocellulose products.

2.1.2 Wood

The main source of cellulose is contributed by the wood material. Due to its abundantly, wood is undoubtedly the most significant industrial source for extracting the cellulosic material. In general, the extraction of nanocellulose from wood sources begins with biomass purification process, in which the non-cellulosic components and impurities are removed. Unfortunately, the increasing demands of woods from various

industry sectors such as furniture, building material production, paper industries, and the combustion process for energy have made it challenging to supply all users with the sufficient quantities at the reasonable price. Besides that, the increasing of wood consumption directs cause of over-deforestation, which further leads to the imbalance of ecology system. For this reason, the low-cost raw materials such as agriculture bio-residues and annual plants are likely to become of increasing interest.

2.1.3 Sea Animals

Tunicates (also known as "sea squirts" or Ascidiaces) are the only sea animals known to produce almost pure highly crystalline nanofibers via cellulose biosynthesis. In nature phase, tunicates have a mantle or tunic which comprised of cellulose microfibrils embedded in the protein matrix. In the mature phase, this thick and leathery mantle is used as a source of cellulose microfibrils. The structure of tunicate nanofiber is quite different as compared with the nanocellulose derived from agro-sources and has a helical organization. Basically, the tunic consists of about 90% water, 60% cellulose and 27% nitrogen-containing components in the fresh condition (dos Santos, Iulianelli, & Tavares, 2016). Recently, these nanofibers have been extensively used by researchers because of their high aspect ratio, high modulus and good compatibility with matrix materials. Briefly, the tunicate shells were ground into small fragments, followed by several steps of the bleaching process. Subsequently, the bleached products were treated by acid hydrolysis for the production of nanocellulose.

It is important to note that the tunicates are abundantly available, which over 2300 species of it has been reported in the literature. The cellulose microfibrils in the tunic are aggregated and deposited in a multilayered texture with a bundled structure that parallels to the epidermis. Even if the structures and properties of cellulose microfibrils

are expected to be similar between species, the cellulose formation process could be varying which may be reflected in the resulting end product. In order to separate the cellulose mantles from the tunicate for isolating the cellulose, the tunicate is treated by potassium hydroxide (KOH) solution at an elevated temperature (Zhang et al., 2013).

2.1.4 Bacterial Cellulose

Other than the plant origins (cell-wall component of plants), cellulose fibers are also secreted extracellularly by some of the bacteria species that belonging to the genera *Acetobacter*, *Acanthamoeba*, *Alcaligenes*, *Achromobacter*, *Agrobacterium*, *Rhizobium*, *Pseudomonas*, *Salmonella,Escherichia* and *Zooglea* (Rojas, Bedoya, & Ciro, 2015). Among these species, one of the most studied types of microorganisms that used to produce cellulose is *Acetobacter*. These microorganisms can procure glycerol, sugar, glucose or other organic substrates, and efficient convert them into pure cellulose.

Bacterial cellulose is produced by cultivation process in a culture medium. Under special culturing conditions, the bacteria secrete cellulose microfibrils by producing a pellicle (a thick gel composed of cellulose microfibrils and 97% water) on the surface of the liquid medium (Siró & Plackett, 2010). The bacterial cellulose can be obtained in both synthetic and non-synthetic medium through an oxidative fermentation process (Esa, Tasirin, & Rahman, 2014). Mostly, the bacteria actively fermented at pH 3–7 with the temperature of 25–30 °C, using saccharides as a carbon source (Castro et al., 2011). After the biosynthesis, the produced cellulose pellicles are washed by the 2% NaOH at boiling point for several hours, and then rinsed under running water for several days with the purpose of removing the bacteria. Posteriorly, the water content is eliminated either by evaporation or the combination with pressing in order to collapse the gel-network to produce a dense film (1.0 g/cm^3). In fact, the produced hydrogels are

composed of an entangled network of cellulose microfibrils formed because of the random movement of the bacteria. Most importantly, in contrast to plant-based derived cellulose sources, bacterial cellulose does not require any further purification to remove non-cellulosic polymers such as hemicellulose and lignin. Although the detailed mechanism for bacteria generate cellulose is still unclear, it has been proposed that it is necessary for their survival, including to act as a barrier to yeasts, fungi, and other organisms, or to guard against ultraviolet light (Kim et al., 2016). Compared to cellulose derived from annual plants, the bacterial cellulose displays as a ribbon-shaped fibril structure, which composed of less than 100 nm width and a bundle of finer nanofibrils, 2–4 nm in diameter. However, the morphology of the cellulose microfibril and its network configuration within the pellicle are significantly affected by the variation in culture conditions, including temperature, carbon source, bacteria type, nutrients, pH and agitation (dos Santos, Iulianelli, & Tavares, 2016).

2.1.5 Algae

Algae are phototrophs that occur in marine and freshwater and environments. In nature, algae can differ from small unicellular microalgae (cyanobacteria and diatoms) to a large multicellular macroalga (*e.g.* giant kelp) (Kouzuma & Watanabe, 2015). They live mostly in shallow seas and coastal rocks (Lee, 2011). Although many species of algae (*e.g.* yellow-green, red, green, gray, *etc*.) available in the Earth, only several species of algae produce cellulose microfibril within its cell wall, namely red algae (*Rhodophyta*), brown algae (*Phaeophyta*) and green algae (*Cladophora* and *Valonia*). The cellulose is composed of manna and xylem that mainly serves as the structure of cell wall of polysaccharides in the algae plant (Mohammad et al., 2014). Compared to the land plants, the cellulose presents in the marine algae is in a smaller and more variable proportion. In both brown and red algae, the cellulose content is relatively low,

whereas most of the green algae have a high cellulose content with a cellulosic cell wall, ranging up to approximately 70% of the dry weight (dos Santos et al., 2016). To some extent, the cellulose content of the green algae is of the same order of magnitude as than that of the wood. Due to this reason, green algae have been widely used for the extraction of cellulose microfibril.

However, there are significant differences in the structure of cellulose microfibril obtained from each algae species due to the dissimilarities in the biosynthesis process. For instance, cellulose derived from *Valoniaor Cladophora*, a type of green algae, is featured with an extensive surface area and exceptionally high crystallinity (George & Sabapathi, 2015). In contrast, the cell wall of *Spongomorpha* consists of a large amount of mercerized-like cellulose (a derivative of native cellulose) which has a randomly oriented chain and a low degree of crystallinity (Mihranyan, 2011). In land plants, the cellulose plays a significant role in providing the tensile strength of the cell wall and considered the only skeletal polysaccharides. However, the real reason for explaining the presence of highly crystallinity cellulose in the marine green algae is still ambiguous. So far, it has been suggested that the strong microfibrils structure in the algae is necessary in order to maintain the turgor, such as osmotic pressure inside the cells in the marine environment that features fluctuating salinity (dos Santos et al., 2016).

Generally, the isolation of cellulose microfibrils from algae biomass requires several steps, including a pretreatment of algal cellulose sources. These pretreatments usually involve culturing methods and followed by purifying steps for removing the wall matrix material. Finally, the cellulose nanoparticles can be extracted from the algae cell wall by either acid hydrolysis or mechanical refining process. Even though algae

cellulose does not have the rod-like structure, the nanomaterial produced are about 20 nm wide and comparable in length (>1 μm) to that of typical wood-based cellulosic material (Mihranyan, 2011).

2.2 Classifications of Cellulosic Nanomaterials

In the chemical hydrolysis system, the amorphous regions of the cellulose matrix will be degraded into oligosaccharide molecules (liquid fraction) while the remaining unaltered cellulose crystallite segments present in nanostructured (solid fraction). This remained solid residue is also known as nanocellulose. During the cellulose biosynthesis, intermolecular hydrogen bonds and van der Waals promote the parallel stacking of several cellulose chains to the formation of elementary fibrils that can be further aggregate into larger microfibrils (diameter of 5–50 nm and up to several microns in length). The inter- and intra-chain hydrogen bonding network makes the cellulose becomes a relatively stable macro-polymer, and provides the cellulose fibrils high axial stiffness. Interestingly, the nanofibrils of cellulose are not perfectly crystalline; they exist in the para-crystalline state (amorphous and crystalline domains). In other words, the cellulose chains have the crystal part and defect (amorphous) part in a row. The highly ordered crystalline part cannot be broken due to the presence of strong hydrogen bonding while amorphous regions of cellulose are easily degraded by strong mechanical force or chemical attack (Islam et al., 2014).

In the literature, there are numerous terminologies used in reference to cellulose nanoparticles. Occasionally, the similar term is used to designate different materials, and this can result in uncertainty with respect to the classification of the nanocellulose. This is due to the fact that there is not yet a standard term for these nanomaterials. In the following section, the current trends in nanocellulose particle terms and classification

are discussed. Basically, there are three principal classes of nanocellulose, namely nanocrystalline cellulose (NCC), nanofibrillated cellulose (NFC) and bacterial cellulose (BNC). The cellulose nanoparticles can be differentiated from one another based on their crystallinity, size, dimensions, morphology and properties (**Table 2.2**). Therefore, optimum content of cellulose and possible formation of nanocellulose are main issues to address in order to form ideal nanocellulose with preferred properties.

Table 2.2: The family of nanocellulose materials (Islam et al., 2014).

Type	Synonyms	Formation and average size
Nanocrystalline cellulose (NCC)	✓ Cellulose nanocrystals ✓ Crystallites ✓ Whiskers ✓ Rod-like cellulose microcrystals	Acid hydrolysis of cellulose Diameter: 5–70 nm Length: 100–250 nm (from plant celluloses); 100 nm to several micrometers (from celluloses of tunicates, algae, bacteria)
Nanofibrillated cellulose (NFC)	✓ Microfibrillated cellulose ✓ Nanofibrils and microfibrils	By mechanical treatment Diameter: 5–60 nm Length: Up to several micrometers
Bacterial nanocellulose (BNC)	✓ Bacterial cellulose ✓ Microbial cellulose ✓ Bio-cellulose	Bacterial synthesis Diameter: 20–100 nm; Different types of nanofiber networks

2.2.1 Nanocrystalline Cellulose (NCC)

NCC is whisker-shaped or rod-like particles obtained after acid hydrolysis of micro-sized cellulose fiber. Different terms have been used in the literature to designate these particles such as cellulose whiskers, nanocrystalline cellulose, cellulose microcrystals and cellulose nanowhiskers. They are mainly referred to as “crystals”. Generally, the size of rigid rod-like NCC formed depends on its origin and can vary from 5–70 nm in width and 100–1000 nm in length. In general, NCC particles are nearly 100% cellulose with highly crystalline (54–88%) (Moon et al., 2011). The

variety of morphologies, dimensions, and degree of crystallinity mainly depends on the source of cellulosic material, hydrolysis conditions under which preparation is carried out as well as rely on the experimental technique used (Habibi et al., 2010). As earlier mentioned, the cleavage of cellulose chains occurred randomly during the acid hydrolysis process, giving rise to the not uniform of NCC dimensions. It was reported that NCC isolated from bacterial and tunicate cellulose is generally larger in dimensions as compared with those derived from cotton or wood-based biomass. This is because bacterial and tunicate cellulose is highly crystalline hence there are lower fractions of amorphous regions that required to be cleaved. Due to their highly crystalline structure, the elastic modulus of NCC can even reach up to 140 GPa, and it can be attributed to its hydrogen bonding capability and the stiff nature of the cellulose polymer.

Regarding the extraction of NCC, a simple approach mostly based on the strong acid hydrolysis is normally utilized. Nickerson and Habrle have first introduced the idea of using acid hydrolysis to isolate NCC (Jonoobi et al., 2015). They treated cellulosic fibers with aqueous sulfuric and hydrochloric acids at boiling temperatures. Thus, the conventional method for NCC production is accomplished by the acidic digestion of the cellulosic amorphous zones. Acid hydrolysis is a well-known process to prepare NCC. This is the most effective method for the production of the high degree of crystallinity NCC by removing the amorphous areas of the raw material (Habibi et al., 2010). In fact, these amorphous fractions are susceptible to acid attacks, and under controlled conditions, results in may be removed leaving crystalline regions intact. Most of the authors in literature have described this procedure, treating the cellulose with aqueous sulfuric acid at high concentration (44–70% wt%), at different temperature (23–70 ºC) and using a wide treatment time range (30 min to overnight).

On the other hand, NCC can be obtained from numerous cellulosic resources, such as sisal, straw, ramie, cotton, wood pulp, sugar beets, kraft pulp, microcrystalline cellulose, mulberry, *etc*. Among these, cotton can be considered as one of the most common sources, especially at the laboratory scale. This is because of its high cellulose content that results in a higher yield and most importantly, no intensive purification process of cellulose is necessary when producing the NCC. To a certain extent, the geometrical characteristics (shape, dimensions, and size) of NCC depend on the hydrolysis conditions, such as temperature and time (Lu et al., 2013). It is widely assumed that the traditional process for nanocellulose production by 64 wt% H_2SO_4 lead to the formation of rod-shaped or whisker-like nanocellulose (Satyamurthy & Vigneshwaran, 2013). In contrast, some NCC extraction pathways may give rise to the semi-spherical or spherical NCC (*i.e.* low aspect ratio) (Lu & Hsieh, 2010). For instance, a combination of pretreatment using dimethyl sulfoxide (DMSO) at high temperature (80 °C) followed by the HCl-H_2SO_4 hydrolysis resulted in the obtaining cellulose nano-spheres product with the diameter range of 60–570 nm (Satyamurthy et al., 2011). However, regarding the conventional hydrolysis approach, varying the reaction variables, including acid concentration, temperature, time, acid to fiber ratio and types of raw material, can lead to smaller crystalline NCC particles (dos Santos et al., 2013). It is widely accepted that the cellulosic source is the main factor affecting the NCC morphology (Morais et al., 2013). Celluloses from different sources present different amorphous/crystalline regions ratio. This fact strongly affects the aspect ratio (L/d) of the resultant NCC.

A key factor for NCC production is the yield, which is highly influenced by the hydrolysis conditions. The NCC yield is normally ranged between 25–30% when the cellulosic feedstocks treated by concentrated H_2SO_4 (64 wt%), under different

hydrolysis conditions, but this value can be considerably with the severity of the applied operational parameters (Xu et al., 2013). Extreme treatments (mild or high temperatures with too short or long period) can result in a very poor impact or lead to the total degradation of cellulose structure (Lu et al., 2013), leading to a terribly low NCC yield. At the same time, the presence of high lignin and hemicellulose content might further reduce the yield of NCC production. **Figure 2.1** shows the micrographs of NCC that previously reported.

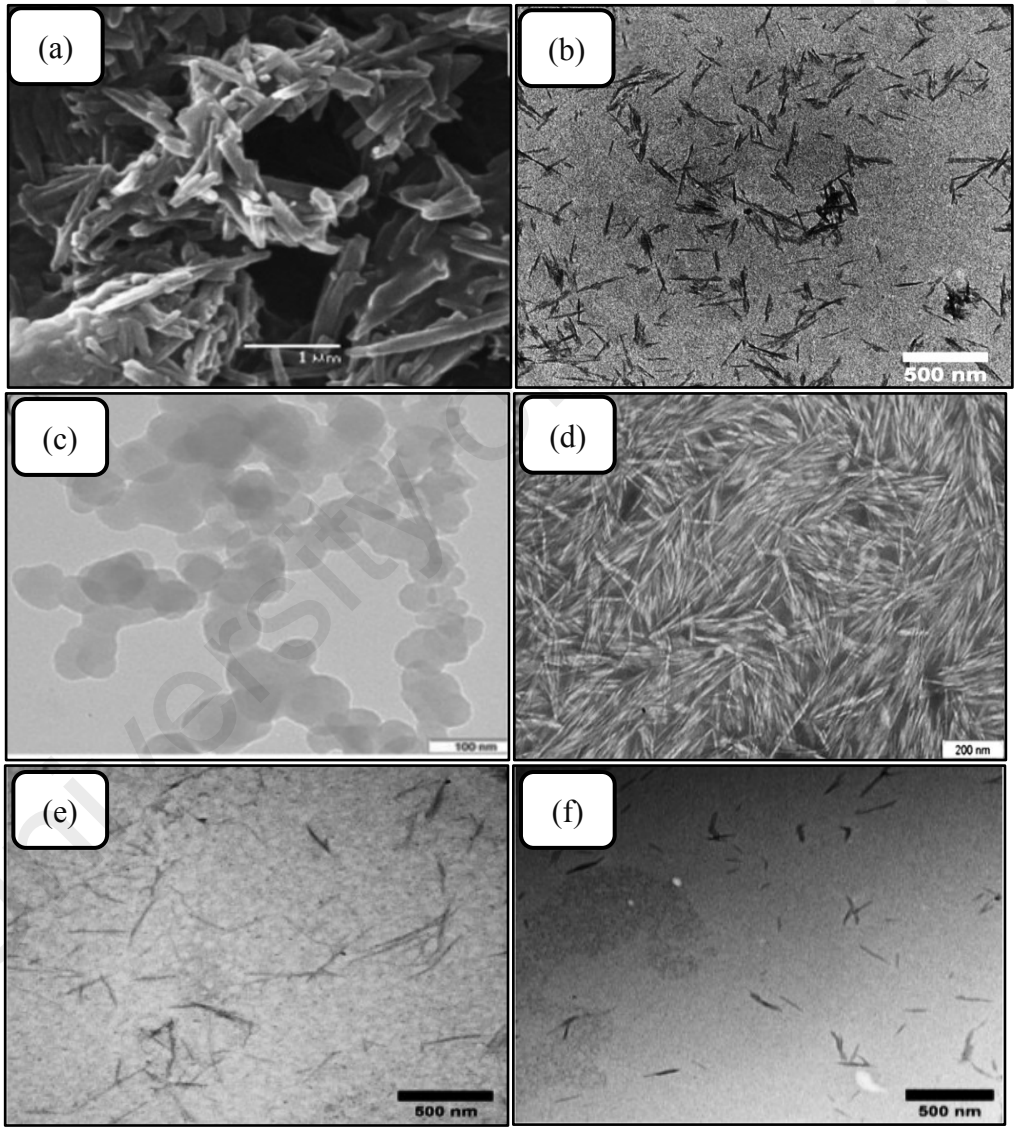

Figure 2.1: Microscopy image of isolated NCC obtained from various sources. (a) orange waste (Tsukamoto, Durán, & Tasic, 2013); (b) bleached softwood (Sacui et al., 2014); (c) grape skin; (d) rice straw (Hsieh, 2013); (e) potato peel; (f) cotton (Chen et al., 2012); (g) oil palm trunk (Lamaming et al., 2015); (h) birch (*Betula pendula*) (B. Li et al., 2015); (i) mengkuang leaves (Sheltami et al., 2012); (j) old corrugated container (Tang et al., 2015); (k) *Agave angustifolia* (Rosli, Ahmad, & Abdullah, 2013); (l) oil palm empty fruit bunch (Al-Dulaimi & Wanrosli, 2016).

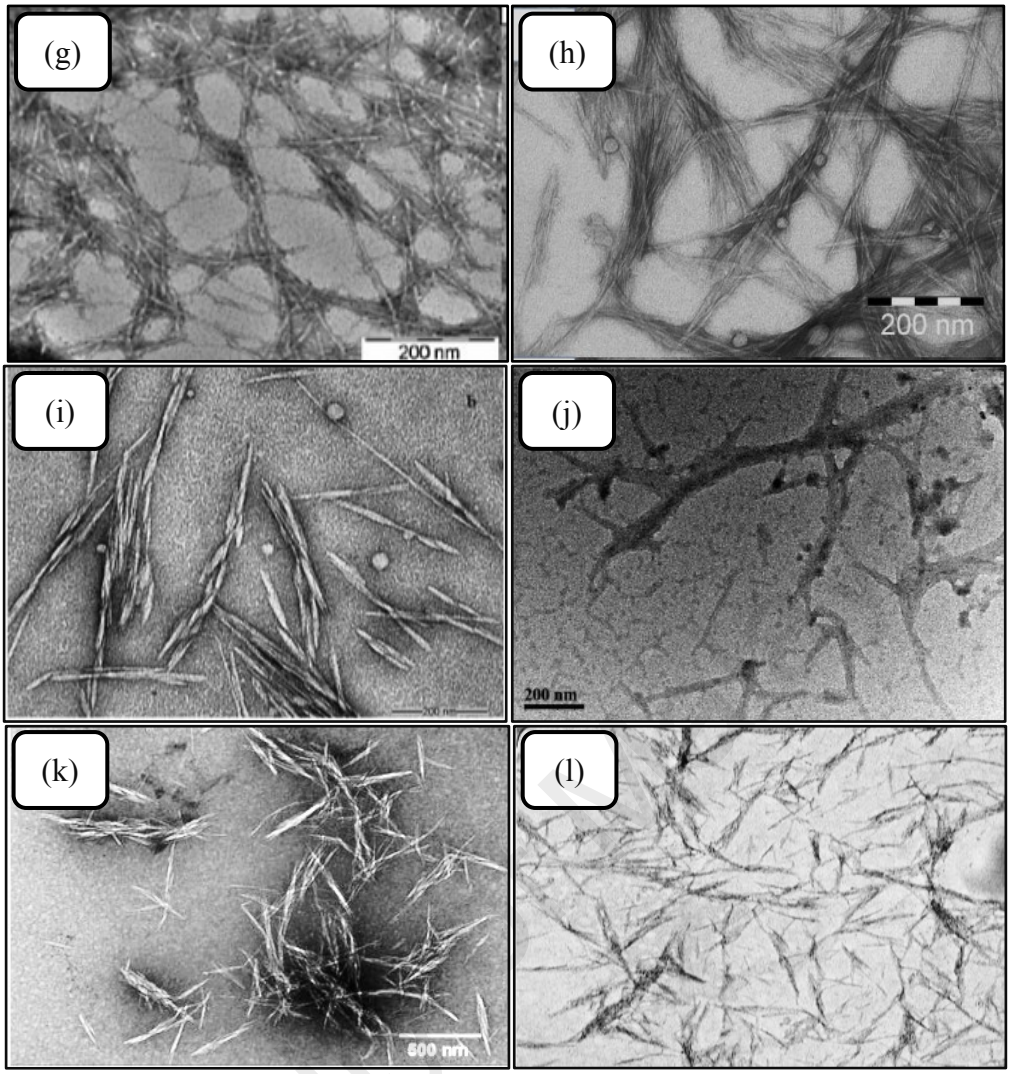

Figure 2.1: Continued.

2.2.2 Nanofibrillated Cellulose (NFC)

In contradiction of cellulose nanocrystals, NFC is long and flexible nano-scaled that composed of more or less individualized cellulose microfibrils. NFC particles are finer cellulose fibrils that can be produced when particular techniques are incorporated to facilitate fibrillation of cellulosic sources in the mechanical refining system (Jonoobi et al., 2015). Generally, these NFC comprise cellulose chains that are tangentially stabilized by dense hydrogen connections between hydroxyl and oxygen groups of adjacent molecules. It is worth mentioning that NFC consists of alternating amorphous and crystalline regions which normally rendered the diameter of varies from 2–20 nm in diameter and up to several microns in length.

There are several isolation methods to obtain NFC including microfluidization, grinding, refining, high-pressure homogenization, high-intensity sonication and cryocrushing with liquid nitrogen. However, the processes requires high energy consumption during the disintegration process with mainly batch processes, resulting in the micro- and nano-scale bundles of microfibrils are obtained most of the time instead of individual microfibrils (García et al., 2016). Due to these reasons, enzymatic and chemical pretreatment has been proposed prior to/after mechanical processes in order to promote the increase the inner surface, accessibility of hydroxyl groups, break down the cellulose hydrogen bonds, alter the cellulose crystallinity and thus, boost the reactivity of the fibers (Khalil et al., 2014). Regarding the chemical pretreatment, the TEMPO-mediated process has been proposed to oxidize the cellulose fibers. By this process, certain repulsive charges are induced on the fiber to make the subsequent fibrillation much easier, and therefore significantly reduce the energy input (Charreau, L Foresti, & Vazquez, 2013). In fact, the TEMPO treatment is an effective chemical process applied in order to minimize the energy consumption during the mechanical process. Liimatainen's group reported that TEMPO-mediated NFC produced able to achieve very good mechanical properties in produced films (8% strain at break, 220 MPa tensile stress and 12 GPa of tensile modulus) due to its high aspect ratio that contributed by more intermolecular hydrogen bonding and network structure (Liimatainen et al., 2013).

Compared to that of chemical pretreatment, the use of enzymatic hydrolysis has been proposed as an interesting way to decrease the NFC processing cost with the advantageous of environmentally-friendly to the biological system. In fact, the combination of enzymatic hydrolysis and mechanical process is able to lower the number of passes required through the homogenizer. Besides that, it is believed that enzymes preferably attack the amorphous regions in the cellulosic substrate and the

process is able to conduct at room temperature. The combination of mechanical shearing and enzymatic hydrolysis is an effective way to produce NFC with controlled nano-dimensional morphology with high aspect ratio (even up to 250) by preserving the junction sites of the network (García et al., 2016). However, the final properties of NFC are significantly affected by the type of enzymes used and contrary to NCC, NFC is more process-dependent than that of raw material source-sensitive (Siqueira, Bras, & Dufresne, 2010). This proves that the selected mechanical process and pretreatment is the main factors that determine the NFC main properties, so the variability of the source is less important than for NCC.

In most of the studies, the isolation of NFC are done by mechanical disintegration without any pretreatment, therefore the energy consumption for overall process is tremendously high (Spence et al., 2011). According to Siro and Plackett's study, it is possible to reduce the energy demand of mechanical processes from relatively high (20,000–30,000 kWh/ton or higher values to approximately 1,000 kWh/ton) (Siró & Plackett, 2010). **Figure 2.2** illustrates the morphological structure of NFC that obtained from respective sources, viewed under the electron microscope.

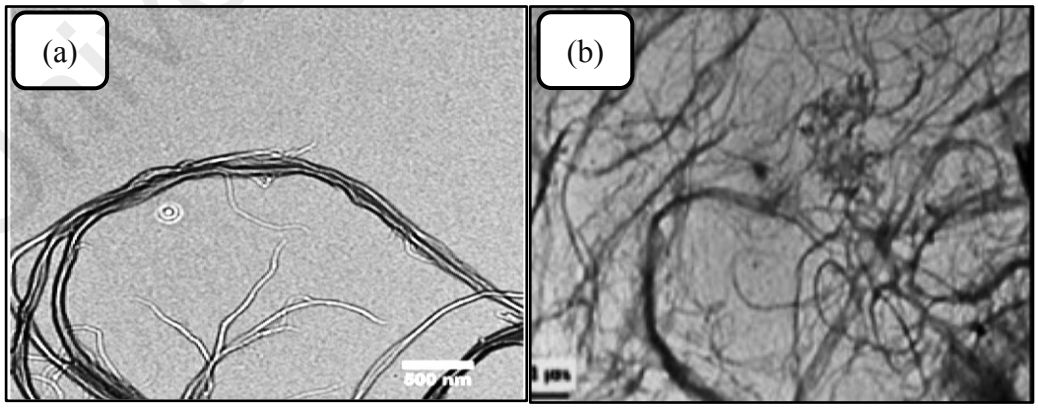

Figure 2.2: Morphological appearance of NFC isolated from (a) bleached softwood (Sacui et al., 2014); (b) bagasse; (c) rice straw (Hassan et al., 2012); (d) banana rachis (Khawas & Deka, 2016); (e) hemp (Pacaphol & Aht-Ong, 2017); (f) kenaf (Jonoobi et al., 2010).

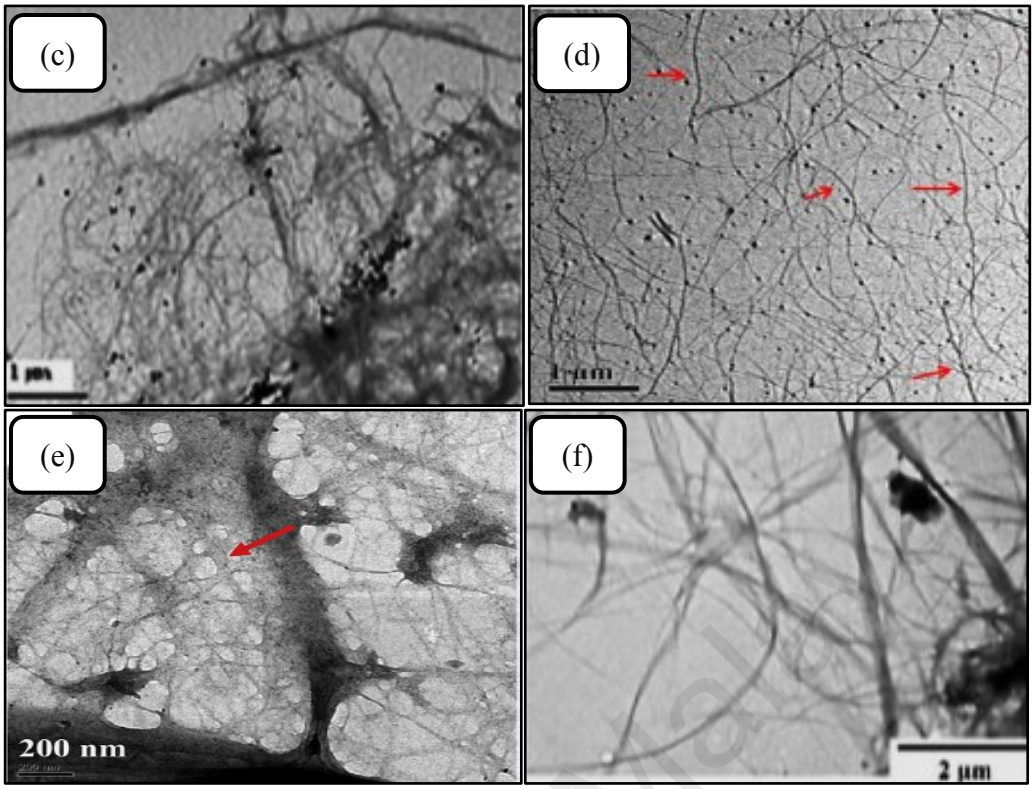

Figure 2.2: Continued.

2.2.3 Bacterial Nanocellulose (BNC)

The last type of nanocellulose that will be discussed is the bacterial nanocellulose (BNC), which is synthesized from special bacteria that build up cellulose fibers with nanosized in diameter and up to micrometer size in length via the bottom-up method. The bacteria produce BNC by manufacturing cellulose and building up bundles of microfibrils. Contrary to NFC and NCC materials isolated from lignocellulosic cellulose sources, BNC is formed as a nanomaterial and polymer by biotechnological assembly processes from low molecular weight sugars or other carbon sources, for instance, D-glucose. Although the produced BNC is identical to nanocellulose isolated from plant origin in terms of molecular formula, bacterial cellulose is quite different.

The BNC offers some excellent chemical, physical and mechanical properties such as high crystallinity (70–90%), extremely pure (with no accompanying substances like

lignin, hemicelluloses, or pectin), fine fiber network structure, good mechanical properties (*i.e.* high tensile strength), biocompatibility, high water holding capacity (up to 200 times of its dry mass), and high degree of polymerization (values up to 8000) (Siró & Plackett, 2010). Due to its relatively pure cellulose membrane, thus no chemical pretreatments are necessary with the purpose of removing non-cellulosic components before undergoes hydrolysis process, as is the case for lignocellulosic biomass cellulose. Owing to these unique characteristics, recent studies have highlighted the potential of BNC in various fields, including surgical and medical health areas such as bandages for skin burn or wound healing and as a substitute for medical materials such as blood vessels (Siró & Plackett, 2010). Some disadvantages with BNC are the inefficient process in synthesizing bacteria cellulose, low availability of the bacterial cellulose and high production costs, which makes it hard to make BNC commercially attractive. Thus, further process development would be requested for large scale production bacteria cellulose in order to the commercialization of BNC. Many researchers isolated NCC from various sources, and they studied the size and morphology of the obtained nanocrystals by microscopes (**Figure 2.3**).

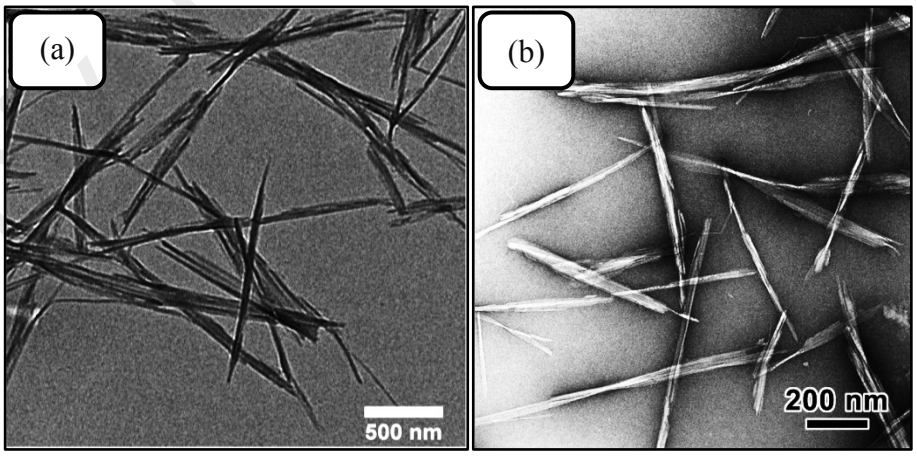

Figure 2.3: Microstructure images of BNC from (a) *Acetobacter xylinum* (Sacui et al., 2014); (b) *Gluconacetobacter xylinus*; (c) *Glaucocystis*; (d) *Halocynthia papillosa* (Kaushik et al., 2015); (e) *Gluconacetobacter* (Klemm et al., 2011) and (f) *Acetobacter xylinum* (Taokaew et al., 2013).

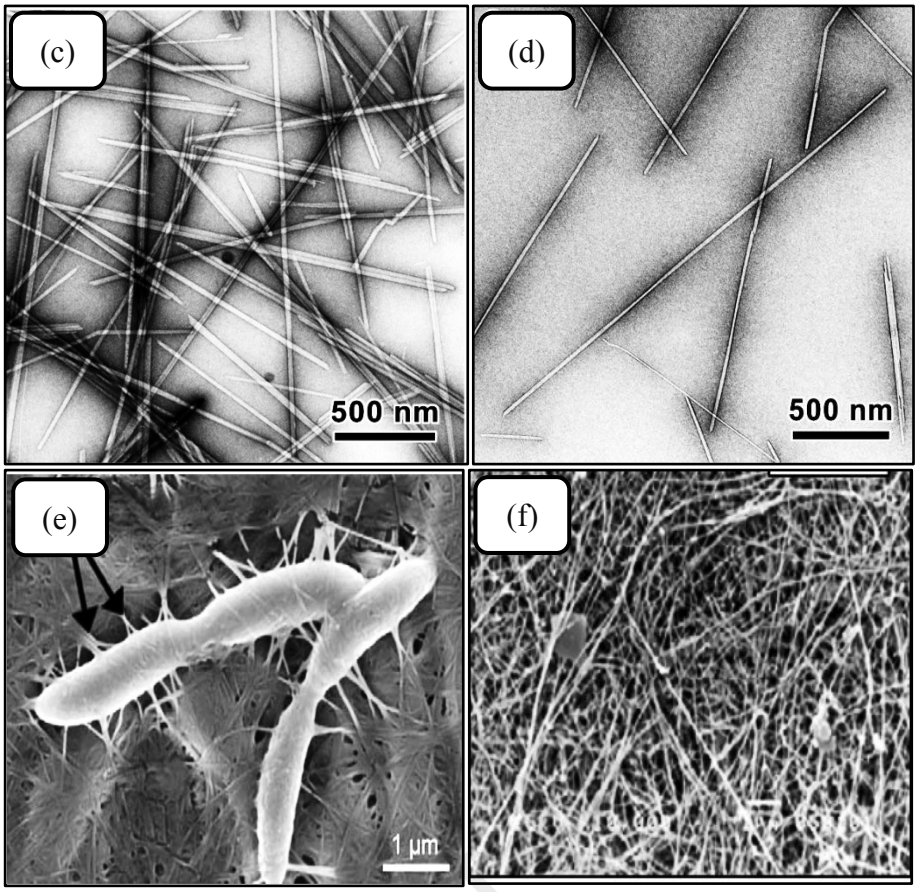

Figure 2.3: Continued.

2.3 Pretreatment of Lignocellulosic Biomass

As discussed earlier, the cellulose contents are normally embedded by the lignin and hemicellulose matrix via physically and chemically linkages to form a cellulose-hemicellulose-lignin complex. Therefore, a pretreatment stage must be implemented to solubilize the hemicellulose, and thus increase the mass fraction of cellulose content in the biomass. It is an important process to increase the porosity and accessibility of cellulose toward the hydrolyzing catalyst attacks during the depolymerization process for the further bioconversion process (Medina et al., 2016). Thus, the main objective of the pretreatment is to remove as much lignin and hemicellulose as much as possible, while simultaneously keeping the cellulose intact and unaltered for subsequent refinery process (Lee, Hamid, & Zain, 2014).

Generally, the isolation of NCC from lignocellulosic biomass occurs in two stages. The first stage is purification and homogenization pretreatment of the source material so that it can react more consistently in subsequent treatments. The particular pretreatment is significantly dependent on the cellulose source material and the desired morphology of the starting cellulose material for the second stage treatments. For pretreatments of plants and wood, it involves the partial or complete removal of matrix materials (lignin, hemicellulose, pectin, *etc*.) and the isolation of individual cellulosic fibers. On the other hand, the pretreatment of tunicate includes the separation of the mantel from the animal source and the isolation of purified cellulose fibrils by removing the protein matrix. For algal cellulose sources, it is typically involve culturing methods, followed by the purifying steps in order to remove the algal wall matrix material. In addition, pretreatment of bacterial cellulose is mainly emphasis on its culturing methods for the growth of cellulose microfibrillar, and subsequently, the washing process is applied to remove the bacteria and other media.

An effective isolation pretreatment is essential to be conducted prior to isolating the high-valuable cellulosic material from the complicated biomass matrix. In order to achieve this, the recalcitrant nature of the lignocellulosic components originating from the biomass must be removed (Medina et al., 2016). In nature, the cellulose contents are normally embedded by the lignin and hemicellulose matrix via physical and chemical linkages to form a cellulose-hemicellulose-lignin complex. Therefore, a pretreatment stage must be implemented to solubilize the lignin and hemicellulose, and thus increase the mass fraction of cellulose content in the biomass. It is an important process to increase the porosity and accessibility of cellulose toward the hydrolyzing catalysts attacks during the acid hydrolysis process for nanocellulose production.

To isolate the cellulosic material from various lignocellulosic biomasses, a series of multiple chemical procedures, namely alkalization treatment, chlorite-bleaching and acid hydrolysis process is the most effective way (Ching & Ng, 2014; Rosa et al., 2010; Sheltami et al., 2012). The purposes of multiple pretreatment steps are to degrade or/and disrupt the hemicellulose and the lignin structure in the biomass, and thereby maximize the accessibility of cellulose during the depolymerization process to produce nanocellulose from micro-sized cellulose. As compared with hemicellulose, the main obstacle in the cellulose isolation process is the presence of complicated lignin complex structure which acts as a protective layer that restricts or minimizes the chemical hydrolysis occurred in the cellulose matrix. This is because most of the hemicellulose can be readily hydrolyzed in water-soluble compounds under milder reaction conditions such as dilute acid; however, more extreme and harsh conditions (*i.e.* high pressure and reaction temperature) are required in order to break down or solubilize the complex lignin structure (Lee, Hamid, & Zain, 2014). Therefore, an effective delignification process by chemical bleaching treatment is a significant step for destroying and removing the lignin in the treated fiber.

Previously, the chemical bleaching process used a large amount of chlorine and chlorite-based chemicals, namely sodium chlorite ($NaClO_2$) to degrade the lignin structure and leave the holocellulose matrix (Ching & Ng, 2014). However, such chemicals lead to negative impacts on the environment by the emancipation of toxic and chlorinated polluting organic products (e.g. chlorinated dioxins) in the biological systems during the pulping process (Saelee et al., 2016). Chlorite (ClO_2) might generate a chlorine radical (Cl•), which reacts and fragments the lignocellulose biomass into highly toxic organochlorine; causing the heavy burden on the surrounding environment. Due to the increasing concern about environmental impact issues within the society, the

demand for the chlorite-free bleaching agent such as hydrogen peroxide (H_2O_2) has increased gradually due to its positive effect on delignification process and more greenery to the environment (Li et al., 2011). Also, the eco-friendly and biodegradable nature of H_2O_2 has begun to replace environmental polluting chlorine-based bleaching agents, which have been used for many decades. In addition, H_2O_2 will not leave any residues on the treated fiber after the bleaching process as H_2O_2 will be degraded into hydrogen and oxygen once the reaction is completed; it poses little danger to the ecosystem (Bensah & Mensah, 2013). According to Goh's finding (Goh et al., 2016), H_2O_2 was capable of penetrating the amorphous domains as well as performing the decolorization of the lignocellulosic biomasses. On the other hand, the alkaline reagents (i.e. NaOH, KOH) are inexpensive, however, the neutralization process utilizes a huge amount of water in order to remove the linked Na–ions, which are strongly incorporated into the biomass (Fiber —OH + NaOH → Fiber —O^-Na^+ + H_2O) and are difficult to be eliminated. Furthermore, the formation of salts upon neutralization of alkalized wastewater may present challenges with disposal.

The second stage is a controlled chemical treatment which involves the separation of the purified cellulose into their crystalline or microfibrillar structure via hydrolysis by removing the amorphous zones of the cellulose. There are several methodologies for isolating the cellulose particles and have been previously reviewed. Basically, the three isolation methods are chemical hydrolysis, mechanical treatment, and enzymatic hydrolysis. In practice, several of these methods can be used in sequence or in combination to obtain the desired nanoparticle morphology. **Section 2.4** will briefly review the most common employed techniques for producing cellulose nanomaterial.

2.4 Potential Hydrolysis Technologies for Isolating Nanocellulose

It is a recognized fact that depolymerization of cellulose into its nano-dimension is generally difficult under mild hydrolysis conditions attributed to the stiff structure and extensive network of intra and intermolecular hydrogen bonding in cellulose (Yuan et al., 2015). The recalcitrance nature of crystalline cellulose to hydrolysis caused the depolymerization process often required harsh conditions such as the use of intensive mechanical treatments, highly concentrated acids, high temperature and pressurized systems are required to break down the strong bonding system in order to open up its structure to expose the reactive groups. These appeared as major difficulty for its further exploitation. Lately, there are a number of existing techniques for producing the nanocellulose, either from the raw materials such as annual plant or other model compounds including filter papers and microcrystalline cellulose.

2.4.1 Mechanical Disintegration

A number of mechanical processes have been used to produce cellulose fibrils from various cellulosic materials. These processes include mainly high-pressure homogenization, high-intensity ultrasonication, microfluidization, cryocrushing and grinding which produce the high shear gradients causing transverse cleavage along the longitudinal axis of the cellulose microfibrillar structure (Qing et al., 2013). As a result, these processes tend to damage the microfibril structure of cellulose by reducing its degree of crystallinity and molar mass to produce long cellulose fibrils. Depending on the types of mechanical treatment and mechanical force levels, interfibrillar hydrogen bonding is broken into a different degree (Wang, Zhao, & Zhu, 2014). The concept of producing nanosized cellulose fibrils from softwood pulps was first introduced by Herrick et al. and Turbak et al. in 1983. This treatment brings about irreversible changes

in the dimensions of fibers by increasing their bonding potential as well as modifying their size and morphology (Moon et al., 2011).

2.4.1.1 High-Pressure Homogenization

Typically, high-pressure homogenization is one of the most promising techniques for mechanical treatment to produce mainly NFC. The impact of the shear forces, as well as the high pressure and velocity produced on fluid generate shear rates in the stream so that it is able to decrease the size of fibers into its nano-dimension (Frone, Panaitescu, & Donescu, 2011). Many researchers reported that this process has been used as an efficient strategy to break up the cellulosic fibers into the nanoscale, which often in combination with other treatments. During homogenization, the dilute refined cellulose fibers (2–7% w/v) are passing through a spring-loaded valve assembly at low velocity, high pressure (8000 psi) and exposed to a pressure drop to atmospheric conditions while the valve closes and opens in a cyclic motion with rapid succession. This result in high impacting and shearing forces produced in a small valve gap maintained at a temperature within 70–80 °C. This combination of forces promotes the high degree of microfibrillation, resulting in the formation of NFC (Chaker et al., 2014).

In general, this method produces NFC with the diameters between 20–100 nm and the lengths of several tens of micrometers without the presence of any organic solvents. During the high temperature and pressurized system, the carbohydrate linkage of the cellulose polymers is subjected to break down and shorter cellulose fractions are released. Despite its efficiency, several problems are encountered such as high energy consumption, clogging of the homogenizer due to smaller diameter size of the orifice, mechanical damage of the crystalline microfibril structure (J. Li et al., 2012). Hence, the fibers required being diminished in advance before subjected to homogenization to

avoid the clogging issue. Besides that, the homogenization process leads to decreases in crystallinity of NFC by increasing the number of passes. This is unpreventable as the homogenization procedure is normally required to be repeated for several times in order to increase the degree of fibrillation or else insufficient disintegration of the pulp fibers (Rebouillat & Pla, 2013). After each path, the cellulose fibers become smaller and more uniform in diameter. It was reported that the number of cycles for producing NFC is varied from 10–15 cycles with high pressure of 30–50 MPa (Khalil et al., 2014).

2.4.1.2 High-Intensity Ultrasonication

It is a mechanical process in which oscillating power is used to prepare NFC via the hydrodynamic forces of ultrasound (He et al., 2014). During the treatment, the cavitation leads to the development of powerful mechanical oscillating power, and thus high intensive waves, which comprises of formation, expansion and implosion of microscopic gas bubbles when these molecules absorb ultrasonic energy. This eventually results in the breaking of cellulose fiber into a smaller dimension. High-intensity ultrasonic treatments normally have been reported to yield less fibrillar, shorter nanocellulose particles in some cases, and yet thin whiskers could be obtained by sonication. In fact, higher temperature and power leads to higher fibrillation, while longer fibers come from lower fibrillation. However, a large distance from the probe to a beaker and a large feed concentration is not advantageous for fibrillation. A typical ultrasonication treatment requires high temperatures, a cylindrical titanium alloy probe tip of 1.5 cm in diameter, 1000 W power, and 20–25 kHz for about 30 min (W. Chen, Yu, Liu, Hai, et al., 2011). Different types of equipment such as the ultrafine grinder and microfluidizer appear to be alternatives to the use of the high-intensity homogenizer as grinding and microfluidization processes are reported to need less energy as compared with homogenization (Spence et al., 2011).

2.4.1.3 Grinding

Cellulose fibers can be fibrillated from a cellulose suspension by passing through an ultrafine grinder (or commercial grinder) where the lower grinding stone is rotating at high speed to avoid the grinder blocking (1400–1500 rpm) and the upper stone is static. In this process, the cell wall structure of cellulose is broken down by the shear forces generating a gel form nanosized individualized fibers due to the heat produced by friction while evaporating the excess water (Rebouillat & Pla, 2013). However, similarly to the high-pressure homogenization process, mechanical damage of the fibers might occur during the grinding process. Compression is a type of modified grinding system by which the highly purified cellulosic fibers are placed in a bed of strips that placed between two plates and subjected to a constant load about 10 tons for several seconds. Unfortunately, such process is only able to obtain micrometer fibers rather in the nanometer size range. It suggested that the increase in the number of cycles or passes by grinding were practically decreased the crystallinity, size, degree of polymerization as well as reduced the strength and failure strain of the NFC (Karande et al., 2011). This might be attributed to the breakage of hydrogen bonding within the crystalline regions of the cellulose matrix after the intensive mechanical actions. These authors also reported that the combination of shear and frictional forces provide the defibrillation effects on the fiber surface by abrasive action.

2.4.1.4 Cryocrushing

Cryocrushing is an alternative defibrillation technique for producing nanofibers by the presence of liquid nitrogen and high shear forces. In this process, the water-swollen cellulosic fibers are immersed into liquid nitrogen in order to freeze it. After that, these brittle frozen fibers are crushed by high impact and shear forces. It is suggested that pressure applied by crushing of ice crystals on the cell walls is the main reason for the

collapse of cellulosic structure and causing them to rupture, thus liberating the microfibrils. The brittle fracture of NFC produced in this process is made possible by the intense freezing, making it brittleness by combining with intense mechanical forces. The cryocrushing treated fibers may then be dispersed uniformly in the water suspension by a disintegrator before the high-pressure fibrillation. This treatment sequence is applicable to different cellulosic materials, and the NFC obtained normally having the diameter ranges of 5–80 nm and the length up to several thousand nanometers (Rebouillat & Pla, 2013).

2.4.1.5 Microfluidization

Similar to homogenization, microfluidization also involves an integrated pressurized system which allows the defibrillation of cellulosic pulps. The fiber suspension is pumped through a thin Z-shaped chamber under very high pressure (up to 30000 psi). The cellulose slurry is accelerated and lead to the interaction chamber where it passes through geometrically fixed microchannel at high velocities. Within the chamber, impact and shear forces are generated for defibrillation of cellulosic fibers due to the interaction between colliding streams and channel walls (Qua et al., 2011). In fact, the thin Z-shaped chambers with dissimilar sizes produce high impact forces and shear rate against colliding streams. It is noticeable that in this process, the repetition of the procedure is also required in order to increase the degree of fibrillation. Generally, the mechanical process can generate the fine fibrils of less than 100 nm in diameter and several micrometers in length. Some studies found that after 10–15 times of passing the material through the equipment, the aspect ratio (L/d) of the NFC fiber bundles increased, whereas the additional passes caused the agglomeration of cellulose fibrils due to the increase in surface area, and thus, a higher concentration of hydroxyl groups (O–H) was found (Pacaphol & Aht-Ong, 2017).

All of the above-listed mechanical defibrillation processes involve high production costs (materials and tools), less efficient and high consumption of energy (20,000–30,000 kWh/ton), which prevents their successful commercialization and becomes less favorable for industries (J. Li et al., 2012). Also, these treatments cause a dramatic decrease in both the fibril length and product yield. Moreover, monitoring and a higher number of cycles which usually consists of several paths via the disintegration device are practically important for producing NFC. For microfluidization and homogenization, the most critical issue is primarily associated with the easily clogging of fiber suspensions within the reaction chamber. Therefore, the current research has mainly focused on the high efficiency, environmental conservative and low costs methods to isolate nanocellulose. The pretreatment or post-treatment of cellulose or a combination of two or more methods have been proved to produce positive results regarding this issue. In summary, microfluidization and homogenization adopted with high-pressure system are able to produce high impact and shear force to form homogeneous size distribution of NFC with the smaller width (Spence et al., 2011). Inversely, grinding and refining process defibrillate the cellulose fibers by abrasive actions in which the heat is produced as the frictional forces for the fibrillar repulsion (Siró & Plackett, 2010). Thus, different mechanical treatments have dissimilar shear mechanisms and varied intensity of shear forces, resulting in the different effects on the characteristics of yielded NFC (crystallinity, size, and degree of polymerization) (Qing et al., 2013).

2.4.2 Enzymatic Hydrolysis

Based on the works of literature, biological treatment (*i.e.* enzymatic hydrolysis) has been proved its effectiveness in the production of nanocellulose (Duran et al., 2011). Similar to acid hydrolysis, the treatment used to obtain the NFC is based on the

enzymatic attack of amorphous areas of the cellulose substrate, while maintaining the crystalline zones. Contrary to chemical treatment, however, it is much more benign from the environment point of view. In this process, the enzyme is used to degrade or modify the hemicellulose and lignin, while preventing the cellulose regions unaltered. This enzyme is produced by cellobiohydrolases, which are A- and B-type cellulases that able to attack the crystalline zones of cellulose. On the other hand, endoglucanases C- and D-type are capable of degrading the amorphous regions (disordered structure) of cellulose (Anderson et al., 2014). Endoglucanases and cellobiohydrolases have strong synergistic effects and therefore, the pretreated fibers subjected to the lowest concentration of enzyme (0.02%) collapsed, while the fiber length and molecular weight are preserved. Exoglucanases plays role in attacking the terminal glycosidic bonds, while endoglucanases mainly focus in the cleavage of the noncovalent internal bonds (non-covalent interaction) to release shorter cellulose chains (Satyamurthy et al., 2011). This ease the further breakdown of glycosidic linkages of shorter chains by betaglucosidases or cellobiases into nanocellulose in which defibrillation apparently occurred (Lee, Hamid, & Zain, 2014). Furthermore, *A. xylinum* and *Trichoderma reesei* produce enzymes that can be used to reduce the size of MCC.

In detail, the enzymatic hydrolysis of cellulose is a multistep procedure process in which the cellulase enzyme is initially adsorbed onto the surface of cellulose. Afterward, the cellulose is breakdown into multiple components via the synergistic action of cellulase. This is because a single enzyme alone is impossible to destroy the cellulosic fiber due to the complex structure of cellulose as well as the presence of different organic compounds within the matrix. Finally, desorption of cellulase from the cellulosic residue renders its release into the supernatant. In order to improve the efficiency of enzymatic hydrolysis, it is usually carried out in combination with acid

hydrolysis or mechanical shearing. During the mechanical process, the NFC is defibrillated by frictional and shearing forces to break down the tight packing structure of cellulose within the crystalline regions. By doing so, it can eventually increase the exposure of cellulose surface area which can more accessible for the adsorption of cellulose enzyme for further hydrolysis. Basically, the rate of enzymatic hydrolysis is relatively slow. Studies found that the significant enzymatic activity is only noticeable after at least 7 to 14 days of incubation. This confirmed that the hydrolysis conditions catalyzed by enzymes are milder than chemical and mechanical routes. The dimension of yielded nanocellulose is reduced as the process time progressed due to the continued hydrolysis catalyzed by the specific enzymes used. A study conducted by (P Satyamurthy & Vigneshwaran, 2013) suggested that the steady reduction in the degree of polymerization of nanocellulose was only able to achieve over the period of 15 days, and the crystallinity of nanocellulose was significant increased to 81% compared to that of 69% of native cellulose. This indicated that the preferential hydrolysis of the amorphous zones of cellulose done by cellulase enzymes. The advantageous of enzyme-induce hydrolysis are potentially higher nanocellulose yield and larger aspect ratio due to its higher selectivity than chemical process (Siddiqui et al., 2011). This technique is beneficial in terms of more environmentally benign and lower energy costs. Regrettably, such process is impeded by several drawbacks such as economical aspect related to the costly cellulase enzyme, long processing period required for a successful cellulose degradation or satisfied conversion (rate limiting step) and the tedious isolation process of the enzymes (Kalia et al., 2014). These issues remain its primary hurdle from commercialization of nanocellulose production even if this process offers numbers of potential benefits (Lee, Hamid, & Zain, 2014).

2.4.3 Chemical Pretreatment

As pointed above, lignin and hemicellulose are the main components of the lignocellulosic biomass. Therefore, removal of hemicellulose and delignification process is carried out as the preliminary step for extracting nanocellulose. An intermediate source like MCC can be a good raw material to prepare NFC or NCC. This can be done by acid hydrolysis, ionic liquids, and TEMPO-oxidation treatment. For acid hydrolysis, it will selectively hydrolyze the cellulose amorphous zones and yield sulfated NCC suspension. During the dissolution, the cellulose fibers are swollen which made it much easier to isolate the crystallite segments from the matrix. On the other hand, ionic liquids are a green solvent which can effectively dissolve cellulose effectively in an eco-friendly way. In TEMPO-mediated oxidation, mild hydrolysis conditions are used to extract nanocellulose which having the width of 3–4 nm with the length of few microns by using 2,2,6,6-tetramethylpiperidine-1-oxyl radical. After the oxidation process, the original fibrous morphology of native cellulose is remained unchanged, only selective surface modification of crystalline cellulose microfibrils are takes place. Each and every procedure has its own merits and demerits; the selection of treatment depends on its demand and potential application to be explored.

2.4.3.1 Acid Hydrolysis

The main process for the isolation of nanocellulose is strong acid hydrolysis which promotes the dissolution of the amorphous regions of the cellulose matrix. In this process, the more accessible, disordered domains (amorphous regions) are preferentially hydrolyzed, whereas the crystalline regions remain undamaged under the acid attack. Since the non-crystalline regions act as structural defects in the cellulose matrix, it is responsible for the transverse cleavage of the long polymeric chains into short size under acidic hydrolysis to produce nanocellulose (Dufresne & Belgacem, 2013).

In the initial stage of the acid hydrolysis, the acid diffuses into the amorphous regions of the cellulose matrix and break down the glycosidic bonds. This phenomenon occurs because of the higher resistance to acid attack in the crystalline regions than those in the amorphous regions. Therefore, the amorphous regions would be first hydrolyzed. After that, the hydrolysis occurs at the reducing end group as well as the surface of cellulose fiber. The hydrolysis of reducing end groups will make the nanocellulose becomes charged, depending on what type of acid used. Generally, several parameters such as reaction temperature, hydrolysis temperature, and acid concentration are some of the most important factors to be controlled for the nanocellulose production. Too long reaction time will hydrolyze the cellulose crystals completely while too short reaction time will produce large undispersed fibers that give a high degree of polymerization. On the other hand, the reaction time and temperature correlate to each other in which a higher hydrolysis temperature will shorten the reaction time or vice versa. Not only temperature and time will affect the properties of nanocellulose, but also the solid-liquid ratio and acid concentration (Lee, Hamid, & Zain, 2014). After the hydrolysis and purification via dialysis, the small crystalline rod-like nanoparticles will be obtained in an aqueous suspension.

The differences in the kinetics of hydrolysis reaction between the crystalline and amorphous regions are able to produce the nanocellulose with high crystallinity (George & Sabapathi, 2015). Acid hydrolysis of cellulosic feedstocks induces a rapid reduction in its degree of polymerization value and therefore leads to the formation of nanoscale particles through the decrement in the cellulose chains size. Acid hydrolysis has been commonly used to extract the crystalline nanoparticles from a variety of lignocellulosic sources, including sugarcane, wood, coconut, etc. However, the isolation of nanocellulose from raw biomass involves a series of pretreatments in order to

selectively remove the hemicellulose and lignin from the fiber by chemical, thermal, physical and biological methods, or by a combination of these methods (dos Santos et al., 2016). Therefore, many researchers have isolated nanocellulose from commercial MCC. When using MCC, many pretreatment processes can be omitted; the process of manufacturing nanocellulose begins with the hydrolysis process.

In order to perform acid hydrolysis, the cellulosic source is mixed into the deionized water with a given concentration of acid. After the addition of acid, the resulting mixture is subjected to strictly control operational conditions of time, temperature, and agitation. Once the reaction completed, the produced suspension is necessary to undergo several separation steps, including filtration or centrifugation and washing or rinsing steps. The last washing step is done by a dialysis against deionized water in order to remove the neutralized salts and remaining acid. Besides that, ultrasonic treatments can be applied to facilitate the dispersion of nanocellulose in suspension form. To obtain powdered nanocellulose, the suspension can be freeze-dried after the dialysis process. Sulfuric acid (H_2SO_4) is the most common acid catalyst for preparing the nanocellulose through chemical hydrolysis. Depending on the operational conditions, the hydrolysis may also occur in the crystalline zones and some of the hydroxyl groups on the fiber surface will convert into sulfate groups (cellulose–OH to cellulose–$OSO_3^-H^+$). Other side reactions such as oxidation and dehydration are also possible during acid hydrolysis (Hamad & Hu, 2010). During the acid hydrolysis, the amorphous regions will be removed; this results in the increment of nanocellulose crystallinity as well as its insolubility against water as the crystalline parts are less accessible (Hamad & Hu, 2010).

There are some other liquid acids besides H_2SO_4 that can be used for the hydrolysis of cellulose material into its nano-dimensional, such as hydrochloric (HCl), phosphoric (H_3PO_4), nitric (HNO_3) and hydrobromic (HBr) acid. When compared to H_2SO_4, HCl and HBr hydrolysis will not introduce any charged groups on the cellulose crystal surface. This is beneficial for the study of enzymatic degradation as the surface groups can hinder the substrate recognition by the enzymes. However, the nanocellulose prepared by these processes will not form a stable colloidal dispersion. Similarity, HNO_3 is expensive compared to H_2SO_4 (Bensah & Mensah, 2013). Thus, sulfuric acid is a more suitable choice of the acid catalyst compared to other liquid acids due to its economically beneficial (Wittcoff, Reuben, & Plotkin, 2012).

In spite of its effectiveness in the production of nanocellulose, acid hydrolysis still remains several critical drawbacks such as excessive usage of concentrated acid, high toxicity and corrosive. In this case, a huge amount of acidic waste will be generated after the hydrolysis process; therefore, proper disposal and waste management are required. Besides that, the hazardous acid waste is highly toxic and corrosive that will eventually cause severe environmental issue and special synthesis reactor with anti-corrosive coating needs to be established. These drawbacks make the production cost becomes relatively expensive. Also, the acid waste is difficult to be regenerated and recovered after the hydrolysis, manifesting that the acid hydrolysis process is economically infeasible. Low product yield is another problem when using acid hydrolysis method for producing the nanocellulose. This is reasonably due to uncontrollable hydrolysis under harsh condition (*i.e.* high temperature and concentrated acid system) would lead to over degradation of cellulose into water soluble reducing sugars and other undesirable side products (Brinchi et al., 2013). Therefore, extra care

and strictly controlled of acid hydrolysis conditions are demanding to manufacture desirable nanocellulose.

2.4.3.2 Ionic Liquids

Ionic liquids are organic salts with the melting point below 100 °C, no flammability, high thermal and chemical stability, no corrosive properties, negligible vapor pressure, low viscosities, high solvency power to dissolve various inorganic and organic substances and low vapor pressure. Ionic liquids play a dual role in the preparation of nanocellulose: (i) dissolve the cellulose; and (ii) initiate re-precipitation of cellulose with the different type of particle morphologies in the presence of co-solvent (Tian et al., 2014). As a matter of principle, ionic liquids have been characterized as promising "green solvent" in literature which can function as an alternative source to replace typical volatile organic solvents (Hu et al., 2013). The cations of ionic liquids are normally containing a cyclic or aromatic structure and long alkyl chain. These common cations are including alkylpyridinium, alkylimidazolium, and quaternary ammonium based, whereas the anions of ionic liquids can be varied from acetate, bromide, chloride, formate, hexafluorophosphate, tetrafluoroborate or methanesulfonate (Gericke, Fardim, & Heinze, 2012).

Ionic liquids have been explored to act as a powerful solvent for dissolution of cellulose and hydrolysis owing to their excellent solvency properties and process benefits. In 2002, a breakthrough was made by Swatloski and his co-workers regarding an innovative new approach for cellulose dissolution by using ionic liquids. They were the pioneer discovered that cellulose (up to 10 wt%) could be dissolved by heating (approximately 100 °C) without derivatization using 1-butyl-3-methylimidazolium chloride ([Bmim]Cl) and the regenerated cellulose was found less crystalline (Wang,

Zheng, & Zhang, 2010). The dissolution of cellulose is mainly due to the hydrogen bonding interaction between the anions of ionic liquids and hydroxyl protons of cellulose (Wang, Gurau, & Rogers, 2012). In particular, the solvation of cellulose might be accredited to the coordination of chloride ions with the hydroxyl protons of cellulose; causing the disruption or weaken in the intermolecular hydrogen bonding within and between the adjoining cellulose polymer chains. The formation of new bonds predominantly between C_3 and C_6 hydroxyl groups of neighbored cellulose chains. In summary, the cellulose dissolution can be explained due to the interaction between anions of ionic liquids with the hydroxyl groups of cellulose; however, the cations of ionic liquids might have a minor role.

Although the use of ionic liquids is under consideration for large scale industrial applications, several challenges such as high solvent loading, high solvent cost, high energy consumption for solvent regeneration, technical challenges and inadequate knowledge on the impact of ionic liquids on the ecological system (Mora-Pale et al., 2011). Besides that, the washing of as recycling of ionic liquids as well as regenerated cellulose via reverse osmosis and evaporation is practically costly which presents challenges for the efficient use of ionic liquids.

2.4.3.3 TEMPO-Mediated Oxidation

TEMPO-mediated oxidation (or oxidation synthesis) is a most well-established process to produce nanocellulose using 2,2,6,6- tetramethylpiperidinyl-1-oxyl (TEMPO) radicals under aqueous and mild conditions. During the treatment, the primary hydroxyl group (C_6) is selectively oxidized to a charged carboxylate or aldehyde functional group, whereas the secondary hydroxyl moieties present in the cellulose fibers remain unaltered (Anderson et al., 2014). Therefore, the presence of aldehyde and carboxylate

groups triggered from oxidation imposed a higher density of negatively charged on the surface of treated fiber. This situation could produce sufficient repulsion between the fibrils as well as modify the surface properties of nanocellulose to overcome the strong interfibrillar hydrogen bonds between the cellulose chains (Masruchin et al., 2015). Eventually, the interfibrillar repulsion forces created via TEMPO-oxidation process facilitated the isolation of nanocellulose by inducing the disintegration ad defibrillation of cellulose microfibrils without change its original fibrous morphologies.

The oxidation process of cellulose occurs in the presence of sodium hypochlorite and catalytic amounts of sodium bromide and TEMPO radical as catalyst at the pH 9–11 and room temperature. The by-product of this reaction is only sodium chloride. In this case, the TEMPO-oxidation reaction only occurs at the surface of cellulose fibrils rather than penetrate into the crystallites interior. Thus, this process is highly selective which contributed to the high product yield and rate of reaction (Rattaz et al., 2011). The oxidation synthesis eases the separation of nanofibrils from each other due to introduction of repulsive force of the ionized groups, which is able to overwhelm the hydrogen bonds. Generally, TEMPO treatment is followed by a mechanical process. Regardless of the potential effectiveness of TEMPO oxidation, there are some limitations with respect to high production cost and environmental concerns caused by toxic TEMPO radicals (Brinchi et al., 2013). **Table 2.3** summarizes the comparison of different hydrolysis processes on the properties of yielded nanocellulose.

Table 2.3: Effect of different hydrolysis techniques on the properties of nanocellulose obtained.

Technique	Yield (%)	Crystallinity (%)	Particle size* (nm)	Surface chemistry	Reference
Mechanical	100	52.1	43.1 ± 25.3	Hydroxyl (neutral)	(Liu et al., 2016)
H_2SO_4 hydrolysis	34.5	55.9	5.5 ± 1.9	Sulfate (negative)	(Liu et al., 2016)
HCl hydrolysis	93.7	88.6	255 ± 5	Hydroxyl (neutral)	(Yu et al., 2013)
HBr hydrolysis	70	91	100–400	Hydroxyl (neutral)	(Sadeghifar et al., 2011)
Ionic liquid	48.33	83.42	12–15	Functionalized	(Chowdhury & Hamid, 2016)
TEMPO-oxidation	78.4	49.9	2.1 ± 1.1	Carboxylate (negative)	(Liu et al., 2016)
Enzymatic	17.58	83.41	200–500	Hydroxyl (neutral)	(Cui et al., 2016)

*Particle size (diameter) was determined based on TEM analysis.

2.4.3.4 Transition Metal Based Catalyst Assisted Hydrolysis

Metal salts have been used for the pretreatment of cellulosic materials as they can induce the degradation of cellulose and able to disrupt the hydrogen bonds (Thulluri et al., 2013; Wang et al., 2013). As compared with common chemical pretreatments such as organic solvents and inorganic acids, metal salts rendered less corrosive to equipment and more environmentally-friendly, resulting in the feasibility of industrial applications for bioconversion of cellulosic material into nanocellulose. Furthermore, a suitable concentration of metal salt can significantly improve the enzymatic hydrolysis of cellulose (H. Liu & Zhu, 2010). Normally, metal salt pretreatment is carried out in aqueous solution or molten state but cannot be performed in solid phase condition because of the poor contact between cellulose and melt salts.

Recently, transition metal salt catalysts have received use as acid homogeneous catalysts for the cellulose hydrolysis process. Transition metal salt catalysts normally can be categorized based on their valence states, such as trivalent ($FeCl_3$, $Fe_2(SO_4)_3$, $CrCl_3$, $AlCl_3$) or divalent ($FeCl_2$, $FeSO_4$, $CuCl_2$), and have high potential for acting as the hydrolysis catalyst for the degradation of the glycosidic linkage of cellulose during acid hydrolysis treatment (Yi et al., 2013). However, the valence state of the transition metal ion plays a significant role in hydrolysis efficiency. (J. Li et al., 2015) reported that the crystallinity of nanocellulose was improved by approximately 19% from native cellulose after being treated by a trivalent Fe^{3+} metal ion catalyst. However, Yahya et al. found that the divalent Ni^{2+} inorganic salt with an optimum pH of 5.0 (1.0 M) was capable of increasing the crystallinity of the treated nanocellulose by approximately 7% compared with untreated cellulose (Yahya, Lee, & Hamid 2015). The results of another study done by Li et al. indicated that Fe^{3+}-treated nanocellulose rendered an extra 7% higher crystallinity compared with Cu^{2+}-treated nanocellulose (Li et al., 2013)

The metal salts were found less corrosive and lower severity conditions than strong mineral acids, and it can be recycled via ultrafiltration process (Wang et al., 2014). It had been proved that the metal ion catalyst was capable of accelerating the cellulose hydrolysis and enhancing the catalytic activity by reducing the activation energy of the hydrolysis reaction (Wang et al., 2014). In addition, the metal salts render high hydrolysis selectivity, which favors targeting the C–O–C and C–H bonds of cellulose in plant wall polymer networks (Wei et al., 2011). However, the key factor to influence hydrolysis efficiency of cellulose into nanocellulose by metal salt catalysts is the valence state of metal ion, where the acidic solution (due to the presence of H^+ ions) was generated during the polarization of metal ions together with water molecules (Kamireddy et al., 2013). Li's research group studied the of two different transition

metals (Fe^{3+} and Cu^{2+}), and the results showed that crystallinity index of yielded nanocellulose treated by trivalent Fe^{3+} metal ion catalyst was about 7% higher than cellulose hydrolyzed by the divalent Cu^{2+} metal ion catalyst under same hydrolysis condition (Li et al., 2013).

Based on reported studies, it has reported that certain metal salts can catalytically hydrolyze carbohydrates effectively into useful feedstock chemicals. Besides that, the presence of the acidic medium (H_2SO_4) can act synergistically to increase the accessibility of transition metal ions in hydrolysis process (J. Li et al., 2015). In fact, the catalytic performance is correlated with the type of metal salt catalyst used in the hydrolysis system. Cao's team investigated the effect of a series of transition metal salts on hydrothermal conversion of lignocellulosic biomass into valuable chemicals and fuels (X. Cao et al., 2015). They reported that Fe^{3+} was able to accelerate the cellulose hydrolysis process into glucose at 200 °C, whereas Ni^{2+} and Co^{2+} metal ions had a significant effect on the conversion of cellulose, glucose, and xylose into lactic acid. These transition metal salts act as Lewis acid catalysts, which anticipated having selective hydrolysis ability by disrupting the glycosidic bond and hydrogen bond of the cellulose chains and had a positive effect on hydrolysis of cellulose into its simpler water soluble monomers at the high reaction temperature (150 °C). On the other hand, Cr^{3+}- and Mn^{2+}-based transition metal catalysts have been found to have highly effective in breakage of the extensive network of glycosidic linkage and hydrogen bonding within the cellulose matrix to separate cellulose fibrils. On the other hand, Peng et al. reported that $CrCl_3$ transition metal salt was highly effective for conversion of cellulose into its simpler form (*i.e.* levulinic acid) under the optimized conditions of 200 °C for 180 min, with the maximum yield of 67 mol% with the presence of 0.02 M of

catalyst loading (Peng et al., 2010). However, it is believed that the intermediate solid nanocellulose can be obtained under the controlled milder conditions.

During the catalytic hydrolysis, the metal salt catalyst possesses of high hydrolyzing ability to depolymerize the cellulose by disrupting its bonding system, and thus enhances the fermentable sugar yield as compared with dilute acid hydrolyzing alone (Ogura et al., 2014). Therefore, by combining a metal ion catalyst with dilute H_2SO_4, one can potentially overcome the drawback of dilute acid hydrolysis since the combination of both pretreatments may initiate a synergistic effect, thus enhancing the hydrolysis efficiency of cellulose depolymerization into nanostructured cellulose under controllable reaction conditions. In fact, the advantage of using transition metal salt instead of strong H_2SO_4 for acid hydrolysis is reducing acid consumption for depolymerization process, which prevents corrosive issues, increase the selectivity of nanocellulose product with lower severity conditions (mild temperature and shorter hydrolysis period).

Besides the cellulose depolymerization process, there are several chemical conversion can be conducted by transition metal-based catalyst such as oxidation and hydrogenation process. Some authors reported that the hydrogenation of cellulose and glucose can produce value-added products, such as sugar alcohols and sorbitol, which are widely used in food industry and precursors of fuels. Up to now, many potential transition metal-based catalysts have been developed for the hydrogenation of cellulose or glucose molecule. A study reported by (de Almeida et al., 2010) found that the sorbitol (a kind of sweetener, thickener) was able to produce from glucose via the hydrogenation process catalyzed by $ZnCl_2$ hydrate media. On the other hand, a simple method was demonstrated by Zhang et al. in order to oxidize the glucose into gluconic acid

in the presence of $FeCl_3$ solution. Via oxidation process, up to 52.3% of gluconic acid, 10–20% of formic and acetic acid was obtained as main coproducts (Zhang et al., 2016). The gluconic acid is mainly used in food additive as an acidity regulator whiles the formic and acetic acids function as preservative and vinegar, respectively. The reaction mechanism of cellulose hydrogenation and oxidation process is shown in **Figure 2.4**.

Table 2.4: Performance and mechanism of transition metal based catalyst for various chemical conversion processes.

	Hydrogenation process	Oxidation process
Catalyst used	$ZnCl_2$, H_2	$FeCl_3$
Product obtained	Sorbitol	Gluconic, formic and acetic acids
Mechanism	Refer **Figure 2.4**- Route (a)	Refer **Figure 2.4**- Route (b)
Reference	(de Almeida et al., 2010)	(Zhang et al., 2016)

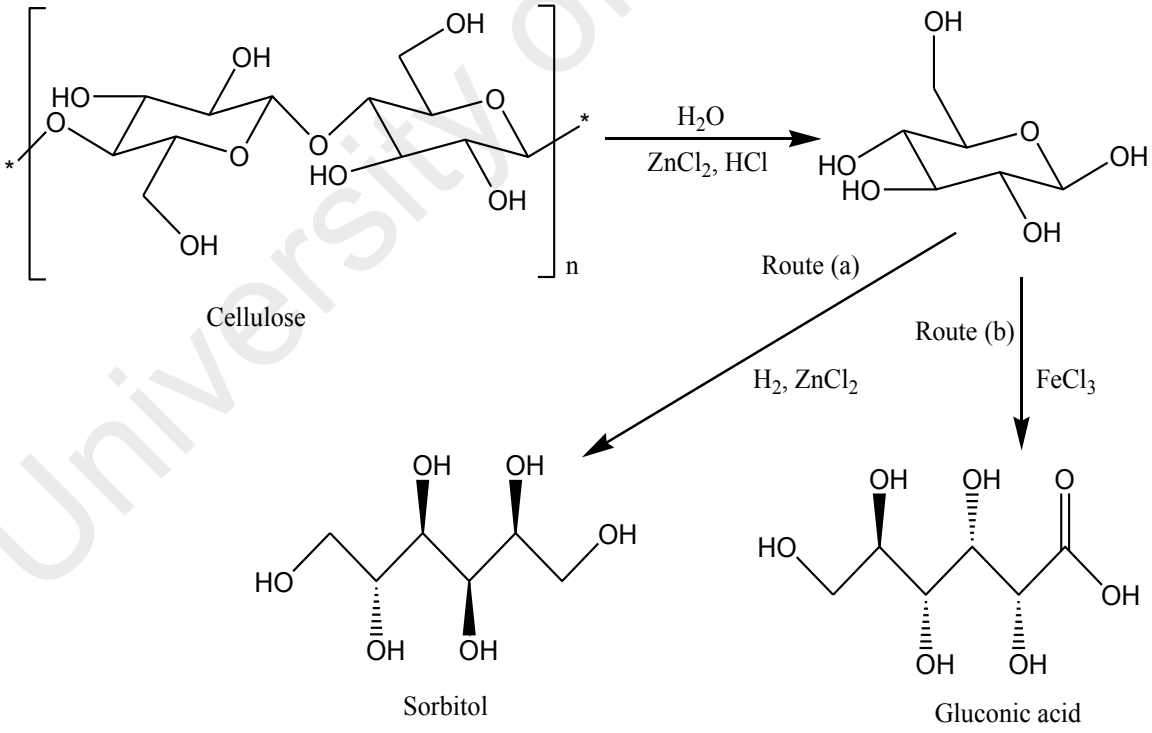

Figure 2.4: The reaction pathway of cellulose hydrolysis of cellulose to glucose, followed by (a) hydrogenation of glucose to sorbitol; and (b) oxidation of glucose to gluconic acid.

2.5 Optimization of Chemical Conversion Process

Optimizing refers to improving the performance of a process, a product, or a system in order to obtain the maximum benefit/outcomes from it. The term "optimization" has been commonly used in analytical chemistry with the meaning of discovering conditions at which to apply a procedure that produces the best possible response(s) (Azami et al., 2012).

Traditionally, optimization of process variables in analytical chemistry can be done by monitoring the impact of one-factor-at-a-time on the experimental output. This suggests that it is possible to systematically study several processes by manipulating one factor while keeping other conditions at a constant level. However, the major disadvantage of this method is that it does not comprise the interaction effects between the each variable studied and it not necessary reflects the overall effects of all the parameters on the selected outcomes (Caldas et al., 2011). Also, it is necessary to consider the influence of each factor and also the interaction between these factors which may be antagonistic and synergistic. Due to these reasons, more experiment sets are necessary to conduct the research in order to enhance the accuracy of the obtained results, which leads it to an increase of capital costs (more expenses for materials and reagents consumption) as well as prolong the duration of the designed studies.

In order to solve this issue, the optimization of analytical procedures has been carried out by using multivariate statistic techniques such as response surface methodology with central composite design, Factorial Design and Taguchi's method. The design of experiment (DOE) is an analytical or experimental method that is commonly used to statistically signify the relationship between input parameters to output response(s), whereby a systematic way of the planning of experiments,

collection, and analysis of data is performed. DOE has wide-ranging applications especially in the field of engineering and science for the purpose of process management, process optimization, and development as well as validation tests (Prasad, Rao, & Rao, 2012). Amongst these, the most relevant multivariate techniques used in analytical optimization is response surface methodology (RSM). RSM is a collection of mathematical and statistical techniques for developing, modeling, simulating and optimizing the complex processes based on the statistical design and analysis (C. Wang et al., 2014). It can be well applied when a response or a set of responses of interest are influenced by several variables. The objective is to simultaneously optimize the levels of these variables to attain the best system performance.

2.5.1 Response Surface Methodology (RSM)

Response surface methodology (RSM) is widely used as a powerful tool to study the interactions of two or more variable. Basically, RSM is useful for modeling and analysis of problems in which a response of interest is influenced by several parameters. RSM usually contains three main stages, namely design and experiments, response surface modeling through regression, and optimization (Yeniay, 2014). This technique has become popular and attractive in optimizing the reaction variables due to several advantages: (i) sufficient information for statistically acceptable result can be obtained without carry out the extensive experimental runs; (ii) the relationship between independent variables on the response(s) within the investigation ranges can be determined readily by the visualization of response surface; and (iii) Can efficiently achieve the optimal reaction conditions at low cost (Chen, Yu, Liu, Hai, et al., 2011; Man et al., 2011). RSM is an experimental strategy that has been employed by research and development personnel in the industrial sectors, with considerable success in a wide variety of situations to obtain solutions for complicated problems.

Before applying the RSM methodology, it is necessary to select an experimental design as well as the experiments that going to perform within the experimental region being studied. There are some experimental matrices for this purpose such as experimental designs for first-order models (e.g., factorial designs) can be used when the data set does not present curvature. If a response function to experimental data that cannot be described by linear functions, the experimental designs for quadratic response surfaces should be used implied, including central composite, Box-Behnken, three-level factorial and Doehlert designs.

2.5.2 Theory and Steps for RSM Application

As above mentioned, RSM consists of a group of statistical and mathematical techniques that are based on the fit of empirical models to the experimental data obtained in relation to experimental design. To achieve this objective, linear or square polynomial functions are employed to describe the system studied and, thus, to explore (displacing and modeling) experimental conditions until reach its optimization (Hosseini et al., 2017). Some essential steps in the application of RSM as an optimization system are as follows:

(1) Selection of independent variables that play the major effects on the system via pre-screening studies and the delimitation of the experimental region, based on the objective(s) of the study as well as the experience of the researcher;

(2) Choice of the experimental design and conducts the experiments according to the selected experimental matrix;

(3) Mathematic–statistical treatment of the experimental data through the fit of a polynomial function;

(4) Evaluation of the model's fitness;

(5) Verification of the possibility and necessity of performing a displacement in direction to the optimal region; and

(6) Obtaining the optimum values for each selected variable.

2.5.3 Central Composite Design

The central composite design was first introduced by Box and Wilson at 1951. **Figure 2.5** illustrates the full central composite design for optimization of two and three variables. This design consists of the three parts:

(1) A fractional factorial or full factorial design;

(2) An additional design, often a star design in which experimental points are set from its center; and

(3) A central point.

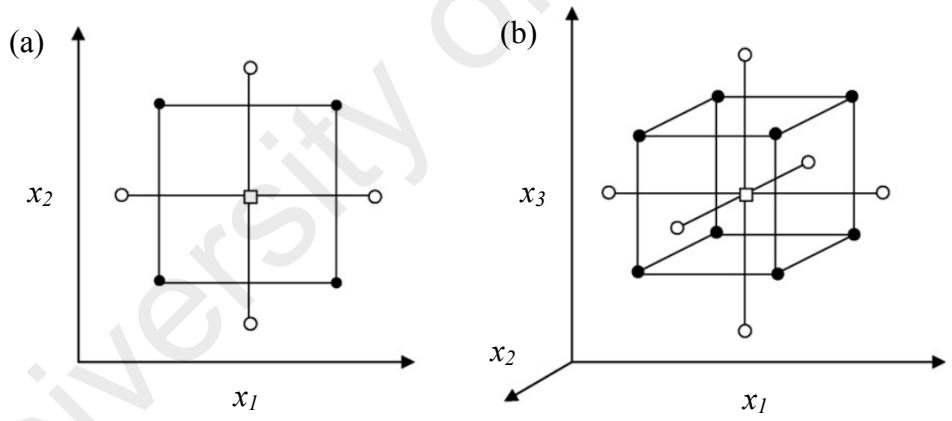

Figure 2.5: Central composite designs for the optimization process of (a) two variables ($\alpha = 1.41$) and (b) three variables ($\alpha = 1.68$) [(●) factorial point, (□) central point, and (○) axial points].

The central composite designs which are fully uniformly routable should have the following characteristics:

(1) An experiment number according to $N = k^2 + 2k + c_p$, where k is the factor number and (c_p) is the replicate number of the central point;

(2) α-values is highly dependent on the number of variables and can be calculated by $\alpha = 2^{(k-p)/4}$.

For two, three, and four variables, they are α respectively, 1.41, 1.68, and 2.00;

(3) All factors are studied in five levels ($-\alpha, -1, 0, +1, +\alpha$).

CHAPTER 3: RESEARCH METHODOLOGY

3.1 Overview

Chapter 3 covers the methodologies for three main sections. First section (**Section 3.3**) provides the information regarding the preparation of nanocellulose from α-cellulose model compound by using different type of transition metal salt catalysts via acid hydrolysis. Second section (**Section 3.4**) mainly focused on the optimization study of nanocellulose product by using response surface methodology (RSM) system, where the responses are crystallinity index and product yield. The best catalyst from **Section 3.3** was selected for the optimization study. Third section (**Section 3.5**) discussed on developing a facile approach for the isolation of nanocellulose from oil palm empty fruit bunch via one-pot oxidative-hydrolysis process. Besides that, the physicochemical properties of nanocellulose were examined using different analytical techniques FESEM, TEM, AFM, FTIR, XRD and TGA.

3.2 Raw Materials and Chemicals Selections

Alpha cellulose (Chemical formula: $(C_6H_{10}O_5)_n$; Source: cotton linters; Molecular weight: ~1.18×10^5 g/mol; Degree of polymerization: ~229; Bulk density: 3.1–4.3 CC/g; Crystallinity: 43.7%) was purchased from Sigma-Aldrich (USA) and used as the cellulose model compound for the production of nanocellulose. On the other hand, oil palm empty fruit bunch (OPEFB; Crystallinity: 42.6%) was supplied by a local oil palm refinery factory and used as raw lignocellulosic biomass. All the chemicals and reagents, such as iron(III) nitrate (ρ=1.68 g/cm^3), chromium(III) nitrate (ρ=1.85 g/cm^3), cobalt(II) nitrate (ρ=1.87 g/cm^3), nickel(II) nitrate (ρ=2.05 g/cm^3), manganese(II) nitrate (ρ=1.536 g/cm^3), sulfuric acid, hydrogen peroxide, toluene, ethanol, sodium chlorite, acetic acid and sodium hydroxide used in this research were purchased from Merck

Company (Malaysia). The purity of transition metal salts was ≥ 99% trace metals basis. All these chemical were in analytical grade and used as received form without further purification processing. In addition, dialysis tubing cellulose membrane from Sigma-Aldrich (USA) was used for dialysis process. Deionized (DI) water was utilized as washing solvent to remove the chemicals or hydrolyzing catalyst during the centrifugation steps. It also functions to quench the hydrolysis reaction by diluting the nanocellulose suspension.

3.3 Catalytic Screening for Hydrolysis of Cellulose to Nanocellulose

3.3.1 Synthesis of Nanocellulose via Transition Metal Assisted Dilute H_2SO_4 Catalyzed Acid Hydrolysis

Different nanocellulose samples were initially synthesized through acid hydrolysis by using various transition metal salts, namely iron(III) nitrate; $Fe(NO_3)_3$, chromium(III) nitrate; $Cr(NO_3)_3$, cobalt(II) nitrate; $Co(NO_3)_2$, nickel(II) nitrate; $Ni(NO_3)_2$, manganese(II) nitrate; $Mn(NO_3)_2$. 1 g of α-cellulose model compound was added to the mixture of 4 wt% H_2SO_4 and 25 mM of transition metal based catalyst with the different cations (Fe^{3+}, Co^{2+}, Ni^{2+}, Mn^{2+}, Cr^{3+}). The suspension was heated up to 80 °C for 45 min with continuous mechanical stirring. Once the reaction completed, the hydrolysis system was quenched and diluted by addition of cold DI water, followed by repeated centrifugation for 10 min interval until neutral pH was achieved. The collected sediment was subjected to lyophilization process after the dialysis process against the distilled water in order to produce dried finely snowy-white powder before further characterization studies.

3.4 Optimization Study of Nanocellulose Production by using Response Surface Methodology (RSM)

3.4.1 Preparation of Nanocellulose

In order to optimize the hydrolysis process, the α-cellulose model compound powder (0.6 g) was placed in a round-bottomed flask and treated with different concentrations of H_2SO_4 and $Cr(NO_3)_3$ catalysts at desired reaction temperatures (30–100 °C). The mixture was heated to different reaction duration varied from 0.5 to 2.5 h under the constant stirring speed. The cellulose hydrolysis reaction was performed according to the pre-set conditions based on a basic design matrix (**Table 3.1–3.2)**. After the definite interval of time, the treated cellulose samples were washed with DI water for several times by repeated centrifugations and subjected to dialysis process to obtain high-purity nanocellulose. The yield of freeze-dried nanocellulose was calculated according to the **Equation 3.1** as follows (Hamid et al., 2014).

Product yield (%) = (Weight of nanocellulose) / (Weight of untreated cellulose) × 100

[Equation 3.1]

3.4.2 Experimental Design for RSM Optimization Study

The experimental design matrix, data analysis, and optimization study were developed by using a software Design-Expert version 9.0.0 (Stat-Ease, Inc., Minneapolis). A standard RSM design called central composite design (CCD) was applied to study the catalytic acid hydrolysis of cellulose for preparing the nanocellulose products. Four independent variables studied were reaction temperature (x_1), reaction time (x_2), concentration of Cr(III)-transition metal based catalyst (x_3), and

concentration of H_2SO_4 (x_4). The responses were crystallinity index (y_1) and nanocellulose yield (y_2).

Table 3.1 lists the range and levels of the four independent variables studied with actual and coded levels of each parameter. The independent variables were coded into two levels: namely, low (-1) and high (+1), whereas the axial points were coded as -2 (-α) and +2 (+α). In this study, the α-value was fixed at 2, which is the distance of the axial point from the center and makes the design rotatable. The experimental design matrix, in terms of real and coded independent variables and the results, is presented in **Table 3.2**. The experiments were run in random order to minimize errors from systematic trends in the variables.

Table 3.1: Five-level, four-factor central composite design of hydrolysis variables.

Coded symbol	Variable	Levels				
		-α	-1	0	+1	+α
x_1	Reaction temperature (°C)	30.0	47.5	65.0	82.5	100.0
x_2	Reaction time (h)	0.5	1.0	1.5	2.0	2.5
x_3	Concentration of Cr(III)-transition metal based catalyst (M)	0.025	0.125	0.225	0.325	0.425
x_4	Concentration of H_2SO_4 (M)	0.2	0.4	0.6	0.8	1.0

Table 3.2: Experimental design matrix and experimental results for nanocellulose preparation via Cr(III)-assisted H_2SO_4 hydrolysis.

Run	Variable levels				Selected responses	
	x_1	x_2	x_3	x_4	Crystallinity, y_1 (%)	Yield, y_2 (%)
1	0 (65.0)	0 (1.5)	0 (0.225)	0 (0.60)	83.33	80.14
2	0 (65.0)	0 (1.5)	0 (0.225)	0 (0.60)	83.08	80.32
3	0 (65.0)	0 (1.5)	0 (0.225)	0 (0.60)	82.24	80.22
4	0 (65.0)	0 (1.5)	0 (0.225)	0 (0.60)	82.85	80.52
5	0 (65.0)	0 (1.5)	0 (0.225)	0 (0.60)	82.72	80.85
6	0 (65.0)	0 (1.5)	0 (0.225)	0 (0.60)	83.74	80.53
7	0 (65.0)	0 (1.5)	2 (0.425)	0 (0.60)	86.23	80.61
8	-2 (30.0)	0 (1.5)	0 (0.225)	0 (0.60)	70.33	88.00
9	2 (100.0)	0 (1.5)	0 (0.225)	0 (0.60)	88.93	83.20
10	0 (65.0)	2 (2.5)	0 (0.225)	0 (0.60)	85.52	80.93
11	0 (65.0)	-2 (0.5)	0 (0.225)	0 (0.60)	66.55	91.02
12	0 (65.0)	0 (1.5)	0 (0.225)	-2 (0.20)	60.11	90.55
13	0 (65.0)	0 (1.5)	0 (0.225)	2 (1.00)	77.44	80.11
14	0 (65.0)	0 (1.5)	-2 (0.025)	0 (0.60)	63.99	89.63
15	-1 (47.5)	1 (2.0)	-1 (0.125)	-1 (0.40)	67.91	88.86
16	1 (82.5)	1 (2.0)	1 (0.325)	-1 (0.40)	83.71	84.45
17	1 (82.5)	1 (2.0)	-1 (0.125)	1 (0.80)	84.16	82.53
18	1 (82.5)	-1 (1.0)	1 (0.325)	1 (0.80)	86.13	80.87
19	-1 (47.5)	1 (2.0)	1 (0.325)	1 (0.80)	84.11	82.56
20	-1 (47.5)	-1 (1.0)	1 (0.325)	-1 (0.40)	60.38	87.49
21	1 (82.5)	-1 (1.0)	-1 (0.125)	-1 (0.40)	65.87	89.63
22	-1 (47.5)	-1 (1.0)	-1 (0.125)	1 (0.80)	83.81	82.99
23	-1 (47.5)	1 (2.0)	1 (0.325)	-1 (0.40)	74.18	86.97
24	-1 (47.5)	1 (2.0)	-1 (0.125)	1(0.80)	67.09	88.33
25	1 (82.5)	1 (2.0)	1 (0.325)	1 (0.80)	88.58	77.19
26	-1 (47.5)	-1 (1.0)	1 (0.325)	1 (0.80)	82.48	81.14
27	-1 (47.5)	-1 (1.0)	-1 (0.125)	-1 (0.40)	62.63	89.27
28	1 (82.5)	-1 (1.0)	1 (0.325)	-1 (0.40)	72.35	85.55
29	1 (82.5)	1 (2.0)	-1 (0.125)	-1 (0.40)	74.25	86.38
30	1 (82.5)	-1 (1.0)	-1 (0.125)	1 (0.80)	82.81	85.55

3.5 Facile Production of Nanocellulose from Oil Palm Empty Fruit Bunch (OPEFB) via One-Pot Oxidative-Hydrolysis Isolation Approach

3.5.1 Preparation of Nanocellulose from OPEFB via One-Pot Approach

The scheme for the preparation of nanocellulose from OPEFB biomass via the one-pot reaction system was illustrated in **Figure 3.1(a)**. Approximately 100 mL of 30% hydrogen peroxide (H_2O_2) was added into 5 g of untreated OPEFB fibers and heated to 90 °C under continuous mechanical stirring for 5 h. During the reaction, a small amount of sample was collected from the reaction flask every hour in order to determine its chemical composition. Upon the reaction completion, the suspension was cooled down to room temperature. Then, 0.22 M of Cr(III)-transition metal based catalyst and 8 wt% of H_2SO_4 were added into the same reaction pot and further heated to 82 °C for 1 h. The final product was separated from the reaction medium via centrifugation and washed repeatedly with cold deionized water. The collected nanocellulose product (OP-NC) was subjected to lyophilization prior to the physicochemical studies. On the other hand, as a control study, the nanocellulose sample further also prepared via Cr(III)-transition metal based catalyzed hydrolysis route without the assistance of dilute sulfuric acid.

3.5.2 Preparation of Nanocellulose via Multistep Chemical Process

Biomass pretreatment is a multiple steps process that used to destruct the complex structure of biomass and isolate individual cellulose fibers from mixture of cellulosic and non-cellulosic compounds. Initially, the oil and wax components coated on the untreated OPEFB were removed via soxhlet extraction by using 2:1 (v/v) toluene/ethanol mixture for 7 h. The extractive-free dewaxed fibers were then washed repeatedly with hot deionized water for several times. For the bleaching process, the dewaxed fibers were further treated with 1.5 g of sodium chlorite ($NaClO_2$) in the

presence of 3 mL of glacial acetic acid (CH_3COOH). The process was conducted at 75 °C for 1 h and repeated for three times until the fibers became snow white ($NaClO_2$-treated sample). The subsequent alkalization treatment was carried out at 80 °C for 4 h by using 2% NaOH solution. The resultant product was subjected to washing process by using deionized water and separated by centrifugation in order to remove all the solubilized non-cellulosic components. For preparing the nanocellulose, the catalytic acid hydrolysis was performed under RSM-optimized reaction conditions (**Section 3.4**). Briefly, 0.22 M of $Cr(NO_3)_3$ solution and 8 wt% of H_2SO_4 was added to the extracted cellulose with a ratio of 1:10 at 82 °C for 1 h. The hydrolysis reaction was quenched by adding 10-fold of cold deionized water and the final product was freeze-dried to yield the white fluffy nanocellulose (MS-NC). **Figure 3.1(b)** shows the diagram of the conventional multistep chemical isolation processes.

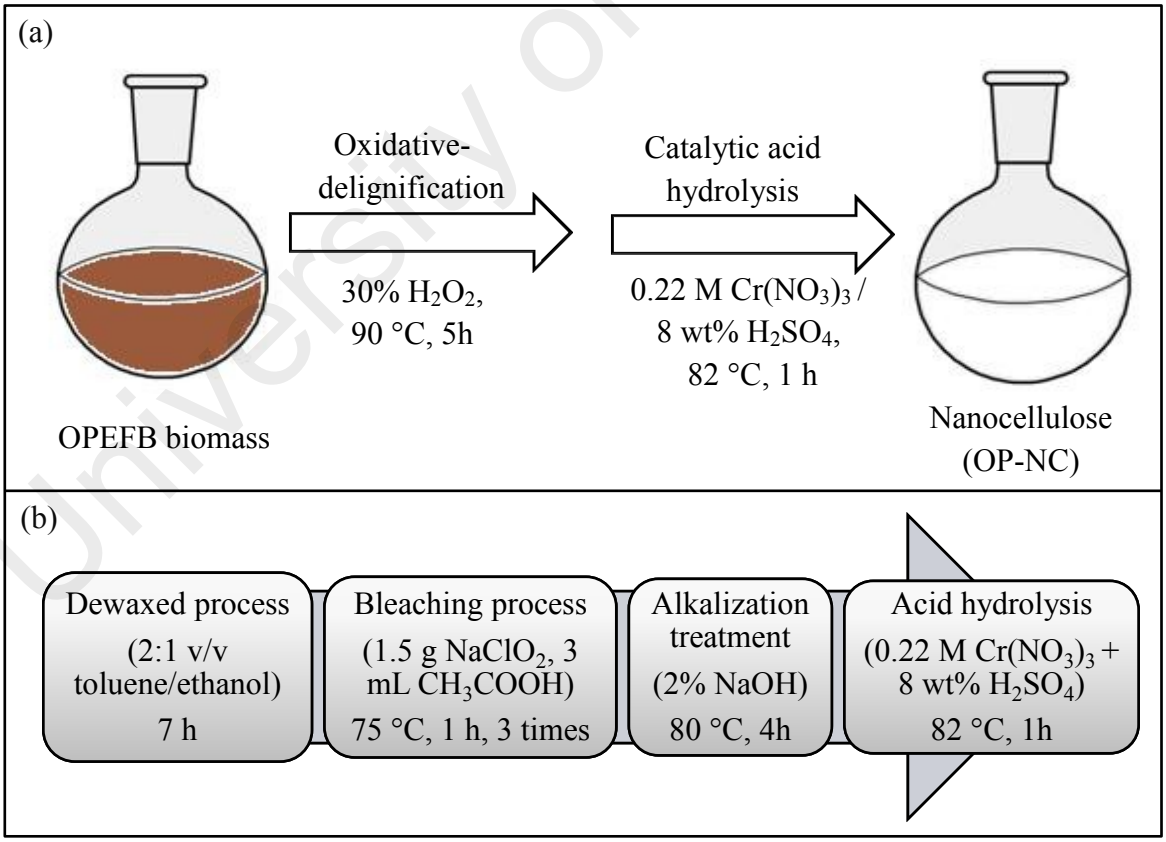

Figure 3.1: Schematic diagram for isolating nanocellulose from OPEFB biomass via (a) one-pot isolation (OP-NC) and (b) multistep purification approach (OP-MS).

3.5.3 Physicochemical Study of OPEFB, Cellulose and Nanocellulose Products

3.5.3.1 ASTM Methods

The chemical compositions of untreated and chemically treated fibers were investigated by using ASTM protocol. The holocellulose, α-cellulose and Klason lignin content were determined based on ASTM D1104-56, ASTM D1103-55T, and ASTM D1106-56, respectively. In contrast, the percentage of hemicellulose can be calculated by the difference between holocellulose and α-cellulose content. The measurement of each sample was conducted in triplicate and the average data were calculated.

Holocellulose content in the fiber was measured by treating the ground raw fiber (4.0 g) with 2.0 mL acetic acid and 5.0 g sodium chlorite at 70 °C for 4 h in a water bath. After that, the suspension was cooled in an ice bath, filtered, and crucible-dried in an oven until constant weight was achieved. The remaining sample obtained after the study of holocellulose content was further treated with 50 mL of 17.5% NaOH solution. Then, the α-cellulose content was determined by weighing the dried sample until constant weight achieved. Lignin composition was studied by treating the ground fiber with 3 mL cold H_2SO_4 at 20 °C for 2 h. Upon completion, the mixture was then diluted to a 3% concentration of H_2SO_4 and further boiled for 4 h under a reflux condenser. The suspension was filtered and washed with hot water and dried in an oven until constant weight was achieved.

3.5.3.2 Fourier Transform-Infrared (FTIR) Spectroscopy

Fourier transform infrared (FTIR) spectroscopy is a powerful characterization method for providing the information on the surface chemical composition of the sample by identifies the functional group present within molecules. FTIR studies were

conducted on each sample in order to identify the effects of biomass pretreatment and hydrolysis process towards the chemical compositions and functional groups of all the fibers. Each type of chemical bond has its own characteristic vibration frequency for indicating the presence of particular functional groups and chemical bonds specific to the molecules. The IR spectrum is displayed as the intensity of light transmitted through the analyzed sample measured against the wavenumber. In general, FTIR is principally essential for identification of organic molecular structure and compounds.

The FTIR spectra of fibers were examined using a Fourier transform infrared spectrometer (Bruker IFS 66/S) in the transmittance mode from the range of 4000 to 400 cm^{-1} with a resolution of 4 cm^{-1}. The samples were ground and mixed with KBr powder in a ratio of 1: 100 (w/w), and then pressed into ultra-thin pellets before the analysis. Then, the KBr pellets were placed in FTIR specimen holder for analysis and IR radiation was passed through it. The intensity of transmittance due to IR radiation was collected as FTIR spectrum.

3.5.3.3 X-Ray Diffraction (XRD)

The crystalline structure of samples was analyzed using a wide-angle X-ray diffraction (WAXRD) powder diffractometer (PANalytical Empyrean, Netherlands) with a CuK_{α} radiation source. The crystallinity index and crystallographic phase of sample was investigated by XRD analysis. Impacts of the catalytic depolymerization process towards the crystallinity index of treated products can be investigated from the generated X-ray diffractograms. The X-ray diffraction patterns were recorded from 5° to 50°, which was generated at an operating power of 40 kV and a current of 40 mA. Crystallinity index (CrI) value of the samples was calculated from diffraction intensity

data by the empirical Segal's method according to the following **Equation 3.2**,

$$\text{CrI}\ (\%) = (I_{200} - I_{am}) / I_{200} \times 100 \qquad \textbf{[Equation 3.2]}$$

where I_{200} represents to the maximum peak intensity at the lattice diffraction (200) of the crystalline regions (2θ = 22.5°) and I_{am} is the minimum value between planar reflections (200) and (110), which refers to reflection intensity of the amorphous parts (2θ = 18.5°) of the samples.

3.5.3.4 Field Emission Scanning Electron Microscopy (FESEM)

Field emission scanning electron microscopy (FESEM) is a non-destructive technique that usually used to visualize topography and morphology details on the surface of a sample. FESEM is predominantly useful to provide a great depth of field to visualize the surface structure of the sample. Surface morphology of the samples was characterized using an FESEM (Hitachi SU8030, Japan). In order to perform the analysis, the dried sample was carefully mounted on the aluminum stubs with double-sided adhesive carbon tapes. The analysis was performed at an accelerating voltage of 5 kV with the working distance of 4 mm and a secondary electron detector. The sample was coated with a layer of platinum using an auto-fine coater (JEOL JFC-1600, Japan) under vacuum environment before analysis to prevent overcharging when exposed to the electron beam. The diameters of fibers were calculated using ImageJ software.

3.5.3.5 Transmission Electron Microscopy (TEM)

Transmission electron microscopy (TEM) is an innovative microscopic technique to visualize the sample dimensions by using a beam of high energy electrons (up to 300 kV accelerating voltage). TEM is one of the important tools for the morphological characterization of nanomaterials. Particle dimensions and structure of nanocellulose

products were observed using a transmission electron microscope (Tecnai G2 F20 Series, FEI, USA) with an accelerating voltage of 200 kV. A diluted sample suspension (0.01 wt%) was ultrasonically treated for a short period to homogeneously dispersed, then dropped on the surface of the glow-discharged carbon-supported copper grid (300-mesh, formvar-carbon, Ted Pella Inc) and dried it naturally in a ventilated place. The dimension of nanocellulose fibers was measured using Image J (National Institutes of Health, USA). The average reading was calculated based on 250 measurements.

3.5.3.6 Atomic Force Microscopy (AFM)

For atomic force microscopy (AFM) analysis, a cantilever with a sharp tip is equipped to scan across the sample surface in order to construct a 3D image. It is able to measure microscopic surface morphological and topographical characterization as well. The yielded nanocellulose samples were visualized by using atomic force microscope with a model Dimension 3100 scanning probe microscope (Brand Veeco, Russia). The measurements were accomplished with a silicon cantilever and operating in the tapping mode at room temperature. Before the AFM imaging, dilute nanocellulose suspension with the concentration of 0.001 wt% was injected and deposited onto a freshly cleaned microscopic slide surface and dried in a vacuum desiccator. The AFM measurements for determining the fibers dimensions were conducted by NanoScope Analysis software. The size and morphology of nanocellulose were examined using NanoScope Analysis software provided by Bruker Company. A histogram was plotted for the diameter of nanocellulose to determine the numerical diameter distribution after measurement of randomly selected nanocellulose.

3.5.3.7 Thermogravimetric Analysis (TGA)

Thermogravimetric analysis (TGA) is a tool commonly used to determine the thermal stability of the material by measuring the variation of mass with respect to temperature under the controlled atmosphere. The basic principle of TGA is to determine the changes of the mass profile when the sample is progressively heated in a furnace. The mass changes can be used to understand the thermal stability of a sample or determine the composition of a material. Generally, the mass loss is normally for the thermal event and can be attributed to the reduction, evaporation, loss or decomposition of the volatile material. The plot of weight percentage of a sample against time or temperature is depicted as a thermogram in order to understand thermal transition behavior of the material.

Thermal stability and decomposition behaviors of samples were analyzed by a model TA Q500 (Australia) thermogravimetric analyzer (TGA). Samples were placed in a crucible, and the operating temperature elevated from room temperature to 600 °C with a constant heating rate of 10 °C/min. All measurements were performed under a nitrogen atmosphere in order to minimize any pre-mature thermo-oxidative degradation as well as the fast pyrolysis of cellulosic materials.

3.5.3.8 Gel Permeation Chromatography (GPC)

In order to determine the molecular weight (M_W) and degree of depolymerization (DP), the extracted cellulose and nanocellulose samples were first modified into its derivative form via the tricarbanilation process before subjecting to GPC analysis (Hubbell & Ragauskas, 2010). In brief, the cellulose tricarbanilate derivative was prepared by adding anhydrous pyridine (4 mL) and phenyl isocyanate (0.5 mL) sequentially to 20 mg of the dry sample via syringe, and the reaction mixture was

heated at 80 °C for 12 h until the sample was completely dissolved. Afterward, 2 mL of methanol was added into the yellowish mixture to eliminate/decompose any excess phenyl isocyanate. The cellulose tricarbanilate was promoted to precipitate by adding dropwise into the 3:7 water/methanol mixtures (100 mL). The derivatized cellulose was finally purified by repeated washing with water/methanol (100 mL, thrice) followed by water (100 mL, twice). Prior to GPC analysis, the derivatized cellulose was dissolved in tetrahydrofuran (THF) with the concentration of 1 mg/mL, filtered through a 0.45 μm PTFE syringe filter and placed in a 2 mL auto sample vial (Hallac & Ragauskas, 2011 Kim et al., 2016). Molecular weight distributions of the tricabanilated cellulose samples were determined by a GPC (Malvern's OMNISEC) instrument. THF solvent was used as the mobile phase/ column eluent with the following conditions: a flow rate of 0.8 mL/min and injection volumes of 100 μL. The degree of polymerization of the samples was calculated according to **Equation 3.3**:

$$\text{Degree of polymerization, } DP_w = M_w / M_{mono} \qquad \textbf{[Equation 3.3]}$$

where M_w is the molecular weight of the sample and M_{mono} refers to the molecular weight of the tricarbanilated cellulose monomer (~ 519 g/mol).

CHAPTER 4: RESULTS AND DISCUSSION

This chapter presents the results obtained from the physicochemical characterization of OPEFB, cellulose and nanocellulose products. As pointed above, the study was divided into three sections. First, production of nanocellulose from α-cellulose model compound via acid hydrolysis process by using different transition metal based catalyst assisted by dilute H_2SO_4. The second section reports on the optimization study of nanocellulose production by using response surface methodology (RSM), which the highest reactivity of transition metal based catalyst was selected for the hydrolysis process. The effect of hydrolysis parameters, namely reaction temperature, reaction time, concentration of Cr(III)-transition metal based catalyst, concentration of H_2SO_4 is evaluated in detail towards the properties and yield of nanocellulose. The third section discusses on developing of a facile route for the production of nanocellulose from OPEFB via one-pot oxidative-hydrolysis method. The physicochemical properties of nanocellulose from one-pot treatment are compared with those extracted via conventional multistep process.

4.1 Catalytic Screening for Hydrolysis of Cellulose to Nanocellulose

In this section, α-cellulose model compound was treated by several potential transition metal nitrate salt (hydrolyzing catalysts) with different metal cations and valence states, namely Fe^{3+}, Cr^{3+}, Ni^{2+}, Co^{2+}, and Mn^{2+}. The aim of this study is to understand the effectiveness of selected transition metal based catalysts in enhancing the hydrolysis efficiency during cellulose depolymerization process. To achieve this purpose, we attempted to treat the macro-sized α-cellulose with selected transition metal based catalysts. The cellulose hydrolysis experiments were conducted under the same operational conditions (4 wt% H_2SO_4, 25 mM transition metal based catalyst, 80 °C and

45 min). Physicochemical properties of yielded nanocellulose were examined and analyzed by using XRD, FESEM, TEM, AFM, FTIR and TGA. The present study will be helpful in assessing the feasibility and practicability of suitable transition metal based catalyst for efficient nanocellulose production with aims of simplicity in operation, milder condition, and no complicated equipment is required.

4.1.1 Physicochemical and Structural Characterization

4.1.1.1 X-Ray Diffraction (XRD)

X-ray diffraction (XRD) is an important analysis use for revealing the chemical characteristic of the bulk crystalline phases and crystallite sizes of nanocellulose. **Figure 4.1** shows the XRD diffraction patterns of α-cellulose and yielded nanocellulose obtained by using different transition metal based catalysts. The nanocellulose products showed similar diffraction patterns to its cellulose material, with diffraction peaks at 2θ = 16.5, 22.5, and 34.6°, which was attributed to the cellulose *I* structure (Yahya, Lee, & Hamid, 2015). This suggested that the crystal structure of yielded nanocellulose products remain unchanged after catalytic acid hydrolysis reaction. On the other hand, the peak intensity of nanocellulose at 2θ = 22.5° gradually increased as compared with cellulose, which indicated the successive removal of amorphous regions and leads to the exposure of cellulose crystallite segments.

Previous studies have been reported that transition metal salts rendered a positive effect on cellulose degradation, however, the catalytic effect of each transition metal ion is dissimilar, which resulted in differing hydrolysis efficiency for cellulose depolymerization during nanocellulose production. Thus, the catalytic screening of cellulose hydrolysis experiments are conducted at same reaction conditions, in order to focus on the catalytic activity of transition metal based catalyst only. Crystallinity index

of nanocellulose is the main factor affecting its mechanical strength in the polymer matrix (Chirayil et al., 2014). Based on the XRD results summarized in **Table 4.1**, the nanocellulose crystallinity (61.1 to 75.6%) increased significantly compared to that of α-cellulose (43.7%). The increment is mainly attributed to the transition metal ion was capable of hydrolyzing and degrading the cellulose amorphous domains (disordered structure) without damaging the crystalline phases (well-organized structure) into unfavorable reducing sugar product (glucose).

Table 4.1: CrI values of α-cellulose and yielded nanocellulose products.

Nanocellulose product	CrI value (%)	Yield[#] (%)
α-cellulose	43.7 ± 0.3	n/a
Dilute acid treated	61.1 ± 0.2	87.8 ± 0.3
Co(II)-treated	66.4 ± 0.4	85.8 ± 0.6
Ni(II)-treated	69.8 ± 0.6	85.3 ± 0.1
Mn(II)-treated	72.3 ± 0.4	85.0 ± 0.5
Fe(III)-treated	74.1 ± 0.2	84.1 ± 0.2
Cr(III)-treated	75.6 ± 0.1	83.5 ± 0.6

#Reaction conditions: temperature, 80 °C; time, 45 min; concentration of H_2SO_4, 4 wt%; concentration of metal salt catalyst, 25 mM

A comparison study by using conventional H_2SO_4 hydrolysis was carried out under the same experimental conditions at reaction temperature (80 °C), reaction time (45 min) and H_2SO_4 concentration (4 wt%), which the experiment was performed without the presence of any transition metal based catalyst. Based on the result, the crystallinity of nanocellulose obtained was only 61.1%, which relatively lower as compared with the transition metal ion assisted H_2SO_4 treated nanocellulose products. This finding further confirmed that the transition metal based catalyst was capable of enhancing the hydrolysis efficiency. Also, this result suggested that dilute acid alone was not sufficient to degrade the amorphous regions and to selectively break down the strong intra- and intermolecular hydrogen bonding in cellulose fibers. In fact, the dilute acid alone is only expected to swell and open up the cellulose fibers without hydrolyzing it

under low severity operating conditions (Kopania, Wietecha, & Ciechańska, 2012). This is in agreement with the observation that has been reported by Li's recent work (Li et al., 2013).

In summary, Cr(III)-transition metal based catalyst rendered the highest capability in preparing the highest crystallinity of nanocellulose (75.6%). For end-product development, the crystallinity of nanocellulose is the important criteria to be considered by industrial applications as it could provide the better mechanical properties and higher tensile strength which is beneficial for nanocomposite applications (Yahya, Lee, & Hamid, 2015). In addition to that, Silvério et al. reported that crystallinity of nanocellulose has a greater influence on the reinforcing properties of nanocomposites than that of its aspect ratio (Silvério et al., 2013).

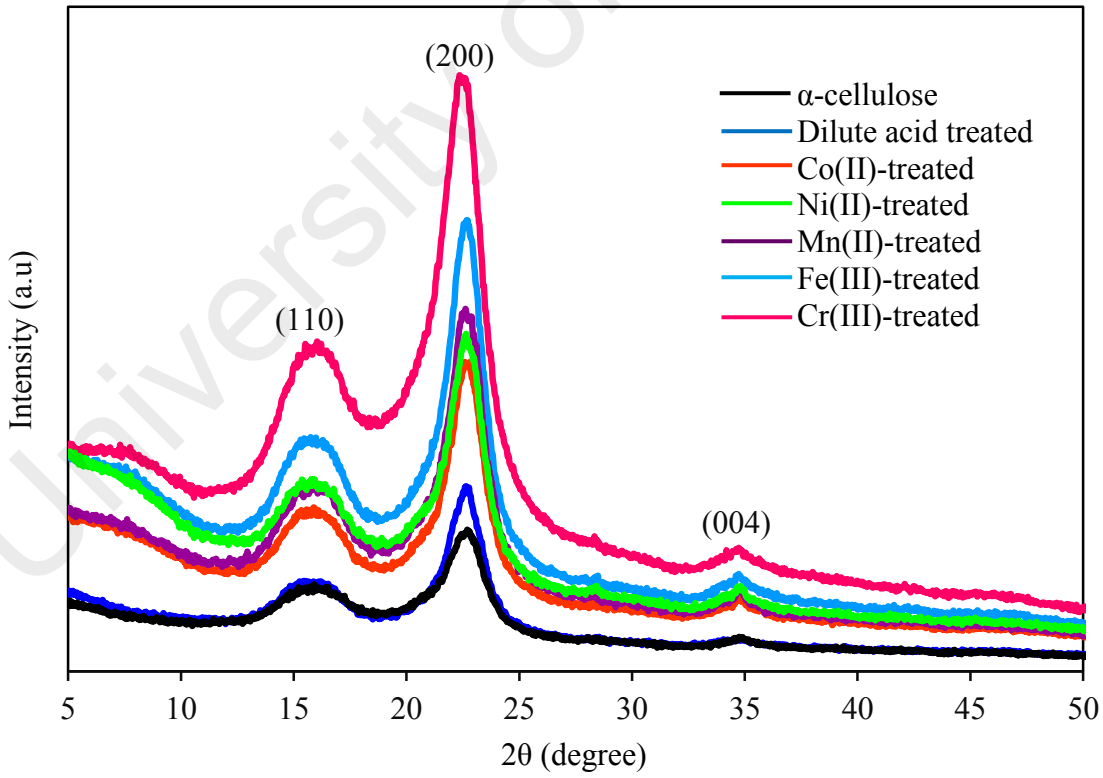

Figure 4.1: XRD patterns of α-cellulose and nanocellulose prepared by dilute acid (H_2SO_4) and different transition metal based catalysts.

In a practical manufacturing process, the yield of nanocellulose obtained after the hydrolysis treatment should take into account in order to optimize the large-scale production with maximum product. Therefore, a compromise should be made between the nanocellulose yield and its crystallinity index to the maximum range. Based on the results, the yield of nanocellulose produced was ranged from 83.5 ± 0.6 to 87.8 ± 0.3 %, as listed in **Table 4.1**. This result is in agreement with those reported for palm biomass derived cellulose (84%) (Hamid et al., 2014) and microcrystalline cellulose (86%) (Karim et al., 2014). They utilized $FeCl_3$ assisted HCl as acidic medium under temperature at 91–98 °C with hydrolysis duration of 4–6 h. Besides that, the nanocellulose prepared via transition metal based catalyzed hydrolysis under milder conditions could gain much higher than the amount reported by others that using concentrated H_2SO_4 as hydrolysis agent. The hydrolysis of cellulosic materials including rice straw cellulose (16.9%) (Jiang & Hsieh, 2013), microcrystalline cellulose (28.6%) (Zhou, 2012), and bamboo bleached fiber (30%) (Brito et al., 2012) via H_2SO_4 (65 wt%) hydrolysis procedure rendered nanocellulose yield with lower amount.

In this study, the yielded nanocellulose prepared via transition metal based catalyzed acid hydrolysis shown higher crystallinity than that of nanomaterial-derived from different biomasses. Son and his coworker conducted a study by preparing the nanocellulose from three major cellulose sources (wood, non-wood and marine pulp) via strong sulfuric acid hydrolysis, and the results revealed that all the yielded nanocellulose (*i.e.* softwood, hardwood; cotton linters, cattail; and red algae) exhibited lower crystallinity (ranged from 61.5–71.7%) (Son & Seo, 2015). This finding suggested that concentrated acid hydrolysis has the high tendency to attack the highly crystalline regions and is accompanied by over-degradation, such that most of the cellulose polymeric chains tended to be solubilized into water soluble reducing sugar

(glucose). This eventually lowers the quality of nanocellulose. A similar study has been reported by Hu et al. in which the authors had proposed two different isolation methods (APS oxidative and H_2SO_4 hydrolysis) for nanocellulose production derived from borer powder. The crystallinity index of both nanocellulose samples was 62.75 and 69.84%, respectively (Hu et al., 2014). The low crystallinity might be due to the harsh conditions applied during the course of treatment.

4.1.1.2 Field Emission Scanning Electron Microscopy (FESEM)

Scanning electron microscopy images of the cellulose and transition metal-treated nanocellulose are shown in **Figure 4.2**. The cellulose material mostly consisted of aggregated long fibrils with an irregular shape (**Figure 4.2a**). In addition, the compact structure of each cellulose fiber appeared to be assembled from hundreds to thousands of microfibrils, and each cellulose fiber was quite long and thus had a low aspect ratio (Tan, Abd Hamid, & Lai, 2015). For transition metal salt-treated nanocellulose, as displayed in **Figure 4.2(c–g)**, it can be clearly observed that the original cellulose fibers were broken down and degraded to a great extent after hydrolysis treatment, which led to the long ribbon-like quality of the original fiber turning into short, rod-like structures.

The micro-sized cellulose fibrils tended to separate from the fibers bundles, which resulted in the intermittent breakdown in its fibrillar structure with more individualized, smaller fragments. These findings are in excellent accordance with the reported literature (Qua et al., 2011). The yielded nanocellulose produced in this study showed a smaller fibrillar structure and reduced fiber diameter compared with α-cellulose. This was accredited to the successive hydrolysis treatment catalyzed by transition metal based catalyst with degradation of defective crystalline regions via metal ions attack and lead to the hydrolytic cleavage of glycosidic linkages of cellulose chains. On the other hand, the

nanocellulose hydrolyzed by dilute H_2SO_4 seems like appeared in larger diameter compared with transition metal treated nanocellulose (**Figure 4.2b**). It could be due to dilute H_2SO_4 was not capable of degrading the cellulose amorphous regions effectively.

In the present analysis, the finer and shorter nano-dimensional fibrils of nanocellulose samples were expected to be observed from FESEM images. However, the present results were not clearly indicated the nanosized of products. This was due to the strong intermolecular hydrogen bonding within the cellulose chains, which the cellulosic fibrils tend to agglomerate during the lyophilizing process (Qua et al., 2011). More insight study on the particle size and morphology of the nanocellulose fibers was further obtained through transmission electron microscopy (TEM) and atomic force microscopy (AFM) analyses.

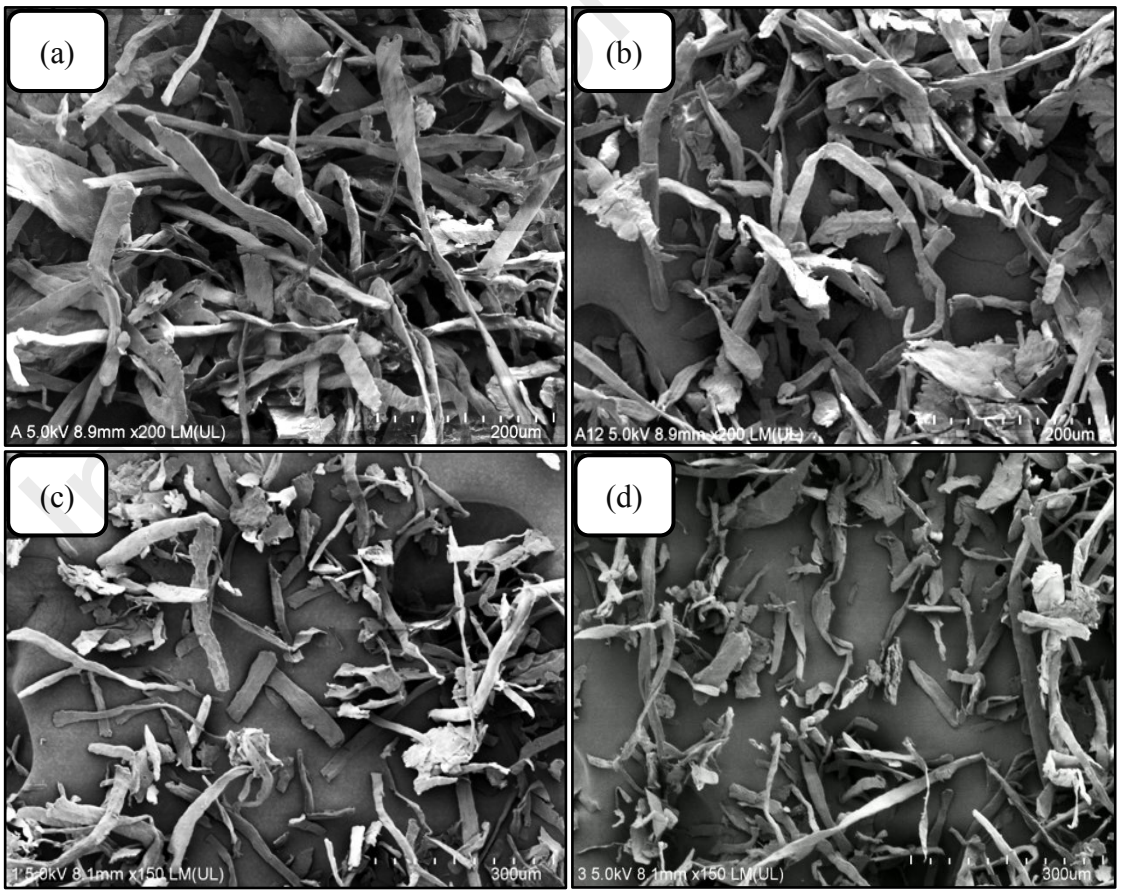

Figure 4.2: FE-SEM images of (a) α-cellulose and nanocellulose treated by (b) dilute acid, (c) Co(II)-, (d) Ni(II)-, (e) Mn(II)-, (f) Fe(III)-, and (g) Cr(III)-metal ion catalyst.

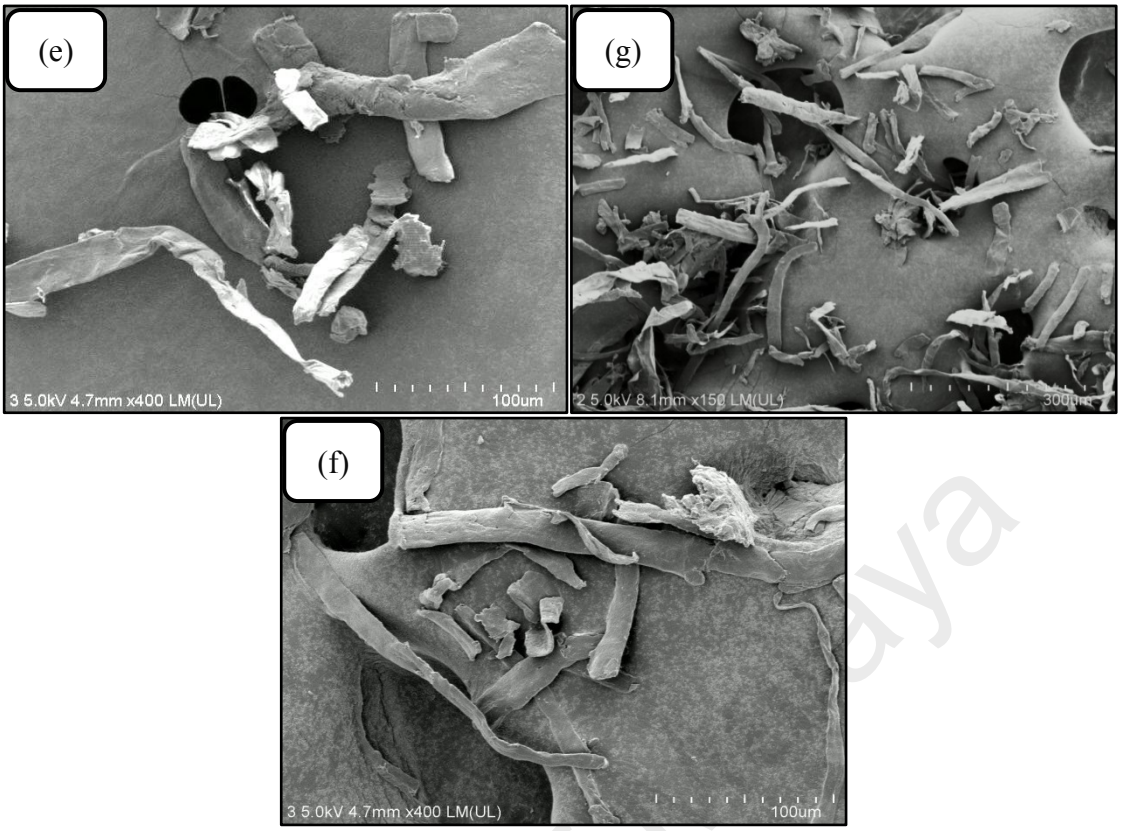

Figure 4.2: Continued.

4.1.1.3 Transmission Electron Microscopy (TEM)

The dimensional profile of prepared nanocellulose was further studied via TEM analysis. As shown in **Figure 4.**3, TEM images of the yielded nanocellulose via transition metal catalyzed hydrolysis pathways formed an entangled, complex spider-like geometry with the presence of porous structures. From the results, it was clearly confirmed that transition metal-catalyzed acid hydrolysis effectively hydrolyzed the micro-dimensional cellulose fiber into the nanometer scale. Based on the TEM micrographs, it was shown that all the yielded nanocellulose fibers shown the diameters less than 100 nm, which mostly ranging between 18.4 ± 6.1 and 31.6 ± 14.4 nm, whereas dilute acid-treated nanocellulose consisted of an average diameter range 59.4 ± 29.6 nm with several microns long. Upon treatment, the micron size of cellulose microfibrils could eventually reduce to its nanoscale scale cellulose fibers via transition metal based catalyzed acid hydrolysis system. The smaller diameter of nanocellulose

indicated that transition metal based catalyst efficiently in depolymerization process of cellulose by attacking the glycosidic linkage of defective crystalline parts at a faster rate than the crystallinity phases, as there are more active sites for chemical reactions to happen.

Additionally, some agglomerated nanocellulose fibrils was observed in TEM images, while the rest are well dispersed. Similar phenomenon was reported by Chirayil's group for the preparation of cellulose nanofibrils from *Helicters isora* via acid hydrolysis (Chirayil et al., 2014). On the other hand, the entanglement structure among the yielded nanocellulose played an important role in force transferring from either fibril to fibril or matrix to fibril to form a strong reinforcement when blended with other polymer materials (Tian et al., 2016). However, the present structure resulted in the limitation of fibers length measurement, as the fibers end is interconnected with each other in network form. It is a common phenomenon reported by many previous studies (Goh et al., 2016; Kargarzadeh et al., 2012; Lu & Hsieh, 2012).

As shown in **Figure 4.3**, each nanocellulose sample rendered the difference of particle diameter distribution. It can be found that trivalent metal salt catalyst (Fe^{3+} and Cr^{3+}) treated nanocellulose possessed of more individual and finer fibers as compared to that of the nanocellulose samples treated with dilute acid and divalent state metal salt catalysts. The homogeneity/uniformity of nanocellulose products in this study was differed, this mainly due to the effectiveness of transition metal based catalyst used for cellulose hydrolysis process. For an effective hydrolyzing catalyst, the cellulose depolymerization process can occur effectively, and the obtained nanocellulose rendered a smaller diameter range.

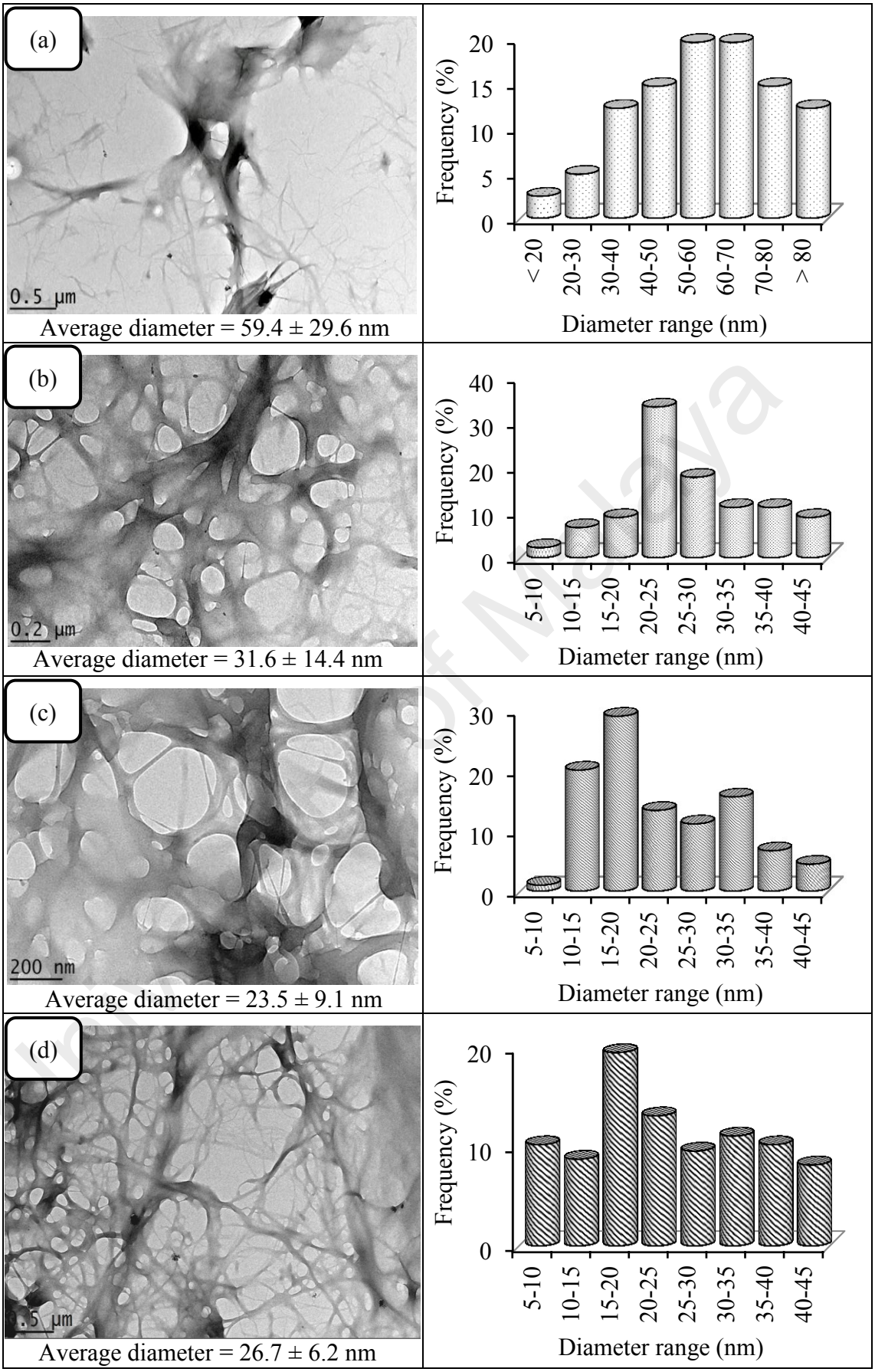

Figure 4.3: TEM images of nanocellulose treated by (a) dilute acid, (b) Co(II)-, (c) Ni(II)-, (d) Mn(II)-, (e) Fe(III)-, and (f) Cr(III)-metal ion catalyst.

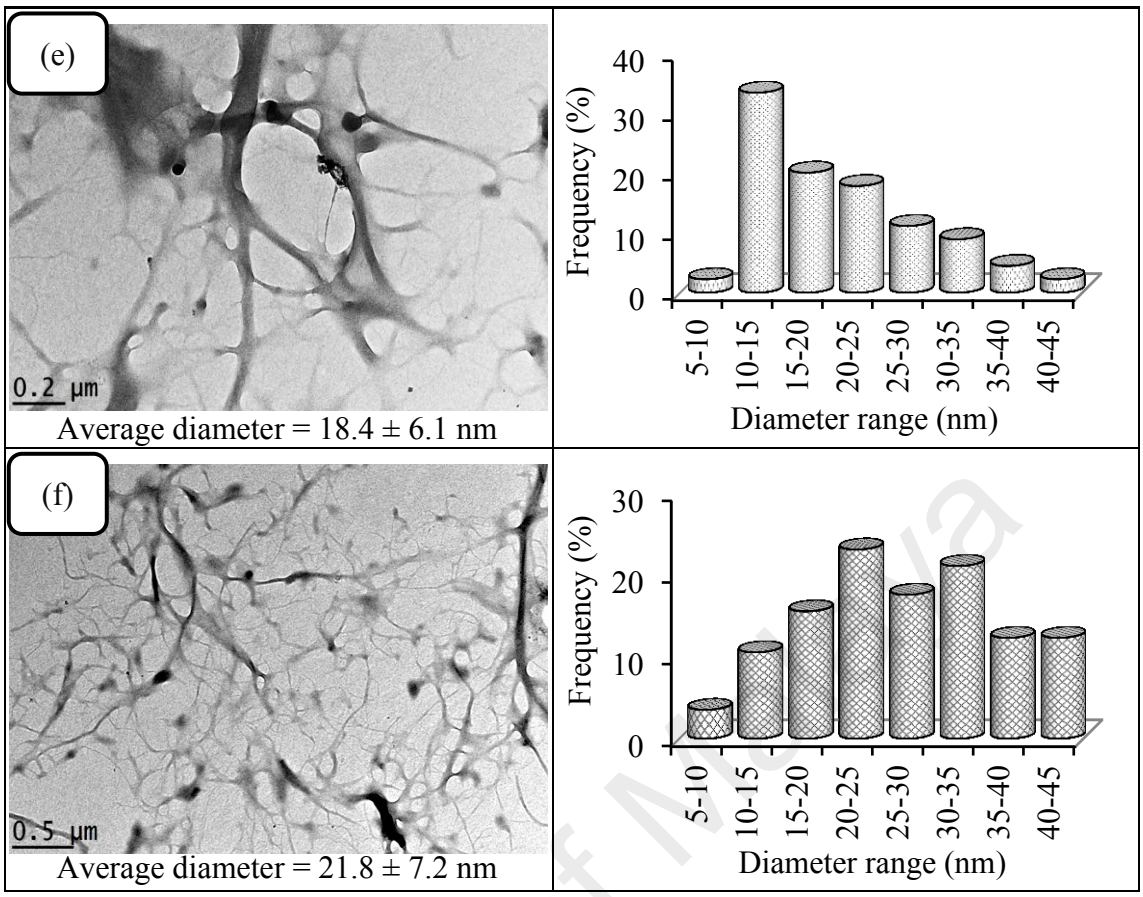

Figure 4.3: Continued.

4.1.1.4 Atomic Force Microscopy (AFM)

Based on the AFM analysis, the whisker nature of the yielded nanocellulose was clearly presented in **Figure 4.4**. This indicated that the transition metal based treatment successfully isolated rod-like nanocellulose from the micro-dimensional cellulose fibers. The current explanation for the process of catalytic acid hydrolysis of cellulose is that it involves the diffusion of acid into the cellulose fiber and subsequently undergoes hydrolytic cleavage of glycosidic bonds by hydronium ions as well as attacked by transition metal ions, transforming the microfibrils into short nanocrystals. However, these steps depend on the reactivity of the transition metal based catalyst (Li et al., 2013).

Atomic force microscopy was used to study detailed nanostructure of the nanomaterial. Results revealed that Fe(III)-treated nanocellulose rendered the smallest fibers diameter as compared to other transition metal salt-treated products. This shown that Fe(III) transition metal assisted H_2SO_4 catalyzed hydrolysis has a greater effect in selectively solubilized amorphous regions in cellulose fibers as compared to other hydrolysis catalysts. In contrast, dilute H_2SO_4 acid treated fiber showed larger fibers size with the average diameter of 308.98 ± 206.60 nm. These results clearly indicated that hydrolysis process with H_2SO_4 without the presence of transition metal base catalyst was not sufficient to isolate nanocellulose from micro-sized fibers completely. The AFM results further confirmed that transition metal catalyzed acid hydrolysis able to break the glycosidic linkages inside the cellulose matrix, mainly in defective amorphous parts, and leads to the gradual disintegration of the micro-scale cellulose fibers into nano-sized cellulose. **Table 4.2** summarizes the dimensional profile of nanocellulose hydrolyzed by difference catalysts. Basically, each transition metal based catalyst has different hydrolyzing ability towards the cellulose depolymerization process. In this study, Cr(III)-transition metal based catalyst treated nanocellulose rendered the smallest average particle width (64.1 ± 31.7 nm) amongst the other nanocellulose products. This was accredited to the successive dilute acid hydrolysis treatment catalyzed by Cr(III)-based catalyst.

Table 4.2: Dimensional profile of nanocellulose samples determined from AFM.

Nanocellulose sample	Average width (nm)
Cr(III)-treated	64.1 ± 31.7
Mn(II)-treated	80.9 ± 30.3
Fe(III)-treated	82.6 ± 21.5
Ni(II)-treated	160.7 ± 51.9
Co(II)-treated	288.1 ± 60.6
Dilute acid treated	308.98 ± 206.6

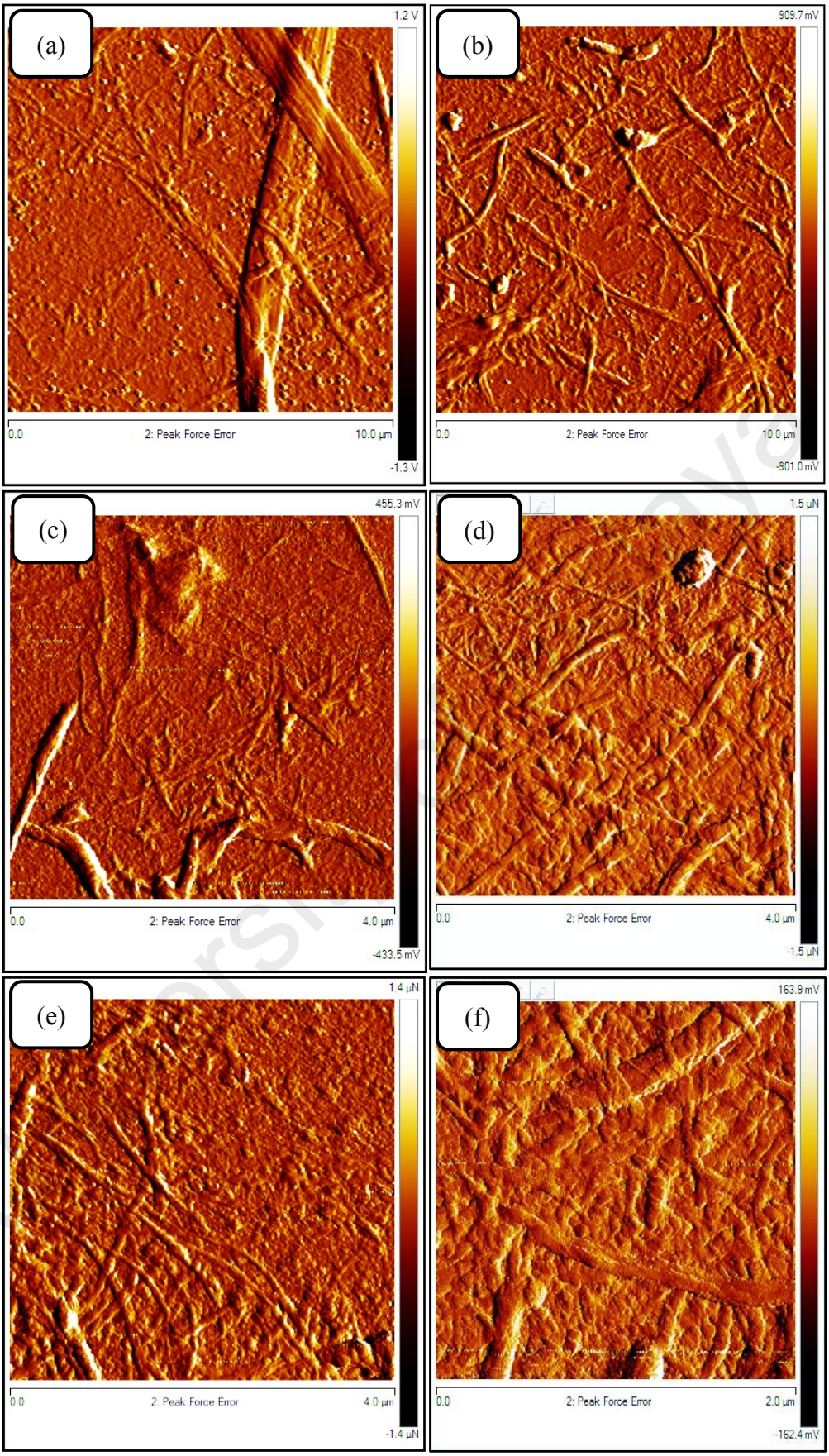

Figure 4.4: AFM micrographs of nanocellulose hydrolyzed by (a) dilute acid, (b) Co(II)-, (c) Ni(II)-, (d) Mn(II)-, (e) Fe(III)-, and (f) Cr(III)-transition metal ion catalyst.

4.1.1.5 Fourier Transform Infrared Spectroscopy (FTIR)

FTIR spectroscopic analysis of the α-cellulose and chemically-treated nanocellulose samples is shown in **Figure 4.5**. The presence of the main peak at 3400 cm^{-1} was attributed to the O–H stretching band, which resulted by the hydrogen bonded hydroxyl group vibrations of cellulose *I* (Yahya, Lee, & Hamid , 2015). In addition, the peak at 2900 cm^{-1} corresponded to the aliphatic saturated symmetric C–H stretching vibration in cellulose (Hamid et al., 2015). The absorption peaks observed at 1640 and 1375 cm^{-1} were caused by the O–H bending mode of absorbed water and C–H bending within the polysaccharide aromatic rings of cellulose, respectively (Tan, Abd Hamid, & Lai, 2015). FTIR peaks at 1430 cm^{-1} (CH_2 scissoring motion in cellulose), 1161 cm^{-1} (C–C ring stretching band), 1110 cm^{-1} (C–O–C pyranose ring stretching vibration), and 898 cm^{-1} (β–glycosidic linkages of cellulose glucose ring) were indicated as the typical bonds of cellulose I_β structure (Kumar et al., 2014). As also illustrated in **Figure 4.5**, similar FTIR patterns were found for all the produced nanocellulose, which indicated that the chemical structures of nanocellulose were not altered after the transition metal catalyzed hydrolysis process, where the typical structure of the parent cellulose was being preserved (Tan, Abd Hamid, & Lai, 2015). When transition metal ions adsorbed on nanocellulose surface, the wavenumbers of the functional groups will be shifted (Singha et al., 2011). However, the wavenumber of the prepared nanocellulose remained similar position as α-cellulose; this suggested that there is no any metal ion introduced to the surface of the nanocellulose fiber. Furthermore, the absence of NO_3^- peak (as nitrate salt) at the signal of 1384 cm^{-1} indicated that the transition metal salt was completely removed during the centrifugation washing and dialysis process (Yahya, Lee & Hamid, 2015).

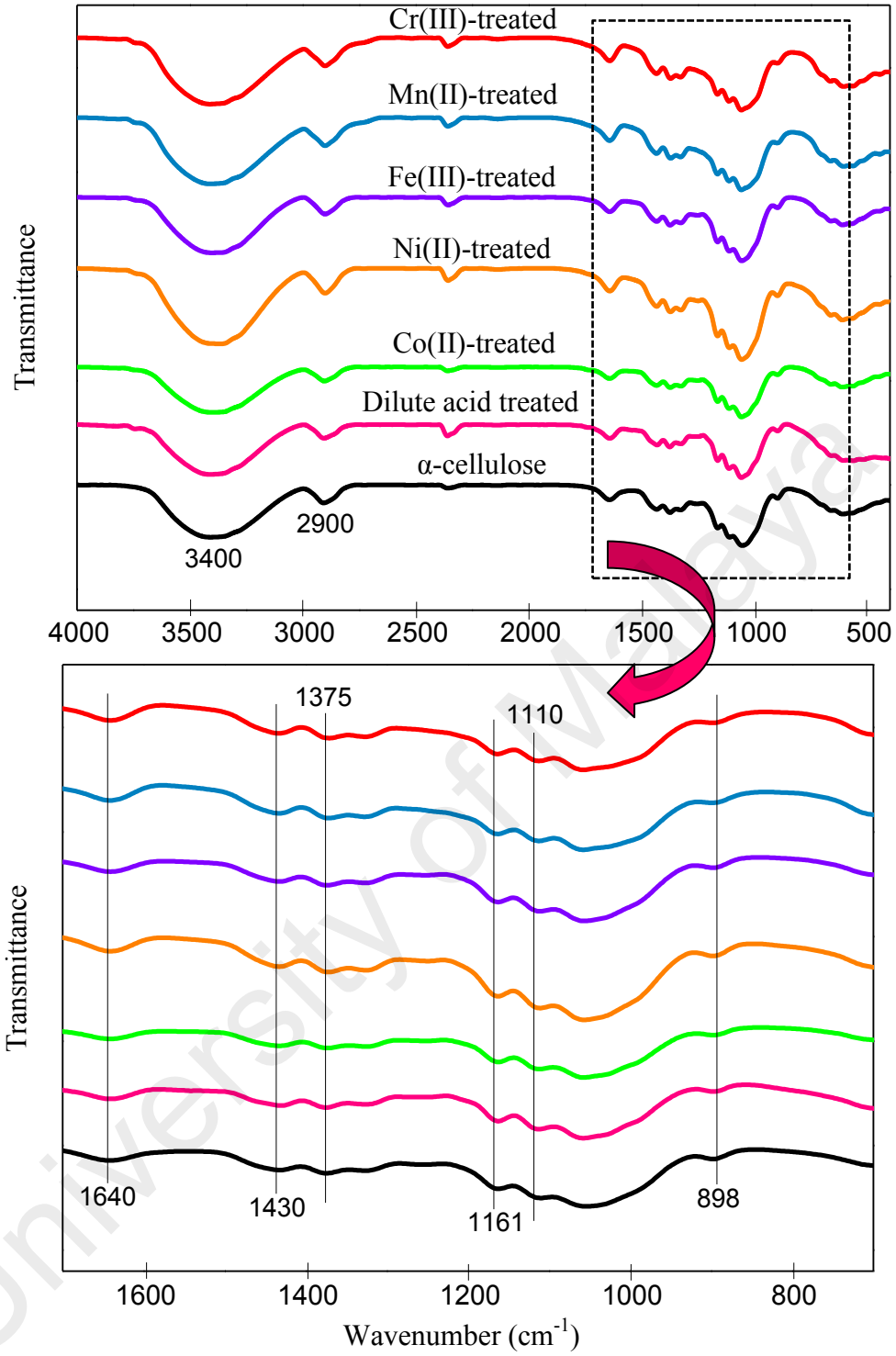

Figure 4.5: FTIR spectra of α-cellulose and yielded nanostructured cellulose treated by different hydrolyzing catalysts.

4.1.1.6 Thermogravimetric Analysis (TGA)

Thermogravimetric (TG) curves and their derivatives (DTG) for cellulose and nanocellulose products are shown in **Figure 4.6**. A minor weight loss that was found for all samples below 100 °C can be attributed to the evaporation of absorbed moisture from the surroundings of the fiber. The α-cellulose showed a typical decomposition behavior with an onset degradation temperature (T_{on}) of 250 °C and a maximum thermal degradation temperature (T_{max}) of 354 °C. The decomposition of the α-cellulose showed only the one-step pyrolysis process, as shown in the DTG curve.

In the case of the produced nanocellulose, the degradation process occurred within a narrower range with lower T_{max} value (331–346 °C) as compared with α-cellulose. It was found that all the yielded cellulose nanoparticles possessed lower T_{max} values. Reduction in thermal stability for yielded nanocellulose was due to several reasons: (i) introduction of active sulfate groups (from H_2SO_4) into the crystals of nanocellulose during the hydrolysis reaction resulted in catalytic effect on the thermal degradation process (Cheng et al., 2014); (ii) higher surface area of yielded product in nano-dimensions leads to higher exposure of fiber toward heat energy applied, thus give rise to faster degradation step as compared to macro-sized cellulose (Tan, Abd Hamid, & Lai, 2015); (iii) increase amount of shorter nanocellulose chains resulted in lower decomposition temperature for free end chains (Kargarzadeh et al., 2012). A similar phenomenon was reported by Saelee's group, where the production of cellulose nanofibrils from sugarcane bagasse via high-pressure homogenization resulted in higher number of contact points that favor to the heating source as compared with crude cellulose (Saelee et al., 2016).

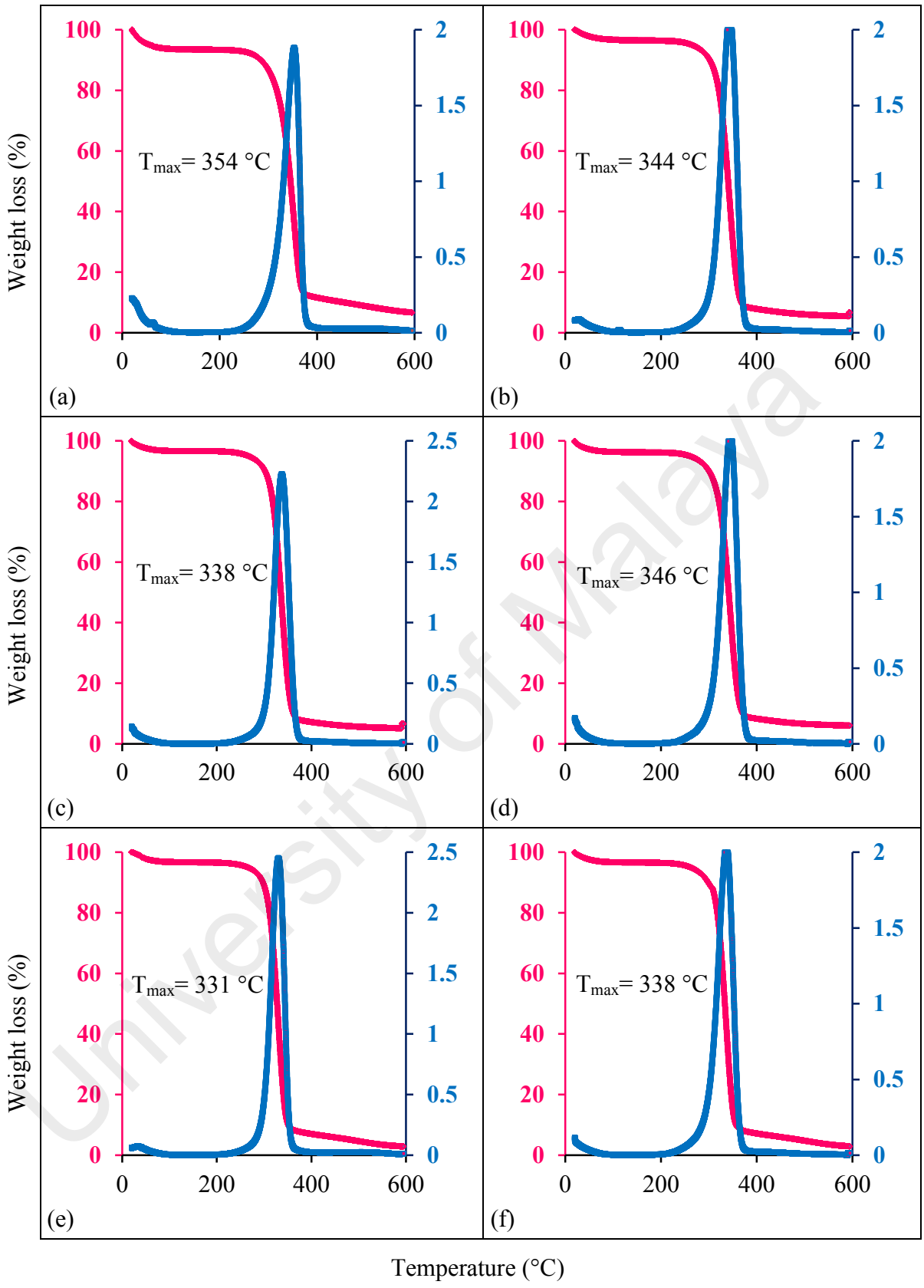

Figure 4.6: TG and DTG curves of (a) α-cellulose and nanocellulose hydrolyzed by (b) Co(II)-, (c) Ni(II)-, (d) Mn(II)-, (e) Fe(III)-, and (f) Cr(III)-transition metal based catalyst.

In addition, the present finding was similar to several studies listed in **Table 4.3**, where the T_{max} value of yielded nanocellulose obtained from various biomass sources rendered lower values than that of crude cellulose material. Fortunately, all the cellulose nanoparticles were stable when the heating temperature was less than 280 °C. This is an important factor for the usage of nanocellulose in various industrial applications, especially the thermoplastics field, as the processing temperature is normally above 200 °C (Cheng et al., 2014). Therefore, the thermal resistance of all the nanocellulose remained sufficient to ensure that nanocellulose can be processed at approximately 200 °C without any risk of degradation. As comparison, concentrated H_2SO_4-treated cellulose nanoparticles exhibited lower thermal stability (150–200 °C) due to the presence of more sulfate groups (Cheng et al., 2014). This behavior was attributed to that the sulfate groups in the nanocellulose fibers tend to play the role of flame retardant by promoting the dehydration reactions, which is conducive to the production of anhydrocellulose and leads to its decomposition to carbonaceous residues, as reported by other authors as Mohamed and his group (Mohamed et al., 2015).

Table 4.3: Thermal properties of cellulosic nanomaterials extracted from various starting materials.

Starting materials	T_{max} (°C)		Hydrolysis method	Reference
	Cellulose	Nanocellulose		
Wheat straw	337.5	332.2	Ultrasonic treatment	(W. Chen, Yu, Liu, Hai, et al., 2011)
Empty fruit bunches	340.0	339.0	Chemo-mechanical	(Jonoobi et al., 2011)
Mulberry bark	397.0	335.0	H_2SO_4 hydrolysis	(R. Li et al., 2009)

4.1.2 Effect of Transition Metal Ion on Acid Hydrolysis Efficiency

Transition metal ions such as Mn^{2+} and Cr^{3+} showed a similar acid hydrolysis mechanism as an inorganic acid for the depolymerization of cellulose fibers. During the typical acid hydrolysis, protons (hydronium ion; H_3O^+) generated from mineral acids (HCl or H_2SO_4) are involved in weakening the bond energy in the cellulose chains by attacking the oxygen electrons from β-1,4-glycosidic linkages between glucose rings, thus triggering the rupture of chemical bonds inti smaller fractions. Compared with single-charge protons (+1), transition metal ions with higher valence states (+2 and +3) were more effective in hydrolytically cleavage of the extensive bonding network of the cellulose chains. This is due to the presence of excessive valence electron from cation, which generate more positive charge and pair with more oxygen atoms to enhance hydrolytic efficiency for nanocellulose production (Zhao et al., 2011).

Furthermore, the metal ions were able to attack oxygen atom with high electronegativity and polarity, which located in the cellulose anhydroglucose unit to form a cellulose-metal ion complex (Zhao et al., 2011). By owning the absorbed metal ions, the bond strength between pyranose rings was weakened by increasing the bond length and bond angle of the intermediate complex. This interaction resulted to the breakage of hydrogen bonding in the cellulose matrix and led to the separation of cellulose fibrils into smaller fiber fragments accompanying by reducing its particle size and improve the degree of depolymerization (J. Li et al., 2014). Consequently, the weakening of C–O–C bonding enhanced the cleavage of the glycosidic linkages and lowered the activation energy of the hydrolysis process (Hamid et al., 2014; Karim et al., 2014). Thus, this process helps to reduces and refined the cellulose fiber into nano-dimension.

Beside the above mentioned advantages, the presence of transition metal ion with several valence electrons could further enhance the efficiency of acid hydrolysis by creating more acidic reaction conditions. It is known that the efficiency of hydrolytic depolymerization of cellulose highly depends on the acidity of the reaction system, where the cellulose is preferable to be degraded under lower pH or higher acidity conditions. The possible mechanism is that the transition metal ion is able to form the metal-ligand complex ions in the presence of an aqueous solvent, such as water, via the formation of coordination covalent bonding with six H_2O molecules. Afterward, the metal-ligand complex ions were deprotonated to yield more H_3O^+ ions in the reaction mixture. This deprotonation process attributed to the increment of H_3O^+ concentration in the solution, thus the glycosidic linkages bonds between the glucose units along the cellulose chain were degraded effectively (Tan, Abd Hamid, & Lai, 2015; Zhao et al., 2011). This process will continue until the metal complex becomes stable. In fact, the oxidation state (valence state) of transition metal ions plays an important role to generate acidic environment. When the metal ion possessed of higher oxidation state, more H_3O^+ would be generated in order to produce a stable complex. This explanation is in good agreement with Li et al.'s recent study (Li et al., 2013) in which the metal ions were tended to be more acidic when they bonded with water, rather than the metal ion alone. Hence, trivalent state (+3) metal ions (Fe^{3+} and Cr^{3+}) is able to produce the higher concentration of H_3O^+ ions as compared with the divalent state (+2) metal ions (Co^{2+}, Ni^{2+} and Mn^{2+}), as shown in **Equations [4.1–4.5]**.

$$[Fe(H_2O)_6]^{3+} + 3\ H_2O \rightarrow [Fe(H_2O)_3(OH)_3] + 3\ H_3O^+ \quad \textbf{[Equation 4.1]}$$

$$[Cr(H_2O)_6]^{3+} + 3\ H_2O \rightarrow [Cr(H_2O)_3(OH)_3] + 3\ H_3O^+ \quad \textbf{[Equation 4.2]}$$

$$[Co(H_2O)_6]^{2+} + 2\ H_2O \rightarrow [Co(H_2O)_4(OH)_2] + 2\ H_3O^+ \quad \textbf{[Equation 4.3]}$$

$$[Mn(H_2O)_6]^{2+} + 2\ H_2O \rightarrow [Mn(H_2O)_4(OH)_2] + 2\ H_3O^+ \quad \textbf{[Equation 4.4]}$$

$$[Ni(H_2O)_6]^{2+} + 2\ H_2O \rightarrow [Ni(H_2O)_4(OH)_2] + 2\ H_3O^+ \quad \textbf{[Equation 4.5]}$$

In 2016, a study reported by Iris et al. found that the difference in performance given by the tested catalysts was correlated with the ionic radius and ionic charge, which were indicative of the binding abilities of metal catalysts (Iris et al., 2016). The promising catalysts of Fe^{3+} and Cr^{3+} are trivalent metals with relatively small effective ionic radius (65 and 62 μm, respectively), resulting in high charge density and strong electrostatic force that favors the coordination of ionic character (Iris et al., 2016). In fact, it was believed that the Cr^{3+} possessed of better hydrolytic efficiency than Fe^{3+} attributed to its smaller ionic radius and better stabilization of the transition state by Cr as a Lewis acid center. This result was in consistence with the previous finding (Wang, Glasper, & Shanks, 2015).

4.1.3 Summary of Catalytic Screening

Dilute acid has been proven to be an effective, simple and effective method for the treatment of the cellulosic sources under milder condition as compared to strong acid hydrolysis. However, dilute acid treatment alone unable to provide a satisfactory economic feasibility due to high temperature or longer hydrolysis period is required to complete the process. In order to enhance the efficiency of the dilute acid process, addition of transition metal based catalyst with the presence of dilute acid was able to create a synergistic effect for selective hydrolysis reactivity. However, not all type of transition metal based catalysts can effectively function in the cellulose depolymerization process. Theoretically, the catalytic system initiated by higher valence state metal ions was able to create stronger hydrolysis efficiency towards the dissolution of cellulose due to lower pH (*i.e.* higher acidity) of reaction medium. The presence of high acidity was due to the generation of a high concentration of H_3O^+ ions in aqueous medium, which beneficial in hydrolyzing the C–O–C bonding in the cellulose matrix.

There are several authors (X. Cao et al., 2015; Peng et al., 2010) reported the major roles of transition metal based catalysts in the cellulose depolymerization process.

A key attribute of nanocellulose is their crystallinity index (CrI). It is a parameter has been widely used to describe the relative amount of crystalline material in cellulose macromolecules (Park et al., 2010). CrI value is an important material characteristic that significantly influences their potential as reinforcing agents for industrial applications, especially nanocomposites, thermoplastics and polymer matrix, and thus affect the composite end-properties (Moriana, Vilaplana, & Ek, 2016). This is because of the high crystallinity index offers a high modulus of elasticity and better reinforcement capability, and makes them as an ideal candidate for polymer synthesis (Silvério et al., 2013). Also, the crystal structure of nanocellulose has been considered as a significant impact to enhance the thermo-mechanical properties as well as the thermal stability of final yielded polymeric composite materials (Goh et al., 2016). Consequently, the crystallinity of nanocellulose is used as evaluation index to evaluate the hydrolysis efficiency of different transition metal salts on the physicochemical properties changes of cellulose.

As we can observe in the XRD spectra of yielded nanocellulose in **Table 4.1**, it clearly indicates that all of the five transition metal based catalyst, namely Fe(III), Co(II), Ni(II), Cr(III) and Mn(II) nitrate salt rendered positive effect for the crystallinity index of nanocellulose. However, the degree of hydrolysis of each catalyst towards the conversion and selectivity of the crystalline product are difference. This suggested that the different transition metal ion could accelerate the dissolution of amorphous regions in cellulose fibers at varying degrees. Among the catalysts, Cr(III)-ion shown a promising effect towards the cellulose conversion, which 31.9% increment of

crystallinity index for Cr(III)-treated nanocellulose as compared with α-cellulose. The result indicated that the use of Cr(III)–transition metal based catalyst with the presence of dilute H_2SO_4 rendered better hydrolytic efficiency on the destruction of glycosidic linkages of defective regions in cellulose chains. Hence, Cr(III)-based transition metal was chosen as the most suitable hydrolyzing catalyst for further study in our current research. To obtain the highest possible nanocellulose crystallinity index and product yield, it is required to optimize the reaction parameters by varying the concentration of hydrolyzing catalysts (namely Cr(III)-transition metal based catalyst and H_2SO_4), reaction time and reaction temperature, and the results are further discussed in the following sections.

In this section, three conclusions could be obtained: (1) all five transition metal salts have significantly higher effects on the cellulose depolymerization compared to dilute acid alone; (2) The hydrolysis efficiency of trivalent state metal ions (Fe^{3+}, Cr^{3+}) is much higher than that of divalent state ions (Co^{2+}, Ni^{2+}, Mn^{2+}); and (3) The effect of Cr(III) ion is higher than that of Fe(III), which is consistent with the result by (Peng et al., 2010)

4.2 Optimization Study of Nanocellulose Production by using Response Surface Methodology (RSM)

In the present work, we investigated the interaction effect of hydrolysis parameters on the production of nanocellulose from cellulosic material by using Cr(III)-transition metal assisted dilute H_2SO_4 hydrolysis process. Thus, optimization study by using five-level, four-factor central composite design coupled with response surface methodology (CCD-RSM) experimental design in order to investigate the individual and interactive effects of hydrolysis parameters towards the nanocellulose crystallinity index and

product yield. Four independent parameters, namely reaction temperature, reaction time, concentration of Cr(III)-transition metal based catalyst, and concentration of H_2SO_4 were chosen to investigate their synergism effect towards the crystallinity index and yield of nanocellulose. The optimization study for nanocellulose production is essential for industrial scale application in order to develop an economically feasible process for high quality and quantity product.

4.2.1 Model Selection and Statistical Analysis

Two regression models describing the nanocellulose yield and crystallinity index were developed. The statistical significance of the model terms was determined by analysis of variance (ANOVA). The responses were crystallinity index and yield of nanocellulose, as determined by the CCD design (**Table 3.2**). Based on the results, nanocellulose prepared via Cr(III)-catalyzed hydrolysis of cellulose rendered the nanocellulose crystallinity (y_1) ranged from 60.38 to 88.93%, and the product yield (y_2) was between 77.19 and 91.02%. The relationship between the crystallinity or nanocellulose yield and the four independent variables was calculated by **Equations [4.6–4.7]**, which are expressed using the coded factors (**Table 3.1**).

Crystallinity index **[Equation 4.6]**

$$y_1 = 82.99 + 3.85\,x_1 + 2.73\,x_2 + 3.66\,x_3 + 5.52\,x_4 + 1.22\,x_1x_2 + 0.25\,x_1x_3 - 0.43\,x_1x_4 + 1.93\,x_2x_3 - 3.13\,x_2x_4 + 0.22\,x_3x_4 - 0.61\,x_1^2 - 1.51\,x_2^2 - 1.74\,x_3^2 - 3.32\,x_4^2$$

Nanocellulose yield **[Equation 4.7]**

$$y_2 = 80.43 - 1.04\,x_1 - 1.06\,x_2 - 1.89\,x_3 - 2.43\,x_4 - 1.06\,x_1x_2 - 0.30\,x_1x_3 - 0.14\,x_1x_4 - 0.16\,x_2x_3 + 0.33\,x_2x_4 - 0.50\,x_3x_4 + 1.21\,x_1^2 + 1.30\,x_2^2 + 1.09\,x_3^2 + 1.14\,x_4^2$$

where y_1 refers to crystallinity index and y_2 is the nanocellulose yield; x_1, x_2, x_3, and x_4 are the independent variables for reaction temperature, reaction time, concentration of Cr(III)-transition metal based catalyst, and concentration of H_2SO_4, respectively.

The regression coefficients of both developed response surface models, corresponding R^2 values, mean, coefficient of variation (CV), and adequate precision are provided in **Table 4.4**. The CV value is the ratio of the standard error of estimate to the mean value of the observed response (as a percentage). It is a measure of reproducibility of the model and as a general rule, a model can be considered reasonably reproducible if its CV is not greater than 10% (Masoumi et al., 2011). It was observed that the CV value for the models of crystallinity index and nanocellulose yield was 5.09 and 2.06, respectively, which implied that there was a high degree of precision and a good deal of reliability of the experimental values in the reaction models. Moreover, the small value of standard deviation (SD) for both responses (y_1 and y_2) at 3.94 and 1.73, respectively, indicated good precision, reproducibility, and reliability of the experimental models (J. Li et al., 2014). The precision of the model reflects the signal-to-noise ratio, and a value larger than 4 is normally desirable (Karim et al., 2014). The obtained precision values of 11.224 and 10.433 for crystallinity index and nanocellulose yield models, respectively. The obtained adequate precision values for both models were well above 4, which indicate an adequate signal, and further suggests that the proposed models can be used to navigate the design space (Mohan, Viruthagiri, & Arunkumar, 2014). On the other hand, the ANOVA for the Cr(III)-transition metal assisted dilute H_2SO_4 hydrolysis model of the response surface of crystallinity index (y_1) and nanocellulose yield (y_2) are shown in **Tables 4.5–4.6**, respectively. Based on the obtained data, the value of probable *F* for both responses, y_1 and y_2, was less than 0.0001. This result was highly significant because it was only a 0.01% chance that a

model F value of this magnitude could occur due to noise (Feng et al., 2015). Furthermore, the prob > F value for the variables (x_1, x_2, x_3, and x_4) in both quadratic models (crystallinity index and nanocellulose yield) was smaller than 0.05, which meant that the model was significant in terms of both responses (y_1 and y_2). In addition, the reaction variable of H_2SO_4 concentration had the greatest effect on both responses, which exhibited the highest F values of 732.21 and 141.68, respectively.

Table 4.4: Statistical parameters for ANOVA analysis of crystallinity index (y_1) and nanocellulose yield (y_2) model regressions.

Statistical Parameters	Crystallinity index, y_1	Nanocellulose yield, y_2
Standard deviation (SD %)	3.95	1.73
R-squared (R^2)	0.9157	0.9138
Mean	77.25	84.21
Coefficient of variation (CV)	5.11	2.06
Adequate precision	11.224	10.433

Table 4.5: ANOVA for the nanocellulose crystallinity index (y_1) regression model.

Source	Sum of squares	Degree of freedom	Mean square	F value	Prob > F
Model	2203.6	14	157.4	10.09	< 0.0001
x_1	356.20	1	356.2	22.83	0.0004
x_2	178.65	1	178.65	11.45	0.0049
x_3	321.51	1	321.51	20.61	0.0006
x_4	732.21	1	732.21	46.94	< 0.0001
x_1x_2	23.86	1	23.86	1.53	0.2380
x_1x_3	0.99	1	0.99	0.063	0.8051
x_1x_4	2.98	1	2.98	0.19	0.6695
x_2x_3	59.83	1	59.83	3.84	0.0720
x_2x_4	156.88	1	156.88	10.06	0.0074
x_3x_4	0.75	1	0.75	0.048	0.8300
x_1^2	10.15	1	10.15	0.65	0.4343
x_2^2	62.39	1	62.39	4.00	0.0669
x_3^2	82.88	1	82.88	5.31	0.0383
x_4^2	302.8	1	302.8	19.41	0.0007

Remark: Prof > F value less than 0.05 designates that model terms are significant.

Table 4.6: ANOVA for the nanocellulose yield (y_2) regression model.

Source	Sum of squares	Degree of freedom	Mean square	*F* value	Prob > *F*
Model	414.36	14	29.60	9.84	< 0.0001
x_1	26.19	1	26.19	8.71	0.0112
x_2	26.88	1	26.88	8.94	0.0104
x_3	85.74	1	85.74	28.52	0.0001
x_4	141.68	1	141.68	47.12	< 0.0001
x_1x_2	17.82	1	17.82	5.93	0.0301
x_1x_3	1.4	1	1.4	0.47	0.5070
x_1x_4	0.33	1	0.33	0.11	0.7456
x_2x_3	0.4	1	0.4	0.13	0.7206
x_2x_4	1.79	1	1.79	0.59	0.4545
x_3x_4	3.97	1	3.97	1.32	0.2714
x_1^2	39.87	1	39.87	13.26	0.0030
x_2^2	46.31	1	46.31	15.4	0.0017
x_3^2	32.33	1	32.33	10.75	0.0060
x_4^2	35.54	1	35.54	11.82	0.0044

Remark: Prof > *F* value less than 0.05 designates that model terms are significant.

Figure 4.7 displays the linear plots of predicted versus actual percentage for the models of crystallinity index and nanocellulose yield. The coefficient of determination (R^2) value should be higher than 0.8000 for a well-fitted model (Hamid et al., 2014). Based on these two plots, the R^2 value of crystallinity index and nanocellulose yield model was 0.9157 and 0.9138, respectively. Because the predicted values were close to 1, the models were expected highly accurate in estimating responses in the range studied (Karim et al., 2014; Tang et al., 2011).

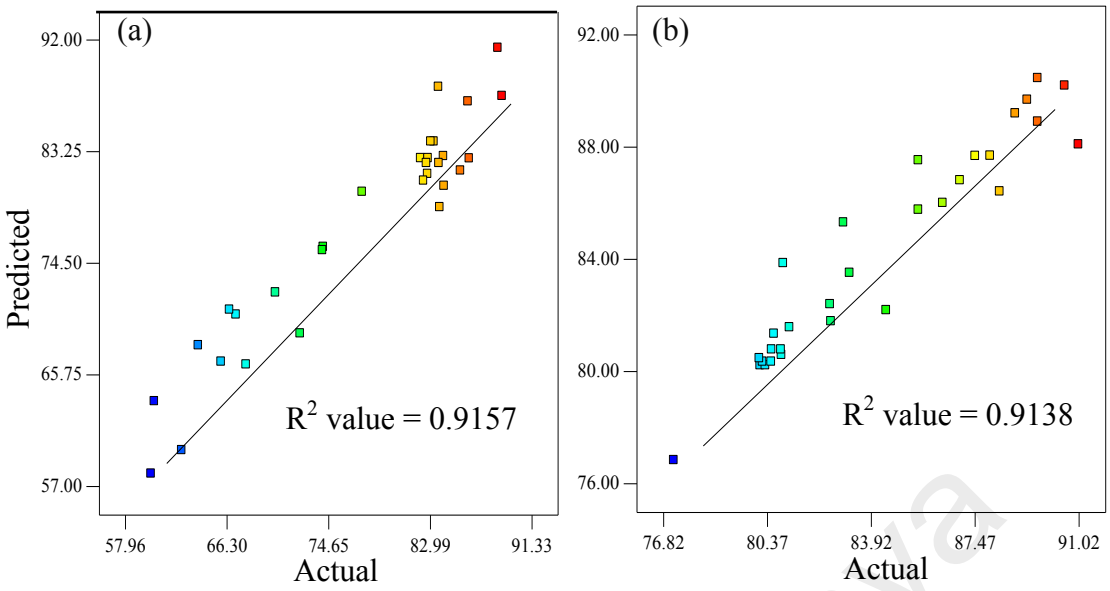

Figure 4.7: The predicted versus actual plots of (a) crystallinity index, and (b) nanocellulose yield models.

4.2.2 Effect of Hydrolysis Variables by using RSM Optimization Study

Amongst four variables including, including reaction temperature (x_1), reaction time (x_2), concentration of Cr(III)-transition metal based catalyst (x_3), and concentration of H_2SO_4 (x_4), RSM predicted that the H_2SO_4 concentration (x_4) and Cr(III) metal salt concentration (x_3) shown the greatest influence on the crystallinity index and nanocellulose yield due to the highest *F*-value. Generally, the effect of the interaction between two hydrolysis variables is demonstrated by response surface plots, while the other variables are kept at zero.

4.2.2.1 Interaction Effect between Reaction Temperature (x_1) and Concentration of H_2SO_4 (x_4)

Figure 4.8 shows 3D plots of the interaction between reaction temperature and concentration of H_2SO_4 and the corresponding effects on the crystallinity index and nanocellulose yield. The reaction time and concentration of Cr(III)-transition metal based catalyst were fixed at 1.5 h and 0.30 M, respectively. The reaction temperature

played an important role in initiating and enhancing the chemical degradation of the cellulose material. The 3D response surface shows that an increase in reaction temperature from low (30 °C) to high (100 °C) was the main parameter contributing to the increase of crystallinity index, as shown in **Figure 4.8(a)**. At a low concentration of H_2SO_4 (0.2 M), an increase in the reaction temperature greatly enhanced the crystallinity index of yielded nanocellulose from 30–100 °C, but it had a negative effect at a high concentration of H_2SO_4 (1.0 M) and reaction temperature (100 °C). The decrease in the crystallinity index of yielded nanocellulose at high H_2SO_4 concentrations and high reaction temperatures was due to over-reaction. When over-reaction occurred under such extreme conditions (*i.e.* excessive heat energy and extensive hydrolysis time), cellulose was tended to be degraded into undesirable liquid fraction monomers such as reducing sugar (Lu et al., 2014). This finding was well agreed with a previous study (J. Li et al., 2014).

Additionally, increasing the reaction temperature from 30 to 100 °C did not greatly improve the crystallinity index of nanocellulose with a high H_2SO_4 concentration (1.0 M). A possible explanation for this result is that the partial crystallite structure was greatly damaged by the concentrated acid when the amorphous regions of cellulose matrix were completely degraded during the catalytic acid hydrolysis process (Karim et al., 2014), even when the reaction was carried out at a low reaction temperature, as shown in **Figure 4.8(a)**. This result was in good agreement with a previous study (J. Li et al., 2014) in which increased reaction temperature and acid concentration would eventually improve the crystallinity index of nanocellulose. However, this reaction conditions must be controlled in order to prevent complete hydrolysis of cellulose into its molecular level, for instance, glucose.

The simultaneous dependence of nanocellulose yield on the reaction temperature and H_2SO_4 concentration is shown in **Figure 4.8(b)**. In a reaction time of 1.5 h, the 3D surface plot revealed that an increase in reaction temperature and amount of H_2SO_4 caused a significant decrease of nanocellulose yield (96 to 87%) at a low reaction temperature (30 °C). The reduction in nanocellulose yield was higher at 100 °C, in which the nanocellulose yield declined from 93 to 82%. This result might indicate that more hydrogen bonds were broken at such a high reaction temperature, which led to more cellulose degradation into water-soluble glucose monomers. This finding was in accordance with a previous study (Hamid et al., 2014).

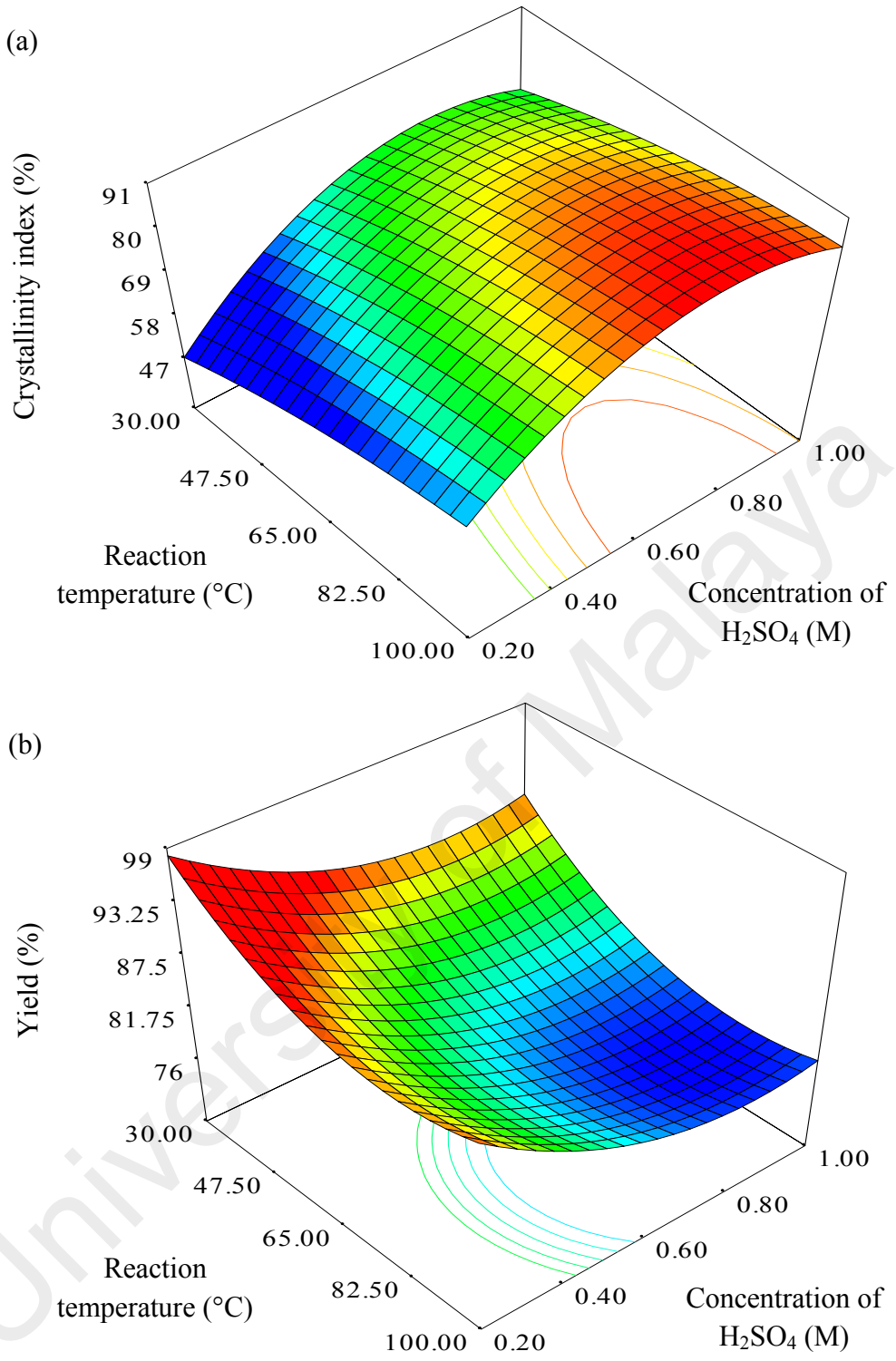

Figure 4.8: Interaction between reaction temperature (x_1) and concentration of H_2SO_4 (x_4), with a fixed reaction time (x_2) of 1.5 h and concentration of Cr(III)-transition metal based catalyst (x_3) of 0.23 M. (a) Crystallinity index and (b) nanocellulose yield model.

4.2.2.2 Interaction Effect between Reaction Time (x_2) and Concentration of H_2SO_4 (x_4)

The effect of reaction time and concentration of H_2SO_4 on the produced nanocellulose crystallinity index and the yield (reaction temperature and concentration of Cr(III)-transition metal based catalyst were kept constant at 65 °C and 0.23 M) are shown in **Figure 4.9**. With a reaction temperature of 65 °C, the 3D surface plot showed that an increase in reaction time caused a significant increase in nanocellulose crystallinity (37 to 72%) at low levels of H_2SO_4 concentration (0.2 M). On the other hand, the crystallinity index of yielded nanocellulose was only slightly influenced by prolonging the reaction time from 0.5 to 1.0 h at high acid concentrations (1.0 M), as the increment of the crystallinity index was low (83 to 85 %). However, further progress of the hydrolysis reaction caused the negative effect in enhancing the crystallinity index, as the over-degradation of cellulose polymeric chain occurred under strong acidic conditions, which resulted in reduction of crystallinity for obtained nanocellulose, as shown in **Figure 4.9(a)**.

Reaction time plays an important role in cellulose depolymerization. In the initial step, increasing contact time (hydrolysis time) was necessary in order to let more acids and metal ion catalysts diffuse into the amorphous regions of cellulose and cause the physical swelling of cellulose (Hamid et al., 2014). Thus, the cellulose matrix was softened, and glycosidic linkages of cellulose fibers were solubilized until an optimal condition was achieved. However, further increases in reaction time and H_2SO_4 concentration did not significantly increase the crystallinity of yielded nanocellulose. The complete dissolution of amorphous regions occurred in high concentrations of catalyst, and the crystallite regions were further damaged by hydrolyzing catalysts at higher reaction temperatures. Eventually, the highly-ordered structure in the cellulose

matrix was reduced, decreasing the crystallinity index of yielded nanocellulose. Prolonging the reaction time could further enhance the crystallinity index of obtained nanocellulose; however, the hydrolysis time must be controlled to minimize over-depolymerization hydrolysis of cellulose (Zhao et al., 2011). Karim and his coworker discouraged increasing the reaction time to produce nanocellulose, as it might decrease the nanocellulose crystallinity and yield (Karim et al., 2016).

For the nanocellulose yield model, the 3D surface plot in **Figure 4.9(b)** showed that an increment of reaction time at a high H_2SO_4 concentration did not cause significant changes in nanocellulose yield as compared with a low amount of acid. This result reflects the fact that majority of cellulose was degraded into glucose monomer at an early reaction time (0.5 h) under strong acid hydrolysis (1.0 M). In the case of H_2SO_4 concentration, the contour plot showed that the nanocellulose yield decreased gradually at a short reaction time with a continuously increasing quantity of acid. At a long reaction time (2.5 h), the nanocellulose yield was reduced from 91 to 84% at 65 °C with 0.23 M of Cr(III)-transition metal based catalyst. However, the response surface plot indicated that both individual factors (reaction time and concentration of H_2SO_4) had negative effects on the yield of hydrolyzed nanocellulose. The model demonstrated that increased sulfuric acid concentration resulted in a marginal decrease of nanocellulose yield for different hydrolysis times. However, the lowest nanocellulose yield (77.2%) was obtained when the hydrolysis reaction was conducted at a high temperature of 82.50 °C for 2 h with a high catalyst loading of 0.325 M Cr(III)-transition metal based catalyst and 0.80 M H_2SO_4 (Sample 25), which reflected the chemical degradation of cellulose polymers.

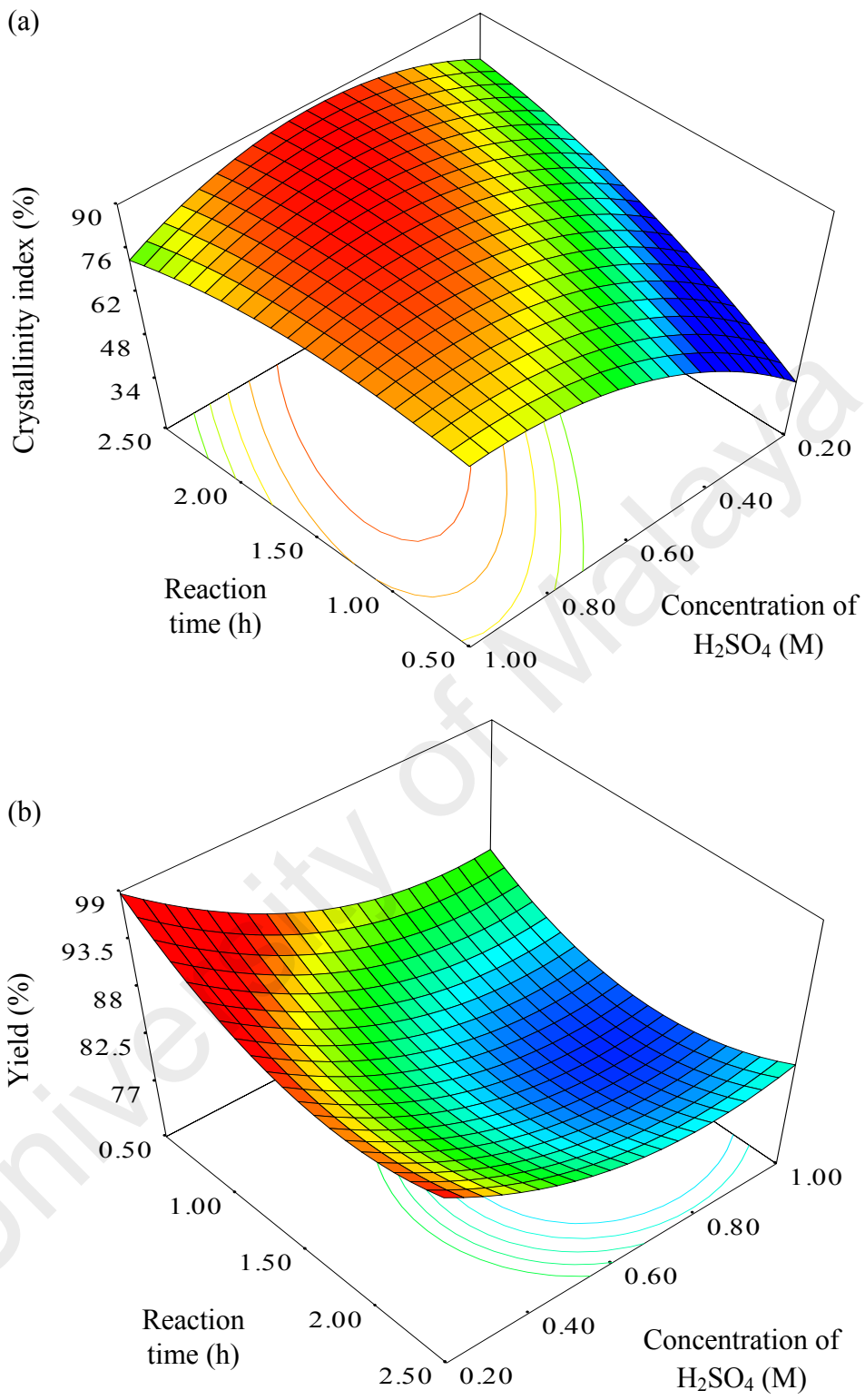

Figure 4.9: Interaction between reaction time (x_2) and concentration of H_2SO_4 concentration (x_4), with a fixed reaction temperature (x_1) of 65 °C and concentration of Cr(III)-transition metal based catalyst (x_3) of 0.23 M. (a) Crystallinity index and (b) nanocellulose yield model.

4.2.2.3 Interaction Effect between Concentration of Cr(III)-transition Metal Based Catalyst (x_3) and Concentration of H_2SO_4 (x_4)

Figure 4.10 illustrates the surface contour plot for the effect of concentration of H_2SO_4 and Cr(III)-transition metal based catalyst on the crystallinity index and yield of produced nanocellulose. The reaction temperature and hydrolysis time were fixed at 65 °C and 1.5 h, respectively. The interaction between these two individual factors created a dome shape, in which the crystalline index of yielded cellulose increased gradually to a certain level, followed by a decrease with higher catalyst loading. This decline indicated that the majority of the amorphous regions of cellulose were hydrolyzed. The remained crystallite regions were further left unaltered at the optimum time, and further increasing the amount of catalyst led to over-degradation of cellulose, facilitating the disintegration of the cellulosic fiber into glucose monomers.

The partial elliptical contour plot showed in **Figure 4.10(a)** indicated that the Cr(III)-transition metal based catalyst greatly enhanced the crystallinity index of nanocellulose. With increasing $Cr(NO_3)_3$ metal salt catalyst at a low concentration of sulfuric acid (0.2 M), the change in crystallinity index was dramatic (45 to 60%). As expected, when increasing the concentration of hydrolyzing catalysts (Cr(III)-transition metal based catalyst or H_2SO_4), the yield of nanocellulose was eventually decreased by the chemical degradation of cellulose in the acid hydrolyzing medium, as indicated in **Figure 4.10(b)**.

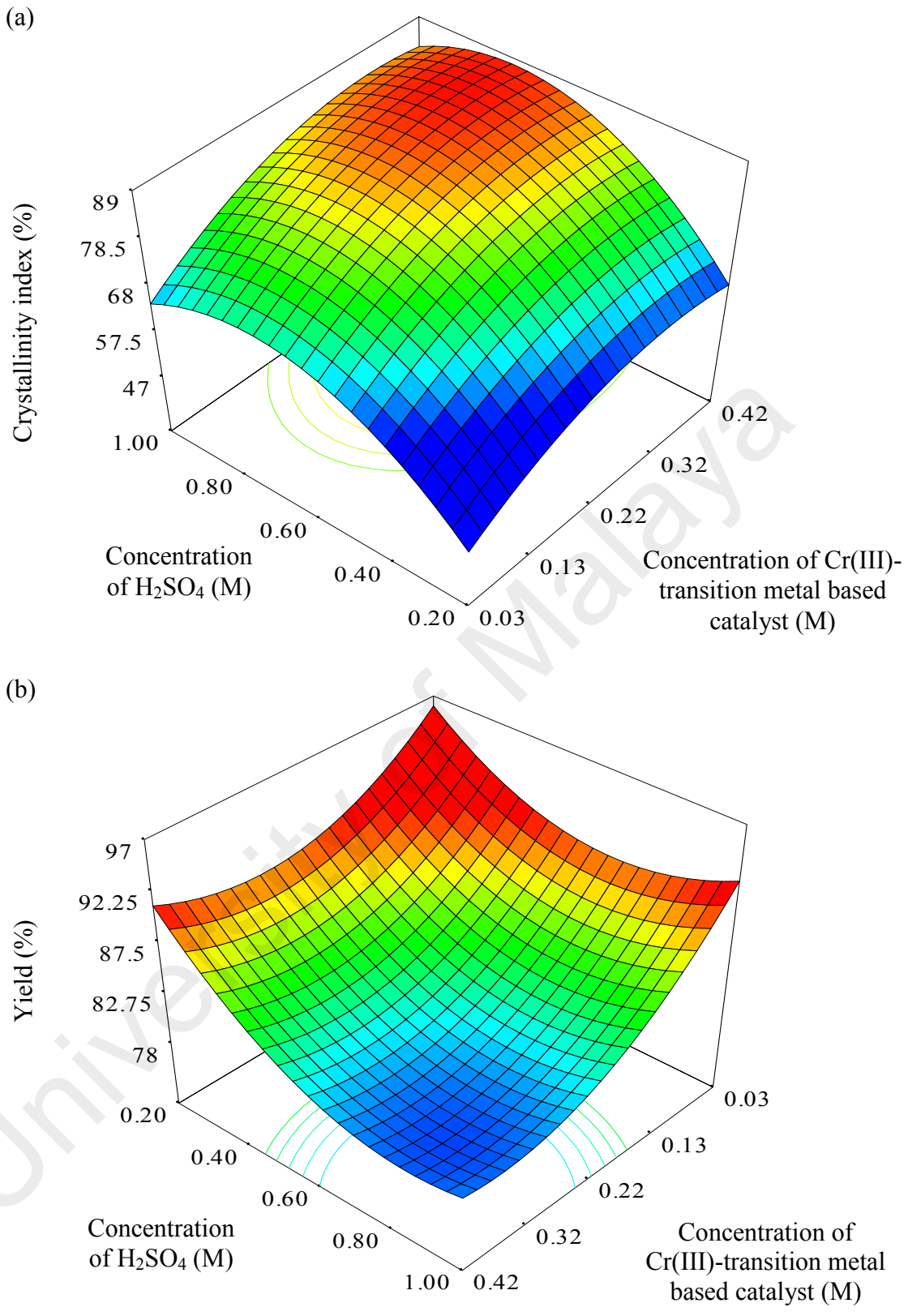

Figure 4.10: Interaction between concentration of Cr(III)-transition metal based catalyst (x_3) and concentration of H_2SO_4 (x_4), with a fixed reaction temperature (x_1) of 65 °C and reaction time (x_2) of 1.5 h. (a) Crystallinity index and (b) nanocellulose yield model.

As reaction scheme shown in Equations **[4.8–4.11]**, Cr(III) ions form a coordination complex with H_2O to yield hydronium ions (H_3O^+), which further enhanced the acidity of the medium, resulting in the disintegration of hydrogen bonds between cellulose polymeric chains as well as the hydrolytic cleavage of glycosidic bonds between glucose units. Furthermore, the Cr^{3+} metal ions were absorbed onto the oxygen atoms of the glucose unit in cellulose to form intermediate complexes. This interaction lowers the activation energy of hydrolysis by increasing the pyranose bond length and its bond angle (Zhao et al., 2011). Thus, the metal ion catalyst could further enhance the efficiency of hydrolysis.

$$Cr(NO_3)_3 + 6H_2O \rightarrow [Cr(H_2O)_6]^{3+} + 3NO_3^- \quad \textbf{[Equation 4.8]}$$

$$[Cr(H_2O)_6]^{3+} + H_2O \rightarrow [Cr(H_2O)_5(OH)]^{2+} + H_3O^+ \quad \textbf{[Equation 4.9]}$$

$$[Cr(H_2O)_5(OH)]^{2+} + H_2O \rightarrow [Cr(H_2O)_4(OH)_2]^{+} + H_3O^+ \quad \textbf{[Equation 4.10]}$$

$$[Cr(H_2O)_4(OH)_2]^{2+} + H_2O \rightarrow [Cr(H_2O)_3(OH)_3] + H_3O^+ \quad \textbf{[Equation 4.11]}$$

4.2.3 Verification and Optimization of Predictive Model

The nanocellulose synthesis process was optimized to generate the highest crystallinity index and the maximum product yield. The independent variables (reaction temperature, reaction time, concentration of Cr(III)-transition metal based catalyst, and concentration of H_2SO_4) were set in low and high levels that were coded as -2 and +2, respectively, while the responses (crystallinity index and nanocellulose yield) were set at the maximum point. However, the economic feasibility of acid hydrolysis operation was needed to be considered. The main concerns were moderate reaction temperature and reaction time, low quantities of Cr(III)-transition metal based catalyst, and low H_2SO_4 concentrations. Although the reaction temperature and hydrolysis time had a positive impact on the crystallinity index of nanocellulose, these parameters needed to be maintained in moderate conditions to minimize the required production energy. To

reduce production costs, only the minimally adequate amounts of the hydrolysis catalysts (Cr(III)-transition metal based catalyst and H_2SO_4 acid) should be used.

To verify the models, the optimum reaction conditions were applied to three independent replicates of the Cr(III)-catalyzed acid hydrolysis reaction (**Table 4.7**) with the following optimized conditions: reaction temperature, 82 °C; reaction time, 1 h; Cr(III)-transition metal based catalyst, 0.22 M; and concentration of H_2SO_4, 0.80 M. Under the optimized hydrolysis conditions, the experimental (actual) results for crystallinity index and nanocellulose yield were 85.35 and 82.86%, respectively, which were close to the predicted values (85.62 and 82.42%). The small error (0.316 and 0.513%) indicated that the developed model was reasonably accurate. In addition to that, the optimal crystallinity index of yielded nanocellulose in this study was higher than previously reported, ranging from 63.6 to 83.5% (**Table 4.8**). This result suggested that the mild hydrolysis conditions and high selectivity of Cr(III)-transition metal assisted dilute H_2SO_4 hydrolysis for hydrolytic cleavage of glycosidic linkages led to the degradation of the cellulose amorphous regions. This effect eventually minimized the possibility of over-depolymerization of cellulose and reduced the production of organic liquids as byproduct with the formation of char.

Table 4.7: Results of model validation for Cr(III)-transition metal assisted dilute H_2SO_4 hydrolysis at optimum experimental conditions.

Temperature (°C)	Time (h)	$[Cr(NO_3)_3]$ (M)	$[H_2SO_4]$ (M)	Crystallinity Index (%)		Yield (%)	
				Actual	Predicted	Actual	Predicted
82	1.0	0.21	0.80	84.63	85.45	81.69	82.59
83	1.0	0.23	0.80	86.63	85.90	83.67	82.17
82	1.0	0.21	0.80	84.78	85.52	83.21	82.49

Table 4.8: Comparisons of crystallinity index (CrI) and nanocellulose yield in literatures.

Starting material	Optimum conditions	CrI (%)	Yield (%)	Reference
α-cellulose	82 °C, 1 h, 0.22 M $Cr(NO_3)_3$, 0.8 M H_2SO_4	85.35	82.86	This study
MCC	91 °C, 6 h, 1 M $FeCl_3$, 2.5 M HCl	83.46	86.98	(Karim et al., 2014)
Eucalyptus pulp	80 °C, 1.2 h, 0.3 M $FeCl_3$, 2.5 M HCl	69.50	–	(J. Li et al., 2015)
Palm tree cellulose	98 °C, 4 h, 0.8 M $FeCl_3$, 3 M HCl	68.66	83.98	(Hamid et al., 2014)
Eucalyptus pulp	88 °C, 1.1 h, 0.4 M $FeCl_3$, 2.46 M HCl	63.59	–	(J. Li et al., 2014)

At the same temperature (82 °C), hydrolysis time (1 h), and H_2SO_4 concentration (0.8 M), the experiment was carried out without Cr(III)-transition metal based catalyst. The crystallinity index of the nanocellulose was 72.24%, which was lower than nanocellulose prepared with Cr(III)-transition metal assisted H_2SO_4 treatment. Thus, Cr(III)-transition metal based catalyst enhanced the nanocellulose crystallinity by 18.15%. The purpose of this experiment was to ascertain the role of Cr(III)-transition metal based catalyst in order to enhance the hydrolytic cleavage of cellulose amorphous regions for higher crystallinity percentage. Moreover, this finding also suggested that dilute H_2SO_4 acid alone was insufficient in cleavage of glycosidic linkages in cellulose amorphous regions and breaking inter- and intramolecular bonding of cellulose. The presence of dilute H_2SO_4 was only capable of swelling and opening the cellulose fibers without further degradation (Kopania et al., 2012). A similar experiment was performed using the optimal conditions of temperature, time, and metal salt concentration (**Table 4.7**) in the presence of HCl (0.8 M) instead of H_2SO_4. These results are summarized in **Table 4.9**. The crystallinity index of yielded HCl-treated nanocellulose was only

65.52%, indicating that HCl is a weaker acid with less dissociated protons than H_2SO_4. Therefore, less hydronium (H_3O^+) ions were available to hydrolytic cleave the intra- and intermolecular hydrogen bonds of the cellulose macromolecules.

Table 4.9: Nanocellulose crystallinity index (CrI) obtained by different reactions.

Nanocellulose sample	Temperature (°C)	Time (h)	$[Cr(NO_3)_3]$ (M)	$[H_2SO_4]$ (M)	[HCl] (M)	CrI (%)
RSM-optimized	82	1.0	0.22	0.80	–	85.35
HCl-treated	82	1.0	0.22	–	0.80	65.52
Hydrolyzed without metal salt	82	1.0	–	0.80	–	72.24

4.2.4 Physicochemical Properties of Cellulose and RSM Optimized Nanocellulose

4.2.4.1 XRD Analysis

The crystalline behaviors of cellulose and RSM-optimized nanocellulose were evaluated by wide-angle X-ray diffraction (WAXRD). Cellulose is a semi-crystalline biopolymer which comprises of both amorphous and crystalline domains in their nature molecular structure. The effects of different chemical treatments on the crystallinity index of cellulose can be calculated and compared from the XRD diffractogram profiles obtained. As shown in **Figure 4.11**, the XRD patterns for both α-cellulose and yielded nanocellulose exhibited similar manner, which indicated that the chemical structure of nanocellulose remained unchanged after catalytic acid hydrolysis.

It is clearly illustrated that the peak intensity around $2\theta = 22.5°$ for nanocellulose product was higher and sharper than that of α-cellulose. This observation suggested that most of the amorphous regions in treated nanocellulose were selectively degraded, and this induced the exposure of well-ordered organized crystallite regions in fiber after the

catalytic acid hydrolysis reaction. The increment in crystallinity was postulated two possible reasons: (i) the H_3O^+ could penetrate into more accessible amorphous regions, promoting the hydrolytic cleavage of glycosidic linkages and thus liberating the elementary solid crystallites (Li et al., 2009); and (ii) the self-assembly properties of nanocellulose resulted in highly ordered organization and realignment occurred, enabling better crystalline interface, close packing and formation of hydrogen bonds (Lu & Hsieh, 2012). Due to these reasons, the crystallinity index for α-cellulose and optimized nanocellulose was calculated based on Segal's equation and found to be 45.8 and 85.4%, respectively. The highly crystalline yielded nanocellulose fibers are expected to be more effective in providing better reinforcement capabilities for composite materials due to its increased rigidity and stiffness (Goh et al., 2016).

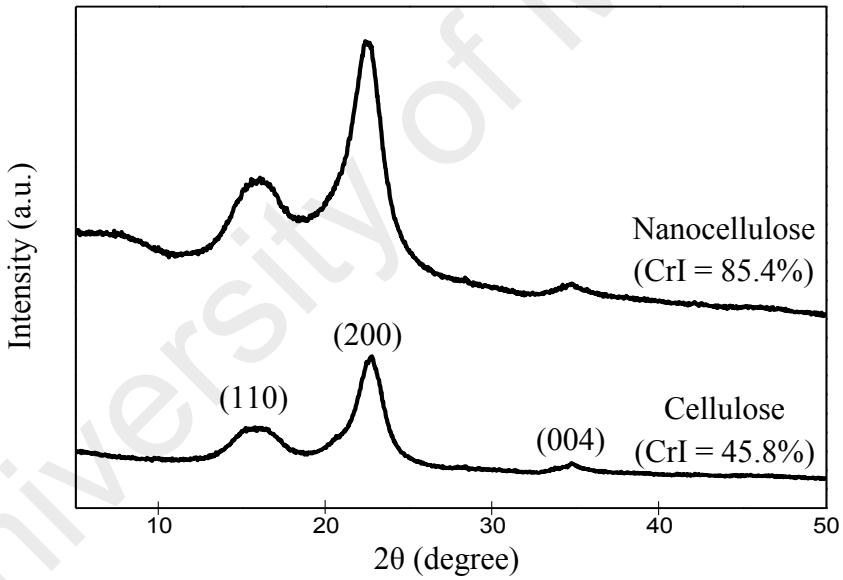

Figure 4.11: XRD patterns of α-cellulose and optimized nanocellulose.

4.2.4.2 FESEM, AFM, and TEM Analyses

Figure 4.12 depicts the FESEM, TEM, and AFM micrographs of cellulose raw material and optimized yielded nanocellulose in order to investigate the morphological and structural features of cellulose raw material and Cr(III)-treated nanocellulose fibers. As shown in **Figure 4.12(a)**, the cellulose fibers exhibited a compact and aggregated

structure of long and irregular length. At higher magnification (×2000), the surface of the cellulose particles was rough, and each fiber had a large diameter with the presence of a large number of crevices and cracks. These cracks allowed the quick diffusion of metal ions and acid inside the fiber bundles and thus, induced the segregation of these cellulose bundles into elementary fibers. Subsequently, the Cr(III)-transition metal assisted dilute H_2SO_4 hydrolysis facilitated to the disintegration of micro-sized cellulose into individual, small fragments with reduced aggregated structure, as illustrated in **Figure 4.12(b)**. Furthermore, the nanocellulose showed a significant decrease in the diameter of the fibrils due to the delamination process, which further diminished intra- and intermolecular hydrogen bonding between cellulose polymers (Hamid et al., 2015). FESEM measurements indicated that the average diameter of nanocellulose decreased from 30.9 ± 10.9 μm to 15.2 ± 6.5 μm.

Based on the TEM measurements in **Figure 4.12(c)**, the nano-scale fibers were successfully isolated from micro-sized cellulose fibers. The nanocellulose fibers were conjoined in a web-like network with average diameters of 18.4 ± 7.4 nm, and the length of these fibers was up to hundred nanometers. The morphology and surface structures of optimized nanocellulose were further explained by AFM micrographs, as revealed in **Figure 4.12(d)**. The nature of the nanocellulose can be clearly seen by the enlarged AFM image. The AFM image further supports the conclusion that the nano-dimension cellulose was successfully hydrolyzed via Cr(III)-transition metal assisted dilute H_2SO_4 treatment, and was characterized by a short, thin, narrow whisker form. However, the dimensions of nanocellulose observed by AFM were remarkably larger than TEM analysis; this difference was attributed to the different sample preparation methods as well as the fact that the samples were placed on different substrates, *i.e.* a carbon-coated copper grid for TEM and a microscope slide for AFM (Feng et al., 2015).

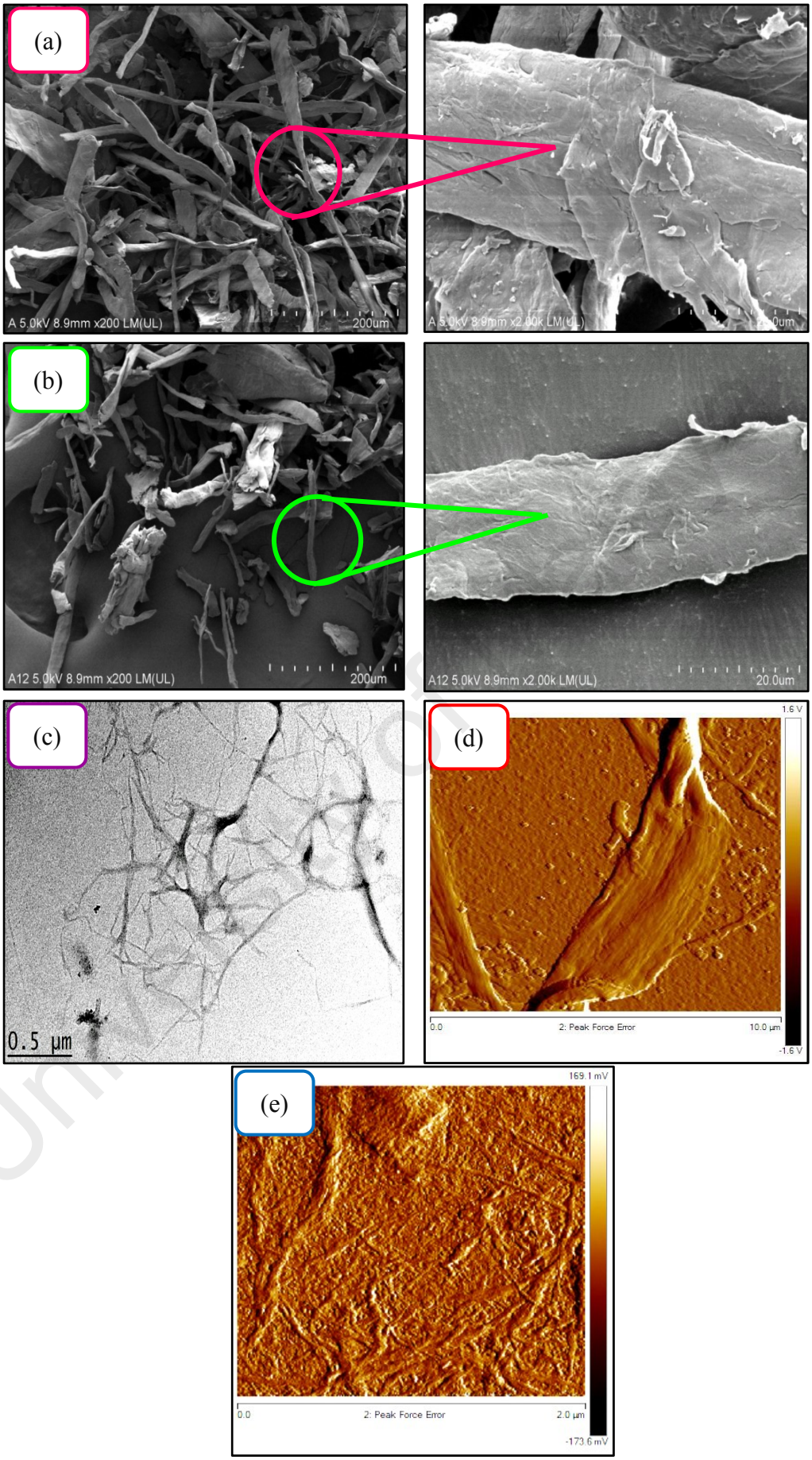

Figure 4.12: FESEM images of (a) α-cellulose and (b) RSM optimized nanocellulose; (c) TEM image of nanocellulose; AFM images of (d) α-cellulose and (e) nanocellulose.

4.2.4.3 FTIR Analysis

Figure 4.13 shows the FTIR spectra of α-cellulose and nanocellulose prepared under optimal conditions. The broad peak observed at 3400 cm^{-1} was attributed to the stretching vibration of O–H bonding from absorbed water molecules of the cellulose chains. In addition, C–H bond stretching vibration was assigned to the dominant peak near 2900 cm^{-1} (Tan, Abd Hamid, & Lai, 2015). A sharp peak observed at 1054 cm^{-1} was corresponded to the stretching vibration of C–O–C pyranose ring (antisymmetric in phase ring) of cellulose molecules (Mandal & Chakrabarty, 2011). Fingerprint region of the FTIR spectra which ranges from 1100 to 600 cm^{-1} indicated the vibration of deformation, wagging and twisting modes of anhydro-glucopyranose which is characteristic of *β*-glucosidic linkages (Johar, Ahmad, & Dufresne, 2012).

Two prominent peaks (1110 and 896 cm^{-1}) that correspond to the C–O–C pyranose ring skeletal vibration and *β*–linkages of $^4C_1$ ring confirmation, respectively, were observed. As reported by (Hamid et al., 2015), both of these peaks reflected the degree of polymerization in cellulose. For RSM optimized nanocellulose, the peak at 1110 cm^{-1} was less intense than in cellulose (**Figure 4.13b**). This indicated that the degradation of glycosidic bonds that linked the *β*–D–glucopyranose monomers of the cellulose chains to produce nanocellulose (Hamid et al., 2015). On the other hand, the FTIR peak at 896 cm^{-1}, which was attributed to *β*–D–glucopyranosyl unit, was the similar in both samples, indicating that the cellulosic structure was retained after treatment (Hamid et al., 2015). The presence of sulfate groups on yielded nanocellulose, not present on the original cellulose material, was illustrated by a small peak at 1205 cm^{-1}, which can be attributed to S=O linkage vibration, as previously described (Beltramino et al., 2016; Flauzino Neto et al., 2013). This tiny peak appears in spectra for nanocellulose samples but seems to be absent for the original fibers (**Figure 4.13**).

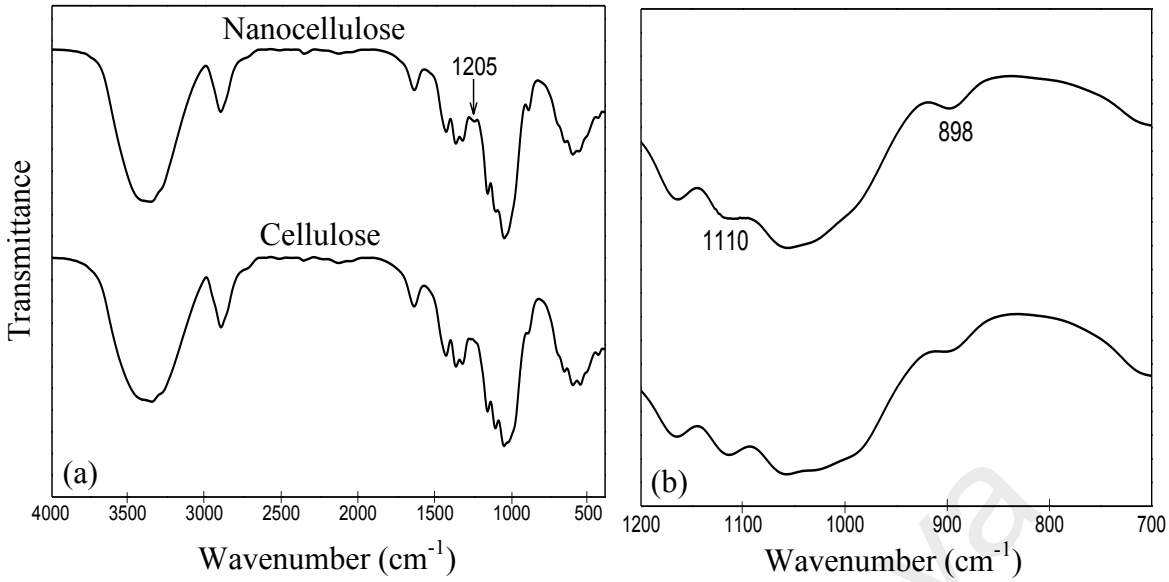

Figure 4.13: (a) FTIR spectra of cellulose material and optimized nanocellulose and (b) enlargement of the spectral region of 1200 to 700 cm^{-1}.

4.3 Facile Production of Nanocellulose from Oil Palm Empty Fruit Bunch via One-Pot Oxidative-Hydrolysis Isolation Approach

In recent years, the production of oil palm (*Elaeis guineensis*) biomass in Malaysia has increased, and Malaysia has been acclaimed as one of the largest exporters and producers in the world (Haafiz et al., 2016). Together with the growing of oil palm production, the amount of solid waste generated, which is known as oil palm empty fruit bunch (OPEFB) is increasing as well. It is estimated that 15 million tons of annual production of solid residue are generated from palm oil mill effluent factories after the crude palm oil is extracted from the OPEFB raw material. Due to the abundant availability of raw material, the development of using waste and residual biomass as the nanocellulose sources is of practical interest (Tang et al., 2015). The lignocellulosic OPEFB mainly consists of cellulose (40–65%), hemicellulose (15–25%) and lignin (12–20%) (Ching & Ng, 2014). Therefore, rational and sustainable utilization of the OPEFB biomass to develop a promising new bio-product (*i.e.* cellulose) would be of great

benefit to minimize the adverse environmental impact, as well as create a new highly value-added biomaterial with excellent properties.

Normally, the conventional biomass pretreatment process requires multiple purification steps for preparing the nanocellulose derived from the complex biomass structure, which is tedious, time-consuming, and generates a large amount of wastewater. Due to this reason, we have developed a new isolation approach for extracting the cellulose in nano-dimensional, which is via a one-pot oxidative-hydrolysis technique. In addition to this, $Cr(NO_3)_3$ metal salt, a promising acid hydrolyzing agent for depolymerization of cellulose was applied in the present study. The main goals of this study are: (i) to determine the feasibility and the practicability of one-pot oxidative-hydrolysis process for isolating nanocellulose from OPEFB; (ii) to perform a comparative study between one-pot oxidative-hydrolysis reaction and multistep purification biomass pretreatment for nanocellulose production; and (iii) to examine the physicochemical properties of starting material (OPEFB), chemically treated fibers and yielded nanocellulose in terms of chemical composition, functional groups, crystallinity index, surface morphology studies, and thermal stability systematically.

4.3.1 Structural Analysis and Characterization

4.3.1.1 Purification and Chemical Composition Analysis

To develop an eco-friendly and simple one-pot isolation process, the present study investigated the effectiveness of multiple-step chemical purification approach and one-pot oxidative-hydrolysis for the isolation of nanostructured cellulose from OPEFB biomass. The chemical compositions, namely lignin, hemicellulose and cellulose content of the fibers treated at every chemical stage were listed in **Table 4.10**. Untreated

OPEFB fiber had the highest percentage of lignin content (25.3%) with approximately 71.8% of holocellulose content that composed of α-cellulose and hemicellulose. In order to extract cellulose from untreated biomass, conventional chemical purification treatment was conducted to remove most of the lignin and hemicellulose content during the multiple-step process. When the dewaxed fibers subjected to chlorite-bleaching treatment by acidified $NaClO_2$, the lignin content of the bleached fibers was reduced significantly from 25.3 to 1.9% as compared to untreated fiber. This was due to the removal of the lignin component chlorine dioxide (ClO_2) generated from the $NaClO_2$ bleaching agent. Besides that, the hemicellulose content was decreased about 55.2% after the bleaching treatment and subsequently decreased to 9.3% when the fiber was further treated with 2% of NaOH solution. This finding suggested that the chlorite-bleaching process plays a noteworthy role in removing most of the lignin and hemicellulose content simultaneously during the reaction, and the subsequent alkalization treatment further hydrolyzed the strong bonding interaction of remaining hemicellulose. Thus, the α-cellulose content of alkali-treated fiber was increased to a certain extent. The chemical composition of NaOH-treated fiber was 86.7% of α-cellulose, 9.3% of hemicellulose, and 2.0% of lignin. The hemicellulose and lignin fractions of the fiber were further reduced when the extracted cellulose was hydrolyzed by $Cr(NO_3)_3$ metal salt catalyst in acidic medium, and the final yielded nanocellulose (MS-NC) comprised of 90.9% α-cellulose, 5.5% hemicellulose, and 1.7% lignin.

Conventionally, $NaClO_2$ bleaching agent is effective in the degradation of lignin and hemicellulose, however, toxic gas may be release during the bleaching process, and the generated chlorite molecules need to be removed from the reaction mixture by washing process after the delignification process was completed. Such bleaching agent is not suitable for one-pot oxidative-hydrolysis process, as the produced chlorite

molecules could affect the efficiency of subsequent acid hydrolysis that are conducted in the same pot of reaction mixture system by $Cr(NO_3)_3$ metal salt catalyst and H_2SO_4, and lead to the formation of unfavorable side products. Due to this reason, H_2O_2 was chosen as an alternative oxidizing agent as it would not leave any residues on the fiber's surface during the bleaching process (Correia et al., 2013). The utilization of H_2O_2 oxidative treatment is an important and necessary step to increase the accessibility of cellulose for the acid depolymerization process to produce nanocellulose because high lignin content in the treated fibers can act as a protective layer of cellulose fibers that avoid them from any chemical attack. Therefore, optimization of the oxidative bleaching treatment period (1–5 h) for the delignification process of OPEFB fiber was investigated in order to estimate the effects H_2O_2 oxidative bleaching process toward the maximal removal of lignin.

Table 4.10 demonstrates that the lignin content of the extracted cellulose was gradually decreasing and α-cellulose content increased with the prolonging of the bleaching period from 1 to 5 h. As expected, the longer the bleaching period, the more lignin content was degraded while more α-cellulose was exposed from the treated fiber. Results showed that the lignin of the treated fibers was greatly reduced from 16.3 to 1.2% and the percentage of hemicellulose decreased from 23.4 to 9.9% after being oxidized by H_2O_2 in the one-pot reaction, which indicated that the majority of lignin and hemicellulose structure were solubilized thus enhancing the exposure of cellulose fibers. This finding was consistent with the literature studies in which the removal of hemicellulose and lignin mostly occurred during the bleaching process (Ching & Ng, 2014). When 5h-bleached fiber was further hydrolyzed by $Cr(NO_3)_3$ in H_2SO_4 medium, the hydrolytic cleavage of the extensive network of hydrogen bonding between cellulose chains and the breakage of glycosidic linkages within the cellulose chains led

to the formation of nanocellulose fiber (Tan, Abd Hamid, & Lai, 2015). Although there were no additional steps for alkalization treatment for one-pot oxidative-hydrolysis process, the hemicellulose content from one-pot isolated nanocellulose was lower (5.2%) than the 5h-bleached fiber (9.9%) after the hydrolysis process. This is because hemicellulose can be easily degraded under mild acidic conditions. The chemical composition of one-pot derived nanocellulose (OP-NC) consisted of 90.8% α-cellulose, 5.2% hemicellulose, and 1.1% lignin, while the corresponding content of Cr(III)-treated nanocellulose (MS-NC) was 90.9, 5.5 and 1.7%, respectively. This suggested that both isolated nanocellulose exhibited similar chemical compositions.

Table 4.10: Chemical composition (wt%) of untreated OPEFB, chemically treated fiber and yielded nanocellulose obtained via different isolation techniques.

Process	OPEFB fiber	α-cellulose	Hemicellulose	Lignin
Multiple chemical purification	Untreated	45.6 ± 1.3	26.2 ± 1.1	25.3 ± 1.8
	$NaClO_2$-treated	85.4 ± 0.9	11.6 ± 1.3	1.9 ± 0.2
	NaOH-treated	86.7 ± 0.3	9.3 ± 0.4	2.0 ± 0.1
	MS–NC	90.9 ± 0.8	5.5 ± 0.9	1.7 ± 0.2
One-pot isolation	1h-bleached	58.6 ± 0.4	23.4 ± 0.3	16.3 ± 1.2
	2h-bleached	69.0 ± 0.6	18.9 ± 0.9	10.7 ± 0.8
	3h-bleached	76.2 ± 0.2	14.6 ± 0.5	5.8 ± 0.7
	4h-bleached	85.4 ± 0.5	9.8 ± 0.2	1.8 ± 0.5
	5h-bleached	87.6 ± 0.7	9.9 ± 0.6	1.2 ± 0.2
	OP–NC	90.8 ± 0.5	5.2 ± 0.1	1.1 ± 0.1

With reference to **Figure 4.14**, the 1h- and 2h-bleached fibers displayed a lighter brown color as compared to untreated fibers after 1–2 h H_2O_2 treatment, which implied that the lignin content of both samples was lower than those of OPEFB fibers. This reflected that the lignin structure of chemically treated fibers started to be removed, dislocated, and/or change during the bleaching treatment, thus the residual lignin after the pretreatment was different from the lignin amount in the raw starting biomass (Saelee et al., 2016). When prolonging the bleaching period, the resulting cellulose fiber

became whiter. Finally, the highly purified and snowy-white appearance bleached fiber was produced due to the breakdown, degradation, and oxidation of phenolic compounds or lignin-based chromophores structures during the bleaching treatment with H_2O_2 (Elanthikkal et al., 2010). A previous study conducted by (Mohamed et al., 2015) has reported that the presence of a slight yellow color on the treated fibers corresponded to the presence of lignin component within the fibers. Consequently, the disappearance of dark brown color from the chemically treated fibers can also be an indication that lignin was removed besides the chemical composition analysis.

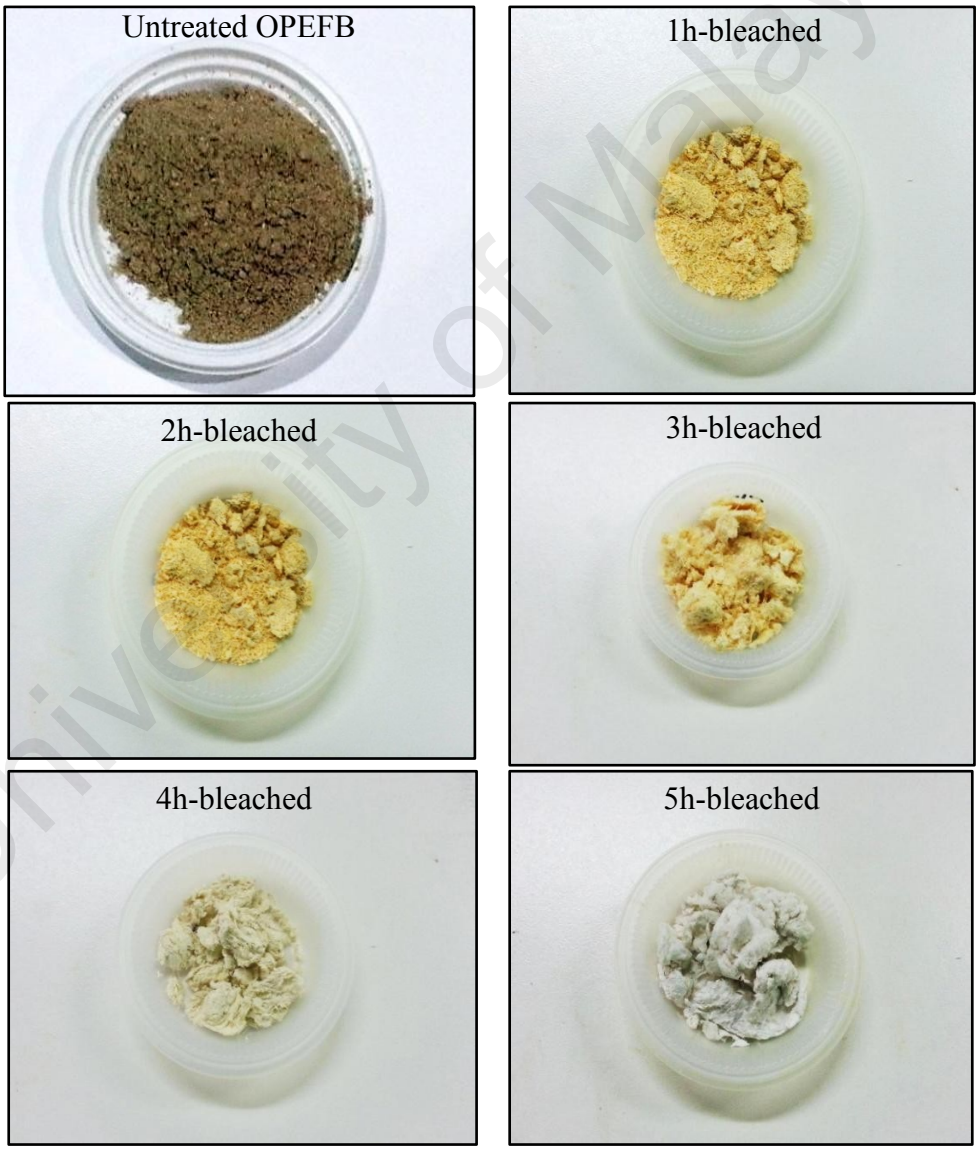

Figure 4.14: Photographs of untreated and H_2O_2-treated fibers obtained from different bleaching periods (1 to 5 h).

4.3.1.2 FTIR Study

FTIR spectroscopy analysis was used to investigate changes in the chemical compositions of fibers in response to all different treatments. **Figure 4.15** presents the FTIR spectra of all untreated and chemically treated OPEFB fibers which were exhibited in two major regions, including high (3600–2800 cm^{-1}) and low wavenumber regions (1700–500 cm^{-1}), which are consistent with the previous studies (Chen, Lee, & Abd Hamid, 2016; Chen, Lee, & Hamid, 2016b). For the first region, the broad peak at 3400 cm^{-1} was attributed to O–H stretching vibrations and the band at 2900 cm^{-1} corresponded to the C–H stretching vibrations (Chen, Lee, & Hamid, 2016a; Tan, Abd Hamid, & Lai, 2015). These two absorption peaks were observed in all the samples. However, a notable change could be observed in the disappearance of FTIR band at 2848 cm^{-1} for all treated fibers. This indicated the absence of C–H stretching which was due to the reduction in the aliphatic fraction of waxes during the successive dewaxed treatment (Sim et al., 2012).

For multistep chemical purification procedures, three main absorption peaks (*i.e.* 1604, 1512 and 1462 cm^{-1}) was designated to the benzene skeleton vibration of the typical lignin aromatic characteristics of OPEFB biomass (Hu et al., 2014). The diminishing of these three peaks from the extracted cellulose and Cr(III)-treated nanocellulose FTIR spectra indicated that the lignin component was degraded after a series of chemical treatments. Besides, the carbonyl peak observed at 1734 cm^{-1} was assigned to the acetyl stretching of polysaccharides such as hemicellulose, pectin, phenolic acids and xylan (Hu et al., 2014). The intensity of this particular peak gradually decreased for the $NaClO_2$-treated fiber. These results were further supported by the chemical composition analysis in **Table 4.10**, where most of the lignin and hemicellulose fraction were solubilized during the chlorite-bleaching process. Besides

that, no significant changes were found in the FTIR spectra of alkaline-treated fiber, except that the peak intensity at 1734 cm^{-1} was further reduced after alkalization. This showed that the remaining small portion of hemicellulose was degraded during the NaOH alkalization treatment and led to the high exposure of purified cellulose.

In the case of yielded nanocellulose isolated via two isolation techniques, significant changes were observed in which the absorption peaks intensities at 898, 1110, 1430 and 1640 cm^{-1} were enhanced. This was owing to the increment of the mass proportion of cellulose content in the treated fiber. In detail, the broad peak at 1640 cm^{-1} was correlated to the O–H bending of water absorption on the cellulose (Rosli et al., 2013). The peak at 1430 cm^{-1} was designated to the scissoring motion of CH_2 in cellulose (Soni & Mahmoud, 2015). This detectable small peak was also ascribed to the intermolecular hydrogen attraction of cellulose at C_6 (aromatic) group (Tan, Abd Hamid, & Lai, 2015). In addition, the presence of the absorption peak at 898 cm^{-1} was owing to β–glycosidic linkages of the cellulose glucose ring (Tan, Abd Hamid, & Lai, 2015). This particular peak was also contributed by the ring vibration of the anhydroglucose units in cellulose molecules (Rosli et al., 2013). The presence of stretching vibration of C–O–C glycosidic ether bond in cellulose pyranose ring contributed to the spectral band observed at 1110 cm^{-1} (Soni & Mahmoud, 2015). (Chirayil et al., 2014) reported that the intensities of these peaks were progressively more intense indicating that cellulose content increased by different chemical treatments.

In this study, FTIR spectra proved that the hemicellulose and lignin contents were fully degraded during the pulping process. In order to further verify this statement, the FTIR spectrum of commercial microcrystalline cellulose (MCC) was used as the

standard comparison. **Figure 4.15** clearly showed that the FTIR spectrum of OP-NC and MS-NC having similar FTIR patterns as commercial MCC. This suggested that the cellulose structures of one-pot isolated nanocellulose product were not affected by oxidation and hydrolysis process, where the typical structure of the parent cellulose remained well-preserved. The success of removing Cr(III)-transition metal ions after the hydrolysis has been assessed by FTIR spectroscopy analysis. This is not surprising because the previous study (Silva et al., 2014) has been reported that the FTIR analysis was extensively used to determine the presence covalent bonds formed between the metal ion and cellulose. But it can be clearly observed that the wavenumber positions of the yielded cellulose nanomaterials remained similar as α-cellulose suggesting that there is no metal ion introduced to the surface of nanocellulose fiber.

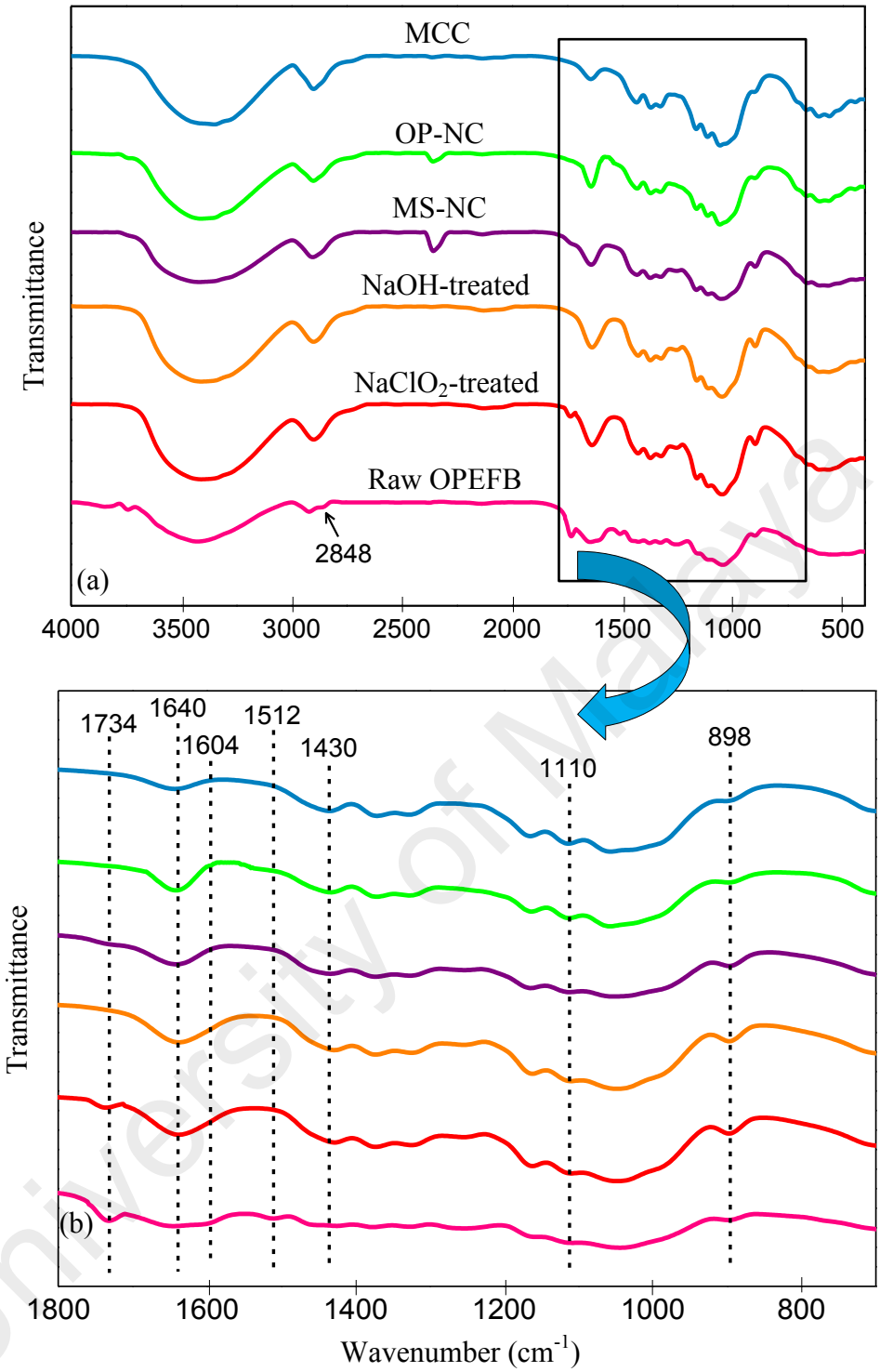

Figure 4.15: (a) FTIR spectra of untreated and chemically treated OPEFB fibers produced at different purification stages, and (b) magnification of the 1800–700 cm^{-1} wavenumber regions.

4.3.1.3 FESEM Analysis

FESEM images illustrated that the fiber surface morphology changed during each purification stage, as shown in **Figure 4.16**. The micrograph of untreated OPEFB fiber, as shown in **Figure 4.16(a)**, displayed a larger diameter and the fiber surface appeared to be smooth, with the average diameter of 137.8 ± 35.3 μm. This was owing to the presence of an outer non-cellulosic layer which consisted of cementing materials (*i.e.* lignin and hemicellulose) and the high percentage of extractives (*i.e.* waxes, oil, and pectin) (Saelee et al., 2016). A clear demonstration of facilitating defibrillation of the fiber bundles via chlorite bleaching followed by alkalization treatment was shown in **Figure 4.16(b)**. The FESEM images showed that the alkali-treated fibers became more individual and had a tougher surface. This indicated a positive effect of bleaching which led to the destruction of lignin through complex formation and depolymerization by chlorine dioxide (ClO_2) (Saelee et al., 2016). Moreover, the alkalization process solubilized most of the hemicellulose found in the fibers and led to the higher exposure of cellulosic fiber. The extracted cellulose was found to have a mean diameter of 26.4 ± 11.8 μm. The destruction of the size of the natural fiber bundles after the alkalization and bleaching process was reported by (Chirayil et al., 2014). They reported that the diameter of the treated fiber was greatly reduced from 125 to 10 μm, and this was mainly due to the removal of lignin and hemicellulose, resulting in the separation of the primary cell wall of the fiber. The further decrement in the fibers diameter was observed by catalytic acid hydrolysis initiated by Cr(III)-transition metal based catalyst and H_2SO_4. These hydrolyzing agents could more readily penetrate into the extracted cellulose for the further refinement step. The acid hydrolysis was capable of disintegrating the cellulose fibers and further defibrillated the micro-sized fibers into nano-sized cellulose product, as presented in **Figure 4.16(c)**.

For one-pot isolation approach, the nanocellulose was extracted directly from untreated OPEFB via oxidative-hydrolysis catalytic reaction. As clearly displayed in **Figure 4.16(d)**, the nanocellulose fibers were successfully prepared from biomass through the one-pot process. By subjecting the H_2O_2 bleaching agent, the majority of the lignin and hemicellulose were degraded and the cellulose material remained as solid residue. This finding was in good agreement with the chemical composition analysis as indicated in **Table 4.9**. The FESEM micrograph of one-pot derived nanocellulose showed a similar particle structure as multiple steps isolated nanocellulose. In this study, finer and shorter nano-sized fibrils were expected in the nanocellulose samples obtained from different isolation techniques; however, this was not obvious from the FESEM micrographs, as shown in **Figure 4.16(c)** and **4.16(d)**. This was accredited to the strong intermolecular hydrogen bonding within the cellulose chains. As a result, the cellulosic fibrils tended to agglomerate with each other during the lyophilizing process.

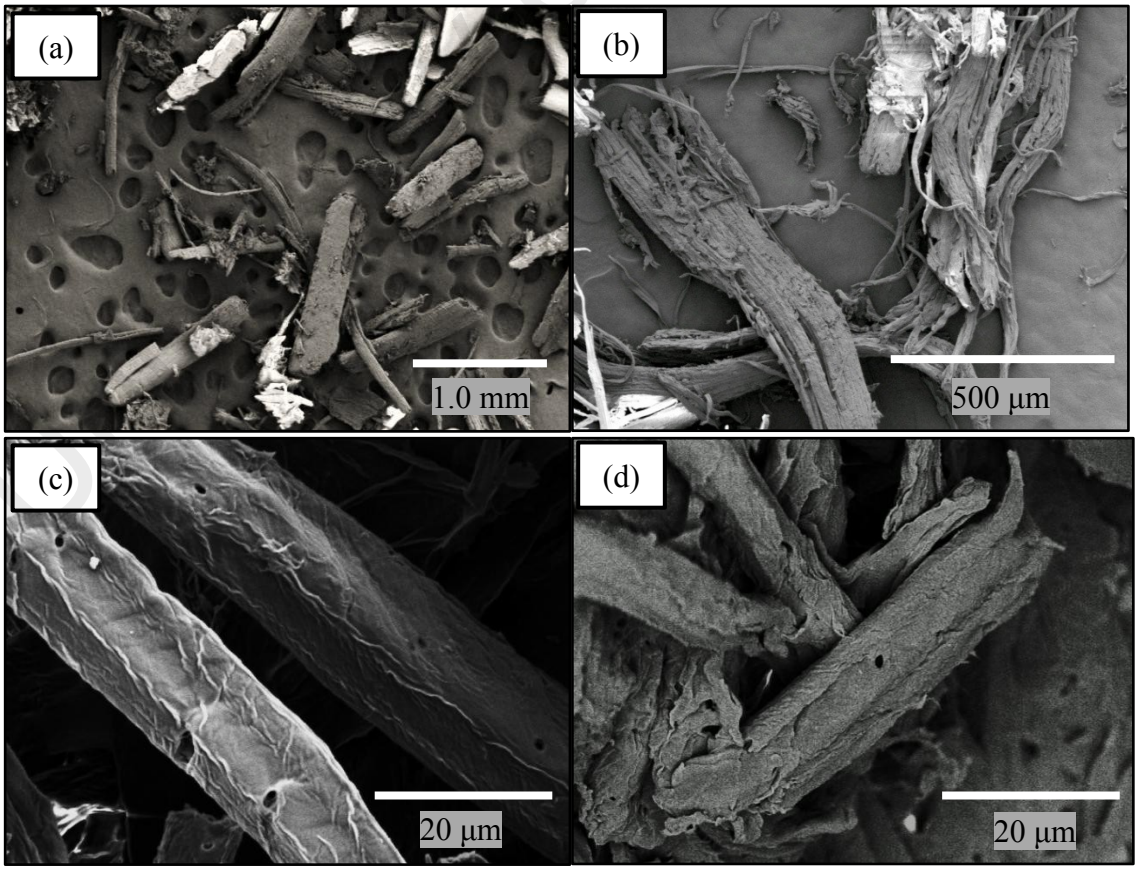

Figure 4.16: FESEM images of (a) raw OPEFB, (b) NaOH-treated fiber, (c) MS-NC and (d) OP-NC.

4.3.1.4 TEM Analysis

In order to confirm that the nano-dimensional cellulose has been isolated successfully from OPEFB biomass via one-pot isolation and multistep purification chemical procedures, TEM analysis was carried out to ensure the presence of nano-scale fiber of the yielded solid product. Based on the TEM micrographs as shown in **Figure 4.17**, it clearly demonstrated that the yielded nanocellulose displayed a spider web-like network structure with nanometer-scale diameter cellulosic fiber. In addition, the individualized fiber connected with each other which led to the formation of a network-structured. In other words, a number of partly individualized nanofibrils or branches of smaller fiber bundles hooked up to produce larger aggregates (Chirayil et al., 2014). A similar phenomenon was reported by (Tang et al., 2014) where two hypotheses were stated: (i) cellulose chains tend to be bundled and twisted together randomly, and joined together with different bundles to produce network configuration; (ii) the acid-hydrolyzed nanocellulose tended to self-assemble into porous networks to overcome the repulsion caused by surface negative charges.

Based on the TEM micrographs, it was revealed that nanocellulose yielded via one-pot isolation approach had the diameters mostly ranging between 20–60 nm with the majority at approximately 51.6 ± 15.4 nm, whereas nanocellulose isolated from multistep chemical procedures consisted of the diameter range between 20–70 nm with a mean value of 47.9 ± 23.7 nm. However, it was very difficult to measure an appropriate fiber's length of both nanocellulose products because of the entanglement, and the difficulty in assigning the ends of individual nanocellulose fibers. This finding was in excellent accordance with a literature study (Dufresne, 2013). Furthermore, some agglomeration of nanocellulose fibrils can be observed in certain places, while the rest are well-separated. A control experiment was performed at the same temperature (82

°C), reaction time (1 h), and H_2SO_4 concentration (8 wt%) without the addition of Cr(III)-transition metal based catalyst. However, the average diameter of the control sample was 75.1 ± 25.3 nm, which rendered a larger fiber dimension than nanocellulose prepared with both H_2SO_4 and Cr(III)-transition metal based catalyst.

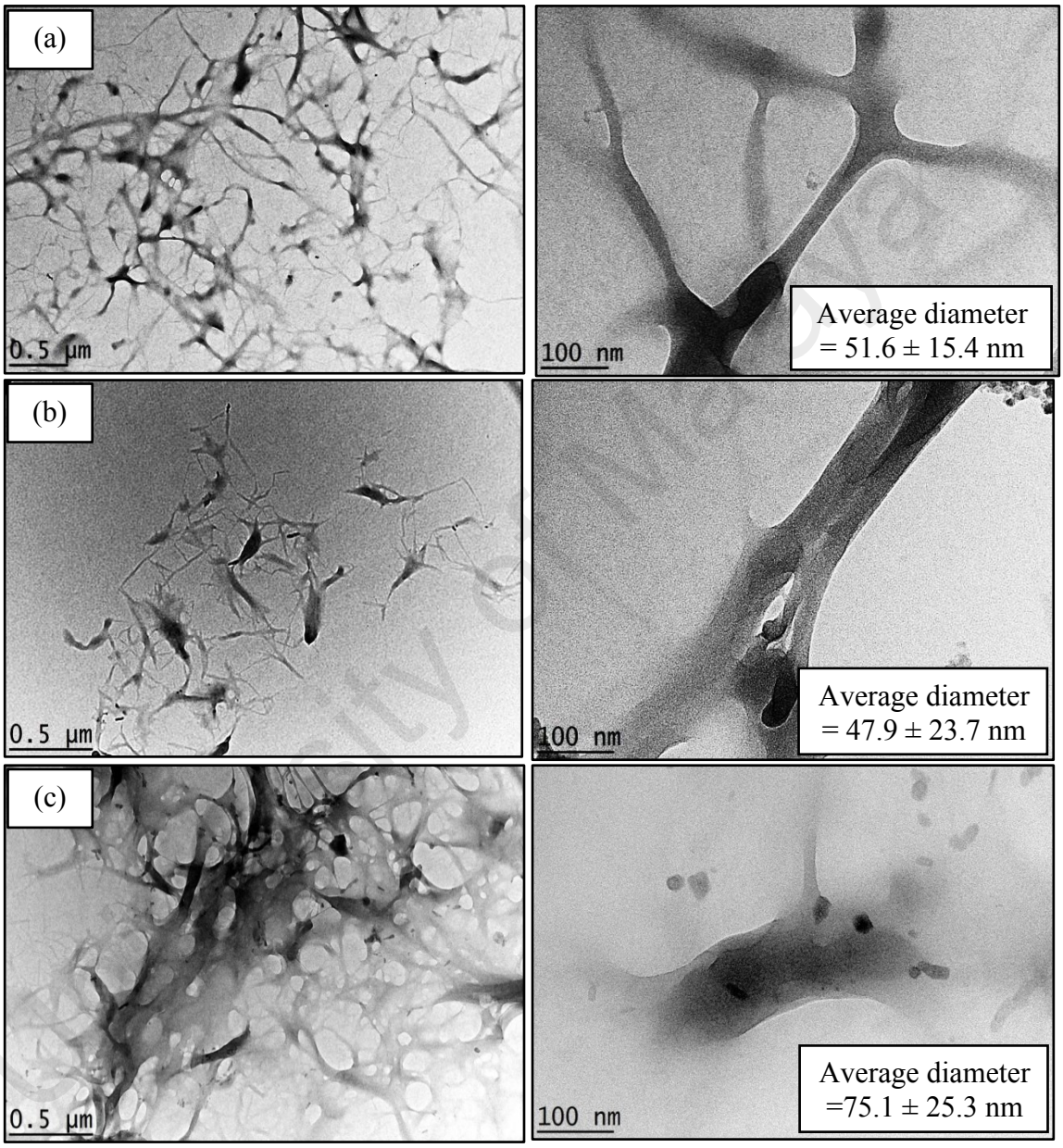

Figure 4.17: TEM micrographs of nanocellulose prepared via (a) one-pot isolation (OP-NC), (b) multistep purification process (MS-NC), and control sample (without the presence of $Cr(NO_3)_3$).

4.3.1.5 XRD Analysis

The crystallinity of samples at the different stages of chemical treatment was determined by XRD analysis (**Figure 4.18**). The untreated fiber showed the lowest crystallinity index (42.6%) as the crystalline cellulose was embedded in the amorphous nature of hemicellulose and lignin components. Therefore, the crystallinity indexes of treated fibers gradually increased due to the removal of lignin and hemicellulose by successive bleaching treatment (61.5%) and alkalization treatment (66.0%) prepared by the conventional multistep chemical process. These findings were in good accordance with a previously published result in which the bleaching and alkalization treatment could enhance the crystallinity index of mengkuang leaves effectively (Sheltami et al., 2012). In addition, the CrI values of yielded OP-NC and MS-NC products (75.4–80.3%) were higher than extracted cellulose (66.0%).

The increment of crystallinity index was accredited to several reasons: (a) the re-arrangement of the crystallite zones into a more highly ordered arrangement, and (b) the further dissolution of the non-cellulosic components and some of the amorphous parts of cellulose by hydrolysis agents (Rosli et al., 2013). The presence of hydronium ions (H_3O^+) and Cr(III)-transition metal based catalysts could penetrate into the more accessible amorphous zones of cellulose during hydrolysis, and thus promoting the hydrolytic cleavage of glycosidic linkages of cellulose, which lead to the formation of individual crystallites (Chirayil et al., 2014). As shown in **Figure 4.18**, the XRD patterns of samples revealed crystallographic peaks at $2\theta = 16.5°$ (110), 22.5° (200) and 34.6° (004), that attributed to the characteristic of cellulose I_β structure (Yahya, Lee, & Hamid, 2015).

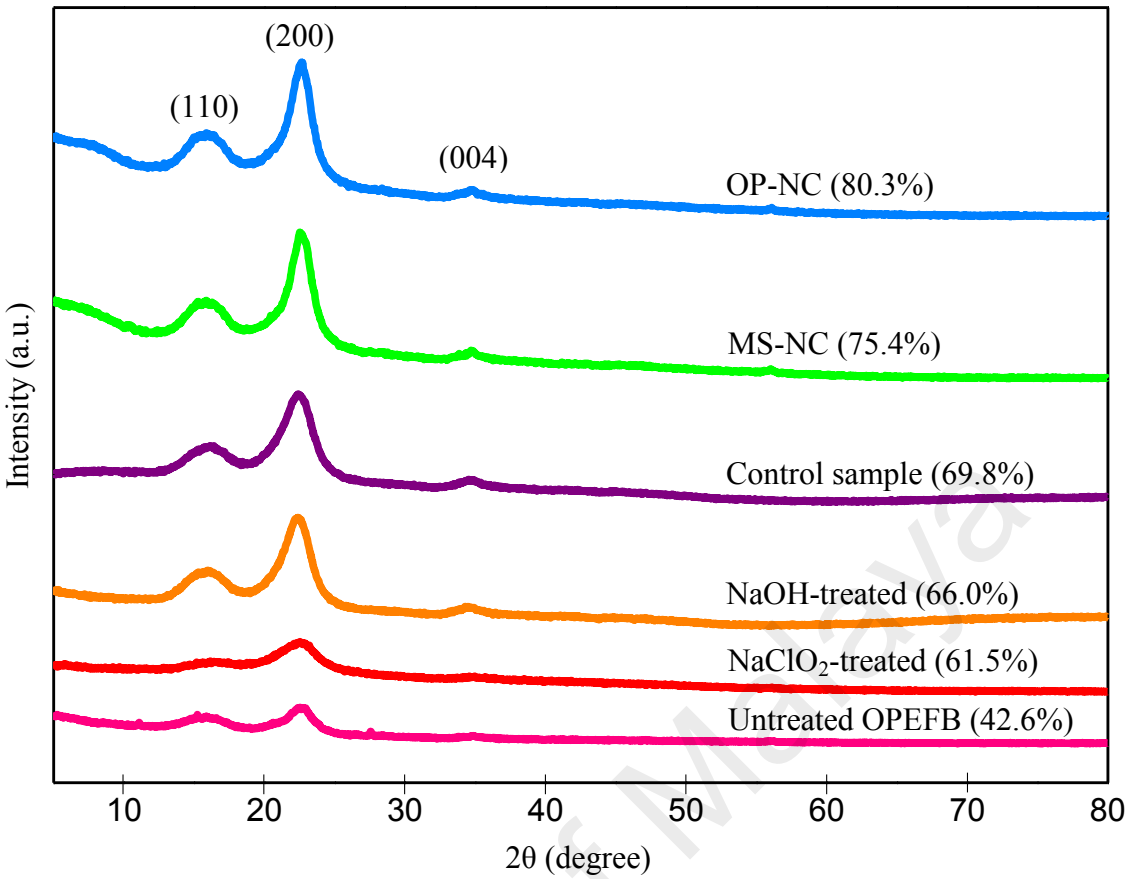

Figure 4.18: X-ray diffraction patterns of OPEFB fibers treated at different purification stages. The parentheses refer to CrI value (%) of the sample.

The crystallinity of yielded nanocellulose increased after each chemical treatment; nevertheless, OP-NC (80.3%) rendered higher crystallinity than the MS-NC (75.4%) product. The lower crystallinity of MS-NC could be attributed to the multiple chemical purification processes which not only degraded the amorphous regions in the fiber matrix, but also tend to partially damage the crystalline domains of the treated fibers. The studies conducted by (Chen et al., 2013) and (Mohkami & Talaeipour, 2011) found that the alkaline reagents, namely sodium hydroxide (NaOH), potassium hydroxide (KOH) and aqueous ammonia (NH_3) play a significant role in breaking and removing the hydrolysable glycosidic linkages of polysaccharides, as well as the hydrogen bonding within the cellulose chains of crystalline regions which led to the decrement in crystallinity index of the treated product. In fact, these studies found that alkali treatment leads to the increase in the percentage of amorphous cellulose at the expense

of crystalline cellulose. In other words, alkalization process conducted in this study was believed to not only solubilize the remaining amorphous hemicellulose content in the fiber matrix, it also contributed to the consuming of crystalline parts of cellulose chains.

Therefore, two types of isolation methods can be used to produce nanocellulose from OPEFB biomass. However, nanocellulose yielded via one-pot isolation rendered higher crystallinity than via conventional multistep chemical purification approach. Increasing the crystallinity index of the sample resulted in the increment of the modulus of elasticity, which eventually enhanced the reinforcement capability (Silvério et al., 2013). For industrial uses, the crystallinity of yielded nanocellulose is a significant factor in determining its mechanical strength and thermal properties. Higher crystallinity nanocellulose prepared via one-pot isolation approach is normally associated with better tensile strength, which is beneficial for manufacturing high-strength nanocomposites materials, and providing better reinforcement and thermal stability, making it more promising to be used in various applications (Yahya, Lee, & Hamid, 2015). On the other hand, the crystallinity index of control nanocellulose was only 69.8%. As above mentioned, the efficient disruption of hydrogen-bonding network and hydrolytic cleavage of glycosidic linkages in cellulose is still a great challenge under mild acid hydrolysis, unless with high-severity conditions. Due to this reason, the successive removal and dissolution of amorphous domains in the cellulose macro-polymer matrix were not so effective, and thus less individual elementary crystallites segments were liberated after the dilute sulfuric acid hydrolysis. In fact, the recalcitrant nature makes cellulose relatively resistant to chemical hydrolysis, and they are only partially hydrolyzed by dilute acid to their monomer components (Alvira et al., 2010; Lee, Hamid, & Zain, 2014).

The yield of nanocellulose obtained via one-pot isolation and the multistep process was determined gravimetrically. Approximately 27.5% acid-treated nanocellulose was successfully extracted from the OPEFB biomass after a series of multiple pretreatment steps. Meanwhile, the extraction process via one-pot isolation was determined to yield about 42% nanocellulose, with respect to the initial amount of dried untreated biomass. This result suggested that one-pot oxidative-hydrolysis technique can produce nanocellulose effectively in large-scale mass production for industrial application uses.

4.3.1.6 TGA Analysis

Figure 4.19 shows the TGA and its differential thermogravimetric (DTG) curves of all untreated and chemically treated OPEFB fibers. Based on the TGA result, an initial small weight loss occurred at <100 °C was observed in all samples, and this was mainly attributed to the evaporation of the intermolecular hydrogen-bonded chemisorbed water and the loosely-bound moisture on the fiber's surface (Chandra, George, & Narayanankutty, 2016). The presence of the chemisorbed water has been confirmed by the FTIR peak at 1640 cm^{-1}. For the multistep process, an increasing trend of decomposition temperature could be observed from untreated fiber to alkali-treated fiber which suggests that the thermal stability of extracted cellulose was improved by a series of chemical purification procedures. The rise in the onset temperature of decomposition of extracted cellulose could be due to several reasons: (i) the degradation of low thermal stability of hemicellulose and lignin into water soluble compounds in the treated fiber (Saelee et al., 2016); (ii) the mass proportion of compact and highly dense structure of cellulose was increased in the sample (Chandra et al., 2016); or (iii) the additional thermal stability of extracted cellulose was associated with the increased crystallinity index of the treated fiber, and thus the sample possessed more highly ordered intermolecular hydrogen bonded domains (Moriana et al., 2016). The T_{max} value of

untreated EFB, $NaClO_2$-treated, and NaOH-treated fiber was 313, 325 and 355 °C, respectively.

A significant reduction in thermal stability was found in the two types of yielded nanocellulose derived via one-pot isolation and multiple chemical purification procedure, although their crystallinity index was higher as compared with other chemically treated fibers. In this study, the yielded nanocellulose via both isolation methods showed lower T_{on} (227–232 °C) and T_{max} (307–320 °C) values compared to extracted cellulose (T_{on}: 249 °C; T_{max}: 355 °C). The decreasing of thermal stability of yielded nanocellulose as compared with the starting material was in good accordance with several previous studies (Cheng et al., 2014; Kargarzadeh et al., 2012; Tan, Abd Hamid, & Lai, 2015). The possible explanations for this phenomenon are:

1. It is widely accepted that the introduction of negative charged active sulfate groups into the surface of the cellulose crystals lead to the reduction in the thermal stability (Tang et al., 2014);
2. The yielded nanocellulose had higher specific surface area and small particle size which resulted in reduction of thermal stability (Cheng et al., 2014); and
3. The number of contact points of nanocellulose towards the heat energy increased compared to cellulose fibers as the number of individualized fibers increased after hydrolysis process (Saelee et al., 2016).

Fortunately, the nanocellulose yielded via both isolation processes was stable when the temperature was below 280 °C. This is a very important factor for yielded nanocellulose in order to be utilized for various industrial applications, especially in thermoplastic application and bio-composite related fields, as the processing temperature for these fields is normally higher than 200 °C (Y. Cao et al., 2015).

Therefore, the nanocellulose prepared remains sufficient for thermal resistance during the material processing without degradation risks. Nevertheless, a notable difference between T_{on} and T_{max} value was observed for OP-NC and MS-NC nanomaterials. This could be explained by the crystallinity index of nanocellulose derived via one-pot isolation approach (80.3%) which was higher than multistep chemical purification procedures (75.4%), as the thermal stability of cellulosic material mainly depends on the intermolecular hydrogen-bonded domains regions and their crystallinity index (Saelee et al., 2016).

Despite that, the char residue of untreated EFB biomass was the highest (25.6%) as compared with other chemically treated fibers. After the bleaching and alkalization process, the char yield of the treated fibers was greatly reduced. This was owing to the removal of lignin and hemicellulose from the biomass matrix, and led to the better accessibility of the cellulose in the treated fibers. The lowest carbon residues (~5.4%) was observed for yielded nanocellulose reflecting the complete absence of non-cellulosic compounds from the OPEFB biomass (Chirayil et al., 2014). This is not surprising because a similar phenomenon had been previously reported for the isolation of nanocellulose from the waste sackcloth (Y. Cao et al., 2015), flax (Chen et al., 2011) and *Helicteres isora* (Chirayil et al., 2014).

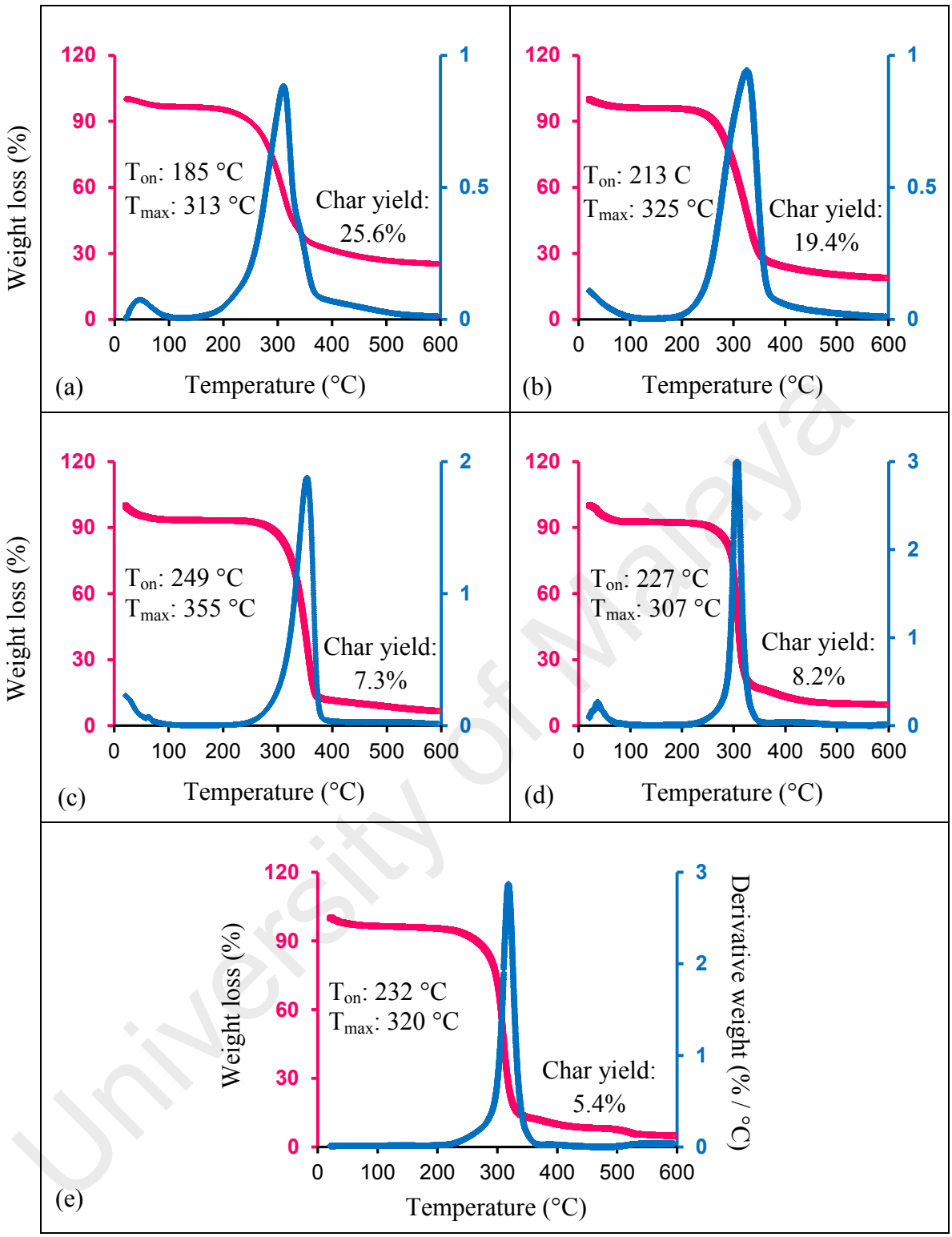

Figure 4.19: TG-DTG analysis of the (a) raw OPEFB, (b) $NaClO_2$-treated, (c) NaOH-treated and nanocellulose products: (d) MS-NC and (e) OP-NC.

4.3.1.7 GPC Analysis

In general, the molecular weight of cellulose in its original form cannot be measured because it is normally insoluble in all common solvents used for GPC system because of its strong intra- and intermolecular hydrogen bonding, high molecular weight, and high crystallinity (Hallac & Ragauskas, 2011). For GPC analysis, the two most practiced techniques for the dissolving of cellulose are nitration and tricarbanilation. Compared to tricarbanilation, nitration technique is rarely used nowadays; due to the uncertainty arising from possible acid hydrolysis of cellulose occurs during derivatization and the instability of the derivative cellulose. The acid hydrolysis catalyzed by phosphoric and nitric acids is more dramatic during the derivatizing of pure cellulose. In contrast, cellulose tricarbanilate is the most utilized derivative for GPC measurements due to several advantages: (i) No depolymerization occurs during derivation; (ii) Highly solubility and stability in THF; (iii) Complete substitution; and (iv) The stability of derivative. Therefore, by modifying the cellulosic sample using phenyl isocyanate and pyridine, the extent of the change of the tricarbanilated nanocellulose products was estimated by measuring the molecular weight and degree of polymerization (**Figure 4.20**).

It was found that the M_w and DP_w of nanocellulose were lower than that of extracted OPEFB cellulose. This trend can be explained by the successive depolymerization process of extracted cellulose when treated by Cr(III)-catalyzed acid hydrolysis. The susceptibility of the glycosidic linkages between the glucose monomers tends to be attacked by hydrolyzing catalysts and caused scission of the chains of cellulose polysaccharide molecules, especially in reactive amorphous regions. The DP value of cellulose (DP_w = 960.85) extracted in this study was smaller than for OPEFB cellulose (DP_w = 1775.6) prepared by (Fahma et al., 2011). The difference in DP values

for similar biomass was mainly due to the different purification procedures, species, composition of lignocellulose components, and most importantly, the analytical techniques used for DP measurement (Karimi & Taherzadeh, 2016). This phenomenon could serve to explain the difference of DP values observed in the case of nanocellulose products, where the MS-NC (170.32) rendered a lower degree of polymerization than OP-NC product (185.56).

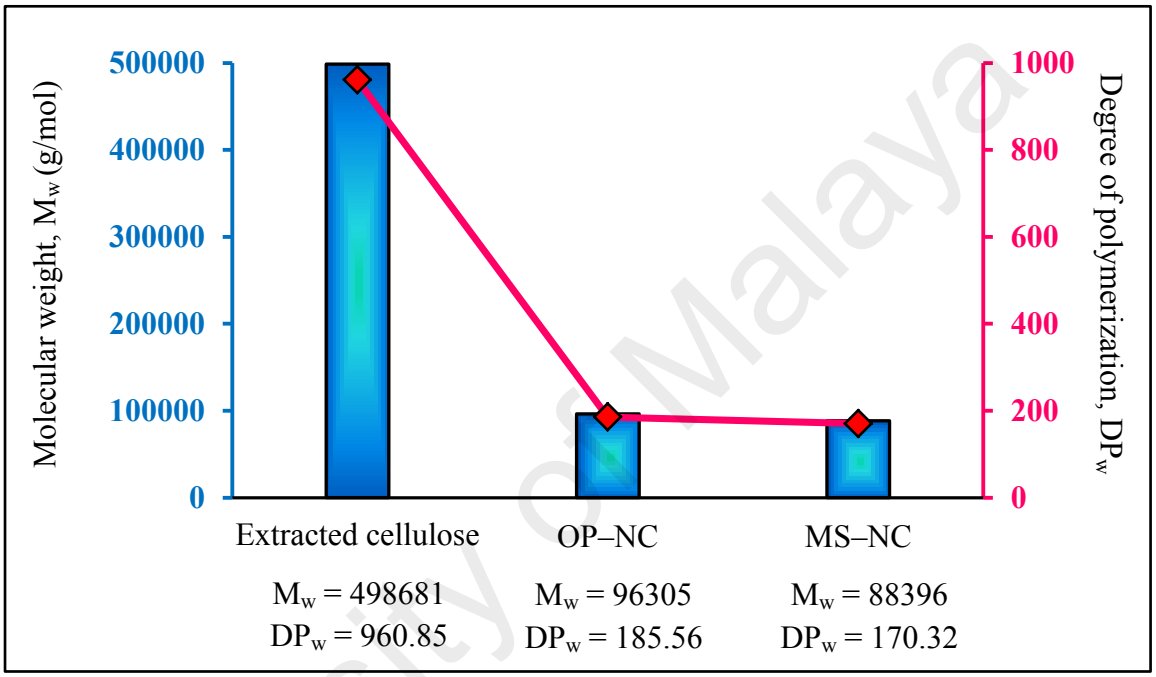

Figure 4.20: Molecular weight (M_w) and degree of polymerization (DP_w) of extracted cellulose and both isolated nanocellulose products (OP-NC and MS-NC).

4.3.2 Comparison between One-Pot Isolation and Multistep Chemical Purification Process

When comparing the two isolation procedures, significant differences are noticed in terms of productivity, fiber quality, environmental impact and economic aspect. In summary, the conventional multistep chemical process involves more sample purification steps (four stages) and requires more time (overall 15 h) than one pot isolation (one purification stage; 6 h). In addition to that, the one-pot process is considered a green and nature-friendly treatment due to the fact of being totally

chlorine-free during the whole process. It is worth mentioning that the wastewater produced from the multistep treatment (*i.e.* alkalized effluent, chlorinated products, and concentrated acid effluent) must be treated further by wastewater processing industry before it can be safely disposed to local waterways.

For the one-pot process, the only generated supernatant (heavy-metal-containing solution) in the final stage can be effectively purified by several cost-effective techniques, such as chemical precipitation, coagulation, adsorption, ion exchange, membrane separation and biosorption (Barakat, 2011). Amongst these techniques for heavy metal removal from wastewater, chemical precipitation is worth mentioning as it is the most widely used. By this process, Cr^{3+} transition metal ion could be transferred to $Cr(OH)_3$ via precipitation reaction with aqueous ammonia (alkaline) or sodium hydroxide, and the $Cr(OH)_3$ is widely used as a pigment, mordant, and catalyst for organic reactions.

Even through the multistep purification process has a lower chemical usage; this treatment suffers from significant pollution involved (or costly wastewater treatment is required) as well as tedious and time-consuming for obtaining nanocellulose. Therefore, high demand of chemical for the one-pot process is balanced by its rapid process and lower pollution involved. The nanocellulose isolated using one-pot isolation showed a higher crystallinity index, as well as better thermal stability; this is beneficial for composite material synthesis applications. In additional, more effort should be focused in order to reduce the usage of chemical as in the multistep isolation process, while maintaining the high quality and quantity of nanocellulose fibers as one-pot isolation approach; that will be however the objective of future studies.

CHAPTER 5: CONCLUSIONS AND RECOMMENDATIONS

5.1 Overall Conclusions

In the present study, different types of transition metal based catalysts, namely $Fe(NO_3)_3$, $Cr(NO_3)_3$, $Co(NO_3)_3$, $Ni(NO_3)_3$ and $Mn(NO_3)_3$ were used as hydrolyzing catalysts for the production of nanocellulose via hydrolysis process with the presence of dilute H_2SO_4. Based on the study, dilute acid alone was insufficient to hydrolyze the recalcitrant nature of cellulose into smaller dimension under mild reaction conditions. Interestingly, the presence of synergistic effect between the transition metal ion and hydronium ions (H_3O^+) from H_2SO_4 created a stronger hydrolyzing effect to degrade the glycosidic linkage of cellulose polymeric chains, especially in the amorphous regions. Therefore, the remained crystallite cellulose segments in nano-dimensional resulted in the high crystallinity index. In the preliminary study (**Section 4.1**), the crystallinity index of dilute H_2SO_4 treated nanocellulose (61.1 ± 0.2%) was relatively lower as compared to that of transition metal based catalyst treated nanocellulose, which lied from the range of 66.4 ± 0.2% to 75.6 ± 0.1%. The TEM morphology study revealed that transition metal based catalyst treated nanocellulose samples appeared in smaller fragments with the spider web-like geometry. FTIR analysis of nanocellulose obtained from transition metal assisted dilute H_2SO_4 hydrolysis indicated that the chemical structures of nanocellulose were not altered after hydrolysis process, where the typical structure of the parent α-cellulose was being preserved. TGA results suggested that the thermal stability of the yielded nanocellulose was mainly affected by the active sulfate groups, which is form H_2SO_4 solution and shorter chain of hydrolyzed cellulose.

Among the transition metal based catalysts, Cr(III)-transition metal based catalyst treated nanocellulose rendered the highest crystallinity index. This indicated that the

Lewis acid active sites of chromium(III) nitrate metal catalyst has contributed significantly in the defibrillation and delamination of cellulose matrix through the dissolution of glycosidic linkages of cellulose. Thus, Cr(III)-transition metal based catalyst was selected as the best hydrolysis catalyst for further optimization study of nanocellulose production by using response surface methodology (RSM) design system (**Section 4.2**).

The RSM technique based on five-level-four-factor CCD was conducted to study the effect of hydrolysis parameters, which including reaction temperature (x_1; 30–100 °C), reaction time (x_2; 0.5–2.5 h), concentration of Cr(III)-transition metal based catalyst (x_3; 0.025–0.425 M), and concentration of H_2SO_4 (x_4; 0.2–1.0 M) with responses of crystallinity index (y_1) and nanocellulose yield (y_2). As a hydrolyzing catalyst, the Cr(III)-transition metal based catalyst significantly enhanced the cellulose hydrolysis efficiency by improving the crystallinity index of yielded nanocellulose as compared to α-cellulose model compound. The optimum hydrolysis process resulted in highly crystalline nanocellulose (85.4%) under a moderate temperature (82 °C) with small amounts of Cr(III)-transition metal based catalyst (0.22 M) and H_2SO_4 (0.80 M). In additional, 82.86% of nanocellulose yield was obtained with the average fiber diameter of 18.4 ± 7.3 nm. The percentage error between the actual and predicted values of crystallinity index and nanocellulose yield was 0.316 and 0.531%, respectively. This result indicated that the developed empirical models were highly accurate, which verified that RSM analysis is a useful method for predicting and optimizing the reaction conditions for nanocellulose preparation via Cr(III)-transition metal assisted dilute H_2SO_4 hydrolysis. From this study, the experimental parameters including reaction temperature, reaction time, concentration of Cr(III)-transition metal based catalyst and H_2SO_4 rendered positive effect in enhancing the crystallinity of yielded nanocellulose.

The study proved that the reaction parameters including reaction temperature, reaction time, concentration of Cr(III)-transition metal based catalyst and H_2SO_4 had positive effect in enhancing the crystallinity index of yielded nanocellulose

In the last section (**Section 4.3**), a simple and novel method for preparing the nanocellulose from oil palm empty fruit bunch (OPEFB) biomass via one-pot oxidative-hydrolysis treatment without assistance of the mechanical disintegrations process was developed. Results revealed that there is a high potential of developing one-pot process for nanocellulose preparation in view of the higher crystallinity (80.3%) and better thermal stability (320 °C) obtained as compared with conventional multistep purification process (75.4% and 307 °C). The simple extraction of nanocellulose from OPEFB via one-pot process was able to reduce the damage of cellulose crystalline segments during the course of treatment and prevent the losing of extra product yield during the washing process. The nanocellulose prepared via one-pot isolation rendered a higher yield of 42% on a weight basis as compared with the multistep process (~27.5%). In addition, the physicochemical properties of yielded nanocellulose from one-pot process showed comparable properties to the multistep process, which is an alternative route for preparing the nanocellulose as less washing steps are required during purification process, therefore reducing the generation of wastewater to the environment.

5.2 Recommendations for Future Work

The use of transition metal based catalyst for acid hydrolysis is an effective approach for the catalytic depolymerization of cellulose into nanocellulose. In addition, the novel one-pot oxidative-depolymerization approach is a simple and versatile route to produce nanocellulose from complex lignocellulosic biomass with rapid and milder reaction conditions as compared to the conventional multistep process.

There are several suggestions and recommendations should be noteworthy for future works are summarized below:

1. To further evaluate the performance of other types of transition metal based catalysts by using RSM optimization study. This will provide in depth understanding on the reaction conditions of the catalytic hydrolysis system for the production of high crystallinity index nanocellulose.
2. To investigate the one-pot isolation approach by using alternative lignocellulosic biomass such as marine biomass, industrial bio-residues, softwoods, hardwoods, fruit and forestry waste. Nevertheless, the cost and availability of raw materials should be taken into consideration to choose the suitable sources for further study and application.
3. The physicochemical properties of obtained nanocellulose can be characterized extensively by different analytical techniques such as gel permeation chromatography (GPC), X-ray photoelectron spectroscopy (XPS), nuclear magnetic resonance (NMR) in future research.

REFERENCES

Abdul Khalil, H. P. S., Bhat, A. H., & Ireana Yusra, A. F. (2012). Green composites from sustainable cellulose nanofibrils: A review. *Carbohydrate Polymers, 87*(2), 963-979.

Achyuthan, K. E., Achyuthan, A. M., Adams, P. D., Dirk, S. M., Harper, J. C., Simmons, B. A., & Singh, A. K. (2010). Supramolecular self-assembled chaos: polyphenolic lignin's barrier to cost-effective lignocellulosic biofuels. *Molecules, 15*(12), 8641-8688.

Adewuyi, Y. G., & Deshmane, V. G. (2015). Intensification of enzymatic hydrolysis of cellulose using high-frequency ultrasound: an investigation of the effects of process parameters on glucose yield. *Energy & Fuels, 29*(8), 4998-5006.

Al-Dulaimi, A. A., & Wanrosli, W. D. (2016). Isolation and characterization of nanocrystalline cellulose from totally chlorine free oil palm empty fruit bunch pulp. *Journal of Polymers and the Environment*, 1-11.

Alvira, P., Tomas-Pejo, E., Ballesteros, M., & Negro, M. J. (2010). Pretreatment technologies for an efficient bioethanol production process based on enzymatic hydrolysis: A review. *Bioresource Technology, 101*(13), 4851-4861.

Anderson, S. R., Esposito, D., Gillette, W., Zhu, J., Baxa, U., & Mcneil, S. E. (2014). Enzymatic preparation of nanocrystalline and microcrystalline cellulose. *TAPPI J, 13*, 35-41.

Anwar, Z., Gulfraz, M., & Irshad, M. (2014). Agro-industrial lignocellulosic biomass a key to unlock the future bio-energy: a brief review. *Journal of radiation research and applied sciences, 7*(2), 163-173.

Azami, M., Bahram, M., Nouri, S., & Naseri, A. (2012). Central composite design for the optimization of removal of the azo dye, methyl orange, from waste water using fenton reaction. *Journal of the Serbian Chemical Society, 77*(2), 235-246.

Barakat, M. A. (2011). New trends in removing heavy metals from industrial wastewater. *Arabian Journal of Chemistry, 4*(4), 361-377.

Beltramino, F., Roncero, M. B., Torres, A. L., Vidal, T., & Valls, C. (2016). Optimization of sulfuric acid hydrolysis conditions for preparation of

nanocrystalline cellulose from enzymatically pretreated fibers. *Cellulose, 23*(3), 1777-1789.

Bensah, E. C., & Mensah, M. (2013). Chemical pretreatment methods for the production of cellulosic ethanol: technologies and innovations. *International Journal of Chemical Engineering, 2013*.

Bettaieb, F., Khiari, R., Dufresne, A., Mhenni, M., Putaux, J., & Boufi, S. (2015). Nanofibrillar cellulose from *Posidoniaoceanica*: properties and morphological features. *Industrial Crops and Products, 72*, 97-106.

Boujemaoui, A., Mongkhontreerat, S., Malmström, E., & Carlmark, A. (2015). Preparation and characterization of functionalized cellulose nanocrystals. *Carbohydrate Polymers, 115*, 457-464.

Brinchi, L., Cotana, F., Fortunati, E., & Kenny, J. M. (2013). Production of nanocrystalline cellulose from lignocellulosic biomass: technology and applications. *Carbohydrate Polymers, 94*(1), 154-169.

Brito, B. L., Pereira, F., Putaux, J.-L., & Jean, B. (2012). Preparation, morphology and structure of cellulose nanocrystals from bamboo fibers. *Cellulose, 19*(5), 1527-1536.

Cabiac, A., Guillon, E., Chambon, F., Pinel, C., Rataboul, F., & Essayem, N. (2011). Cellulose reactivity and glycosidic bond cleavage in aqueous phase by catalytic and non catalytic transformations. *Applied Catalysis A: General, 402*(1), 1-10.

Caldas, L. F. S., Francisco, B. B. A., Netto, A. D. P., & Cassella, R. J. (2011). Multivariate optimization of a spectrophotometric method for copper determination in Brazilian sugar-cane spirits using the Doehlert design. *Microchemical Journal, 99*(1), 118-124.

Cao, X., Peng, X., Sun, S., Zhong, L., Chen, W., Wang, S., & Sun, R. C. (2015). Hydrothermal conversion of xylose, glucose, and cellulose under the catalysis of transition metal sulfates. *Carbohydrate Polymers, 118*, 44-51.

Cao, Y., Jiang, Y., Song, Y., Cao, S., Miao, M., Feng, X., . . . Shi, L. (2015). Combined bleaching and hydrolysis for isolation of cellulose nanofibrils from waste sackcloth. *Carbohydrate Polymers, 131*, 152-158.

Castro, C., Zuluaga, R., Putaux, J.-L., Caro, G., Mondragon, I., & Ganán, P. (2011). Structural characterization of bacterial cellulose produced by *Gluconacetobacter*

swingsii sp. from Colombian agroindustrial wastes. *Carbohydrate Polymers, 84*(1), 96-102.

Chaker, A., Mutjé, P., Vilar, M. R., & Boufi, S. (2014). Agriculture crop residues as a source for the production of nanofibrillated cellulose with low energy demand. *Cellulose, 21*(6), 4247-4259.

Chandra, J., George, N., & Narayanankutty, S. K. (2016). Isolation and characterization of cellulose nanofibrils from arecanut husk fibre. *Carbohydrate Polymers, 142*, 158-166.

Chang, B., Fu, J., Tian, Y., & Dong, X. (2013). Multifunctionalized ordered mesoporous carbon as an efficient and stable solid acid catalyst for biodiesel preparation. *The Journal of Physical Chemistry C, 117*(12), 6252-6258.

Charreau, H., L Foresti, M., & Vazquez, A. (2013). Nanocellulose patents trends: a comprehensive review on patents on cellulose nanocrystals, microfibrillated and bacterial cellulose. *Recent patents on nanotechnology, 7*(1), 56-80.

Chen, D., Lawton, D., Thompson, M., & Liu, Q. (2012). Biocomposites reinforced with cellulose nanocrystals derived from potato peel waste. *Carbohydrate Polymers, 90*(1), 709-716.

Chen, H. (2014). Chemical composition and structure of natural lignocellulose *Biotechnology of Lignocellulose* (pp. 25-71): Springer.

Chen, W., Yu, H., Liu, Y., Chen, P., Zhang, M., & Hai, Y. (2011). Individualization of cellulose nanofibers from wood using high-intensity ultrasonication combined with chemical pretreatments. *Carbohydrate Polymers, 83*(4), 1804-1811.

Chen, W., Yu, H., Liu, Y., Hai, Y., Zhang, M., & Chen, P. (2011). Isolation and characterization of cellulose nanofibers from four plant cellulose fibers using a chemical-ultrasonic process. *Cellulose, 18*(2), 433-442.

Chen, Y., Stevens, M. A., Zhu, Y., Holmes, J., & Xu, H. (2013). Understanding of alkaline pretreatment parameters for corn stover enzymatic saccharification. *Biotechnology for Biofuels, 6*(1), 1-10.

Chen, Y. W., Lee, H. V., & Abd Hamid, S. B. (2016). Preparation and characterization of cellulose crystallites via Fe(III)-, Co(II)-and Ni(II)-assisted dilute sulfuric acid catalyzed hydrolysis process. *Journal of Nano Research, 41*, 96-109.

Chen, Y. W., Lee, H. V., & Hamid, S. B. A. (2016a). Preparation of nanostructured cellulose via Cr(III)-and Mn(II)-transition metal salt catalyzed acid hydrolysis approach. *BioResources, 11*(3), 7224-7241.

Chen, Y. W., Lee, H. V., & Hamid, S. B. A. (2016b). A response surface methodology study: effects of trivalent Cr^{3+} metal ion-catalyzed hydrolysis on nanocellulose crystallinity and yield. *BioResources, 11*(2), 4645-4662.

Chen, Y. W., Lee, H. V., Juan, J. C., & Phang, S.-M. (2016). Production of new cellulose nanomaterial from red algae marine biomass *Gelidium elegans*. *Carbohydrate Polymers, 151*, 1210-1219.

Cheng, M., Qin, Z., Liu, Y., Qin, Y., Li, T., Chen, L., & Zhu, M. (2014). Efficient extraction of carboxylated spherical cellulose nanocrystals with narrow distribution through hydrolysis of lyocell fibers by using ammonium persulfate as an oxidant. *Journal of Materials Chemistry A, 2*(1), 251-258.

Chin, S. X., Chia, C. H., Zakaria, S., Fang, Z., & Ahmad, S. (2015). Ball milling pretreatment and diluted acid hydrolysis of oil palm empty fruit bunch (EFB) fibres for the production of levulinic acid. *Journal of the Taiwan Institute of Chemical Engineers, 52*, 85-92.

Ching, Y. C., & Ng, T. S. (2014). Effect of preparation conditions on cellulose from oil palm empty fruit bunch fiber. *BioResources, 9*(4), 6373-6385.

Chirayil, C. J., Joy, J., Mathew, L., Mozetic, M., Koetz, J., & Thomas, S. (2014). Isolation and characterization of cellulose nanofibrils from *Helicteres isora* plant. *Industrial Crops and Products, 59*, 27-34.

Chowdhury, Z. Z., & Hamid, S. B. A. (2016). Preparation and characterization of nanocrystalline cellulose using ultrasonication combined with a microwave-assisted pretreatment process. *BioResources, 11*(2), 3397-3415.

Correia, J. A., Junior, J. E., Goncalves, L. R., & Rocha, M. V. (2013). Alkaline hydrogen peroxide pretreatment of cashew apple bagasse for ethanol production: study of parameters. *Bioresource Technology, 139*, 249-256.

Cui, S., Zhang, S., Ge, S., Xiong, L., & Sun, Q. (2016). Green preparation and characterization of size-controlled nanocrystalline cellulose via ultrasonic-assisted enzymatic hydrolysis. *Industrial Crops and Products, 83*, 346-352.

Davison, B. H., Parks, J., Davis, M. F., & Donohoe, B. S. (2013). Plant cell walls: basics of structure, chemistry, accessibility and the influence on conversion. *Aqueous Pretreatment of Plant Biomass for Biological and Chemical Conversion to Fuels and Chemicals*, 23-38.

de Almeida , R. M., Li, J., Nederlof, C., O'Connor, P., Makkee, M., & Moulijn, J. A. (2010). Cellulose Conversion to Isosorbide in Molten Salt hydrate Media. *ChemSusChem, 3*(3), 325-328.

Dixon, R. A. (2013). Microbiology: break down the walls. *Nature, 493*(7430), 36-37.

dos Santos, F. A., Iulianelli, G. C., & Tavares, M. I. B. (2016). The use of cellulose nanofillers in obtaining polymer nanocomposites: properties, processing, and applications. *Materials Sciences and Applications, 7*(05), 257.

dos Santos, R. M., Neto, W. P. F., Silvério, H. A., Martins, D. F., Dantas, N. O., & Pasquini, D. (2013). Cellulose nanocrystals from pineapple leaf, a new approach for the reuse of this agro-waste. *Industrial Crops and Products, 50*, 707-714.

Dufresne, A. (2013). Nanocellulose: a new ageless bionanomaterial. *Materials Today, 16*(6), 220-227.

Dufresne, A., & Belgacem, M. N. (2013). Cellulose-reinforced composites: from micro- to nanoscale. *Polímeros, 23*(3), 277-286.

Duran, N., Lemes, A. P., Duran, M., Freer, J., & Baeza, J. (2011). A minireview of cellulose nanocrystals and its potential integration as co-product in bioethanol production. *Journal of the Chilean Chemical Society, 56*(2), 672-677.

Dutta, S., De, S., & Saha, B. (2013). Advances in biomass transformation to 5-hydroxymethylfurfural and mechanistic aspects. *Biomass and Bioenergy, 55*, 355-369.

Dutta, S., De, S., Saha, B., & Alam, M. I. (2012). Advances in conversion of hemicellulosic biomass to furfural and upgrading to biofuels. *Catalysis Science & Technology, 2*(10), 2025-2036.

Elanthikkal, S., Gopalakrishnapanicker, U., Varghese, S., & Guthrie, J. T. (2010). Cellulose microfibres produced from banana plant wastes: isolation and characterization. *Carbohydrate Polymers, 80*(3), 852-859.

Esa, F., Tasirin, S. M., & Rahman, N. A. (2014). Overview of bacterial cellulose production and application. *Agriculture and Agricultural Science Procedia, 2*, 113-119.

Fahma, F., Iwamoto, S., Hori, N., Iwata, T., & Takemura, A. (2011). Effect of pre-acid-hydrolysis treatment on morphology and properties of cellulose nanowhiskers from coconut husk. *Cellulose, 18*(2), 443-450.

Feng, X., Meng, X., Zhao, J., Miao, M., Shi, L., Zhang, S., & Fang, J. (2015). Extraction and preparation of cellulose nanocrystals from dealginate kelp residue: structures and morphological characterization. *Cellulose, 22*(3), 1763-1772.

Flauzino Neto, W. P., Silvério, H. A., Dantas, N. O., & Pasquini, D. (2013). Extraction and characterization of cellulose nanocrystals from agro-industrial residue – soy hulls. *Industrial Crops and Products, 42*(0), 480-488.

Frone, A. N., Panaitescu, D. M., & Donescu, D. (2011). Some aspects concerning the isolation of cellulose micro-and nano-fibers. *UPB Buletin Stiintific, Series B: Chemistry and Materials Science, 73*(2), 133-152.

García, A., Gandini, A., Labidi, J., Belgacem, N., & Bras, J. (2016). Industrial and crop wastes: a new source for nanocellulose biorefinery. *Industrial Crops and Products, 93*, 26-38.

George, J., & Sabapathi, S. (2015). Cellulose nanocrystals: synthesis, functional properties, and applications. *Nanotechnology, science and applications, 8*, 45.

Gericke, M., Fardim, P., & Heinze, T. (2012). Ionic liquids—promising but challenging solvents for homogeneous derivatization of cellulose. *Molecules, 17*(6), 7458-7502.

Gírio, F. M., Carvalheiro, F., Duarte, L. C., & Bogel-Łukasik, R. (2012). Deconstruction of the hemicellulose fraction from lignocellulosic materials into simple sugars. In S. S. da Silva & K. A. Chandel (Eds.), *D-Xylitol: Fermentative Production, Application and Commercialization* (pp. 3-37). Berlin, Heidelberg: Springer Berlin Heidelberg.

Goh, K. Y., Ching, Y. C., Chuah, C. H., Abdullah, L. C., & Liou, N.-S. (2016). Individualization of microfibrillated celluloses from oil palm empty fruit bunch: comparative studies between acid hydrolysis and ammonium persulfate oxidation. *Cellulose, 23*(1), 379-390.

Haafiz, M. K. M., Hassan, A., Khalil, H. P. S. A., Fazita, M. R. N., Islam, M. S., Inuwa, I. M., . . . Hussin, M. H. (2016). Exploring the effect of cellulose nanowhiskers isolated from oil palm biomass on polylactic acid properties. *International Journal of Biological Macromolecules, 85*, 370-378.

Habibi, Y. (2014). Key advances in the chemical modification of nanocelluloses. *Chemical Society Reviews, 43*(5), 1519-1542.

Habibi, Y., Lucia, L. A., & Rojas, O. J. (2010). Cellulose nanocrystals: chemistry, self-assembly, and applications. *Chemical Reviews, 110*(6), 3479-3500.

Hadar, Y. (2013). Sources for lignocellulosic raw materials for the production of ethanol *Lignocellulose Conversion* (pp. 21-38): Springer.

Hallac, B. B., & Ragauskas, A. J. (2011). Analyzing cellulose degree of polymerization and its relevancy to cellulosic ethanol. *Biofuels, Bioproducts and Biorefining, 5*(2), 215-225.

Hamad, W. Y., & Hu, T. Q. (2010). Structure–process–yield interrelations in nanocrystalline cellulose extraction. *The Canadian Journal of Chemical Engineering, 88*(3), 392-402.

Hamid, S. B. A., Chowdhury, Z. Z., & Karim, M. Z. (2014). Catalytic extraction of microcrystalline cellulose (MCC) from *Elaeis guineensis* using central composite design (CCD). *BioResources, 9*(4), 7403-7426.

Hamid, S. B. A., Chowdhury, Z. Z., Karim, M. Z., & Ali, M. E. (2016). Catalytic isolation and physicochemical properties of nanocrystalline cellulose (NCC) using HCl-$FeCl_3$ system combined with ultrasonication. *BioResources, 11*(2), 3840-3855.

Hamid, S. B. A., Zain, S. K., Das, R., & Centi, G. (2015). Synergic effect of tungstophosphoric acid and sonication for rapid synthesis of crystalline nanocellulose. *Carbohydrate Polymers, 138*, 349-355.

Hassan, M. L., Mathew, A. P., Hassan, E. A., El-Wakil, N. A., & Oksman, K. (2012). Nanofibers from bagasse and rice straw: process optimization and properties. *Wood science and technology, 46*(1-3), 193-205.

He, W., Jiang, X., Sun, F., & Xu, X. (2014). Extraction and characterization of cellulose nanofibers from *Phyllostachys nidularia Munro* via a combination of acid treatment and ultrasonication. *BioResources, 9*(4), 6876-6887.

Hosseini, S. A., Nouri, S., Hashemi, S., & Akbari, M. (2017). Investigation of performance of Ni/Clinoptilolite nanoadsorbents in desulfurization of gas oil: experimental design and modeling. *Iranian Journal of Oil & Gas Science and Technology, 6*(1), 13-25.

Hsieh, Y.-L. (2013). Cellulose nanocrystals and self-assembled nanostructures from cotton, rice straw and grape skin: a source perspective. *Journal of Materials Science, 48*(22), 7837-7846.

Hu, X., Xiao, Y., Niu, K., Zhao, Y., Zhang, B., & Hu, B. (2013). Functional ionic liquids for hydrolysis of lignocellulose. *Carbohydrate Polymers, 97*(1), 172-176.

Hu, Y., Tang, L., Lu, Q., Wang, S., Chen, X., & Huang, B. (2014). Preparation of cellulose nanocrystals and carboxylated cellulose nanocrystals from borer powder of bamboo. *Cellulose, 21*(3), 1611-1618.

Huang, Y.-B., & Fu, Y. (2013). Hydrolysis of cellulose to glucose by solid acid catalysts. *Green Chemistry, 15*(5), 1095.

Hubbell, C. A., & Ragauskas, A. J. (2010). Effect of acid-chlorite delignification on cellulose degree of polymerization. *Bioresource Technology, 101*(19), 7410-7415.

Ioelovich, M., Leykin, A., & Figovsky, O. (2010). Study of cellulose paracrystallinity. *BioResources, 5*(3), 1393-1407.

Iris, K., Tsang, D. C., Yip, A. C., Chen, S. S., Ok, Y. S., & Poon, C. S. (2016). Valorization of food waste into hydroxymethylfurfural: dual role of metal ions in successive conversion steps. *Bioresource technology, 219*, 338-347.

Islam, M. T., Alam, M. M., Patrucco, A., Montarsolo, A., & Zoccola, M. (2014). Preparation of nanocellulose: a review. *AATCC Journal of Research, 1*(5), 17-23.

Jawaid, M., & Khalil, H. A. (2011). Cellulosic/synthetic fibre reinforced polymer hybrid composites: a review. *Carbohydrate Polymers, 86*(1), 1-18.

Ji, W., Shen, Z., & Wen, Y. (2015). Hydrolysis of wheat straw by dilute sulfuric acid in a continuous mode. *Chemical Engineering Journal, 260*, 20-27.

Jiang, F., & Hsieh, Y.-L. (2013). Chemically and mechanically isolated nanocellulose and their self-assembled structures. *Carbohydrate Polymers, 95*(1), 32-40.

Johar, N., Ahmad, I., & Dufresne, A. (2012). Extraction, preparation and characterization of cellulose fibres and nanocrystals from rice husk. *Industrial Crops and Products, 37*(1), 93-99.

Jonoobi, M., Harun, J., Mathew, A. P., Hussein, M. Z. B., & Oksman, K. (2010). Preparation of cellulose nanofibers with hydrophobic surface characteristics. *Cellulose, 17*(2), 299-307.

Jonoobi, M., Harun, J., Tahir, P. M., Shakeri, A., SaifulAzry, S., & Makinejad, M. D. (2011). Physicochemical characterization of pulp and nanofibers from kenaf stem. *Materials Letters, 65*(7), 1098-1100.

Jonoobi, M., Khazaeian, A., Tahir, P. M., Azry, S. S., & Oksman, K. (2011). Characteristics of cellulose nanofibers isolated from rubberwood and empty fruit bunches of oil palm using chemo-mechanical process. *Cellulose, 18*(4), 1085-1095.

Jonoobi, M., Mathew, A. P., & Oksman, K. (2012). Producing low-cost cellulose nanofiber from sludge as new source of raw materials. *Industrial Crops and Products, 40*, 232-238.

Jonoobi, M., Oladi, R., Davoudpour, Y., Oksman, K., Dufresne, A., Hamzeh, Y., & Davoodi, R. (2015). Different preparation methods and properties of nanostructured cellulose from various natural resources and residues: a review. *Cellulose*.

Jordan, D. B., Bowman, M. J., Braker, J. D., Dien, B. S., Hector, R. E., Lee, C. C., . . . Wagschal, K. (2012). Plant cell walls to ethanol. *Biochemical Journal, 442*(2), 241-252.

Kalia, S., Boufi, S., Celli, A., & Kango, S. (2014). Nanofibrillated cellulose: surface modification and potential applications. *Colloid and Polymer Science, 292*(1), 5-31.

Kamireddy, S. R., Li, J., Tucker, M., Degenstein, J., & Ji, Y. (2013). Effects and mechanism of metal chloride salts on pretreatment and enzymatic digestibility of corn stover. *Industrial & Engineering Chemistry Research, 52*(5), 1775-1782.

Karande, V., Bharimalla, A., Hadge, G., Mhaske, S., & Vigneshwaran, N. (2011). Nanofibrillation of cotton fibers by disc refiner and its characterization. *Fibers and Polymers, 12*(3), 399-404.

Kargarzadeh, H., Ahmad, I., Abdullah, I., Dufresne, A., Zainudin, S. Y., & Sheltami, R. M. (2012). Effects of hydrolysis conditions on the morphology, crystallinity, and thermal stability of cellulose nanocrystals extracted from kenaf bast fibers. *Cellulose, 19*(3), 855-866.

Karim, M. Z., Chowdhury, Z. Z., Hamid, S. B. A., & Ali, M. E. (2014). Statistical optimization for acid hydrolysis of microcrystalline cellulose and its physiochemical characterization by using metal ion catalyst. *Materials, 7*(10), 6982-6999.

Karim, Z., Chowdhury, Z. Z., Hamid, S. B. A., & Ali, E. (2016). Optimizing pretreatment process conditions using Lewis acid catalyst for higher crystallinity of α-cellulose. *Science of Advanced Materials, 8*(3), 534-544.

Karimi, K., & Taherzadeh, M. J. (2016). A critical review on analysis in pretreatment of lignocelluloses: degree of polymerization, adsorption/desorption, and accessibility. *Bioresource Technology, 203*, 348-356.

Kaushik, M., Putaux, J., Fraschini, C., Chauve, G., & Moores, A. (2015). Transmission electron microscopy for the characterization of cellulose nanocrystals. *The Transmission Electron Microscope, Intech, 129*, 163.

Khalil, H. A., Davoudpour, Y., Islam, M. N., Mustapha, A., Sudesh, K., Dungani, R., & Jawaid, M. (2014). Production and modification of nanofibrillated cellulose using various mechanical processes: a review. *Carbohydrate polymers, 99*, 649-665.

Khalil, H. A., Hassan, A., Zaidon, A., Jawaid, M., & Paridah, M. (2012). Oil palm biomass fibres and recent advancement in oil palm biomass fibres based hybrid biocomposites. In *Composites and Their Applications*. InTech.

Khawas, P., & Deka, S. C. (2016). Isolation and characterization of cellulose nanofibers from culinary banana peel using high-intensity ultrasonication combined with chemical treatment. *Carbohydrate Polymers, 137*, 608-616.

Kim, D.-Y., Lee, B.-M., Koo, D. H., Kang, P.-H., & Jeun, J.-P. (2016). Preparation of nanocellulose from a kenaf core using E-beam irradiation and acid hydrolysis. *Cellulose, 23*(5), 3039-3049.

Kim, H. C., Mun, S., Ko, H.-U., Zhai, L., Kafy, A., & Kim, J. (2016). Renewable smart materials. *Smart Materials and Structures, 25*(7), 073001.

Klein, M., Varvak, A., Segal, E., Markovsky, B., Pulidindi, I. N., Perkas, N., & Gedanken, A. (2015). Sonochemical synthesis of HSiW/graphene catalysts for enhanced biomass hydrolysis. *Green Chemistry, 17*(4), 2418-2425.

Klemm, D., Kramer, F., Moritz, S., Lindström, T., Ankerfors, M., Gray, D., & Dorris, A. (2011). Nanocelluloses: a new family of nature-based materials. *Angewandte Chemie International Edition, 50*(24), 5438-5466.

Komanoya, T., Kobayashi, H., Hara, K., Chun, W.-J., & Fukuoka, A. (2011). Catalysis and characterization of carbon-supported ruthenium for cellulose hydrolysis. *Applied Catalysis A: General, 407*(1), 188-194.

Kopania, E., Wietecha, J., & Ciechańska, D. (2012). Studies on isolation of cellulose fibres from waste plant biomass. *Fibres & Textiles in Eastern Europe, 6B*(96), 167-172.

Kotarska, K., Świerczyńska, A., & Dziemianowicz, W. (2015). Study on the decomposition of lignocellulosic biomass and subjecting it to alcoholic fermentation: study on the decomposition of lignocellulosic biomass. *Renewable Energy, 75*, 389-394.

Kouzuma, A., & Watanabe, K. (2015). Exploring the potential of algae/bacteria interactions. *Current Opinion in Biotechnology, 33*, 125-129.

Kulasinski, K., Keten, S., Churakov, S. V., Derome, D., & Carmeliet, J. (2014). A comparative molecular dynamics study of crystalline, paracrystalline and amorphous states of cellulose. *Cellulose, 21*(3), 1103-1116.

Kumar, A., Negi, Y. S., Choudhary, V., & Bhardwaj, N. K. (2014). Characterization of cellulose nanocrystals produced by acid-hydrolysis from sugarcane bagasse as agro-waste. *Journal of Materials Physics and Chemistry, 2*(1), 1-8.

Lamaming, J., Hashim, R., Sulaiman, O., Leh, C. P., Sugimoto, T., & Nordin, N. A. (2015). Cellulose nanocrystals isolated from oil palm trunk. *Carbohydrate Polymers, 127*, 202-208.

Lee, H., Hamid, S., & Zain, S. (2014). Conversion of lignocellulosic biomass to nanocellulose: structure and chemical process. *The Scientific World Journal, 2014*.

Lee, S.-Y., Ahn, J.-W., Hwang, H.-J., & Lee, S.-B. (2011). Seaweed biomass resources in Korea. *KSBB Journal, 26*(4), 267-276.

Li, B., Xu, W., Kronlund, D., Määttänen, A., Liu, J., Smått, J.-H., . . . Xu, C. (2015). Cellulose nanocrystals prepared via formic acid hydrolysis followed by TEMPO-mediated oxidation. *Carbohydrate polymers, 133*, 605-612.

Li, C., Zhao, X., Wang, A., Huber, G., & Zhang, T. (2015). Catalytic transformation of lignin for the production of chemicals and fuels. *Chemical Reviews, 115*(21), 11559-11624.

Li, H.-Y., Sun, S.-N., Wang, C.-Z., & Sun, R.-C. (2015). Structural and dynamic changes of lignin in *Eucalyptus* cell walls during successive alkaline ethanol treatments. *Industrial Crops and Products, 74*, 200-208.

Li, J., Wei, X., Wang, Q., Chen, J., Chang, G., Kong, L., . . . Liu, Y. (2012). Homogeneous isolation of nanocellulose from sugarcane bagasse by high pressure homogenization. *Carbohydrate Polymers, 90*(4), 1609-1613.

Li, J., Xiu, H., Zhang, M., Wang, H., Ren, Y., & Ji, Y. (2013). Enhancement of cellulose acid hydrolysis selectivity using metal ion catalysts. *Current Organic Chemistry, 17*(15), 1617-1623.

Li, J., Zhang, X., Zhang, M., Xiu, H., & He, H. (2014). Optimization of selective acid hydrolysis of cellulose for microcrystalline cellulose using $FeCl_3$. *BioResources, 9*(1), 1334-1345.

Li, J., Zhang, X., Zhang, M., Xiu, H., & He, H. (2015). Ultrasonic enhance acid hydrolysis selectivity of cellulose with HCl-$FeCl_3$ as catalyst. *Carbohydrate Polymers, 117*, 917-922.

Li, L., Lee, S., Lee, H., & Youn, H. (2011). Hydrogen peroxide bleaching of hardwood kraft pulp with adsorbed birch xylan and its effect on paper properties. *BioResources, 6*(1), 721-736.

Li, W., Yue, J., & Liu, S. (2012). Preparation of nanocrystalline cellulose via ultrasound and its reinforcement capability for poly(vinyl alcohol) composites. *Ultrasonics Sonochemistry, 19*(3), 479-485.

Li, Y., Zhu, H., Xu, M., Zhuang, Z., Xu, M., & Dai, H. (2014). High yield preparation method of thermally stable cellulose nanofibers. *BioResources, 9*(2), 1986-1997.

Liimatainen, H., Visanko, M., Sirviö, J., Hormi, O., & Niinimäki, J. (2013). Sulfonated cellulose nanofibrils obtained from wood pulp through regioselective oxidative bisulfite pre-treatment. *Cellulose, 20*(2), 741-749.

Liu, C., Li, B., Du, H., Lv, D., Zhang, Y., Yu, G., . . . Peng, H. (2016). Properties of nanocellulose isolated from corncob residue using sulfuric acid, formic acid, oxidative and mechanical methods. *Carbohydrate Polymers, 151*, 716–724.

Liu, H., & Zhu, J. (2010). Eliminating inhibition of enzymatic hydrolysis by lignosulfonate in unwashed sulfite-pretreated aspen using metal salts. *Bioresource technology, 101*(23), 9120-9127.

Liu, Y., Wang, H., Yu, G., Yu, Q., Li, B., & Mu, X. (2014). A novel approach for the preparation of nanocrystalline cellulose by using phosphotungstic acid. *Carbohydrate Polymers, 110*, 415-422.

Loow, Y.-L., Wu, T. Y., Tan, K. A., Lim, Y. S., Siow, L. F., Md. Jahim, J., . . . Teoh, W. H. (2015). Recent advances in the application of inorganic salt pretreatment for transforming lignocellulosic biomass into reducing sugars. *Journal of Agricultural and Food Chemistry, 63*(38), 8349-8363.

Lu, P., & Hsieh, Y.-L. (2010). Preparation and properties of cellulose nanocrystals: rods, spheres, and network. *Carbohydrate Polymers, 82*(2), 329-336.

Lu, P., & Hsieh, Y.-L. (2012). Preparation and characterization of cellulose nanocrystals from rice straw. *Carbohydrate Polymers, 87*(1), 564-573.

Lu, Q., Tang, L., Lin, F., Wang, S., Chen, Y., Chen, X., & Huang, B. (2014). Preparation and characterization of cellulose nanocrystals via ultrasonication-assisted $FeCl_3$-catalyzed hydrolysis. *Cellulose, 21*(5), 3497-3506.

Lu, Z., Fan, L., Zheng, H., Lu, Q., Liao, Y., & Huang, B. (2013). Preparation, characterization and optimization of nanocellulose whiskers by simultaneously ultrasonic wave and microwave assisted. *Bioresource Technology, 146*, 82-88.

Ludueña, L., Vecchio, A., Stefani, P., & Alvarez, V. (2013). Extraction of cellulose nanowhiskers from natural fibers and agricultural byproducts. *Fibers and Polymers, 14*(7), 1118-1127.

Man, Z., Muhammad, N., Sarwono, A., Bustam, M. A., Kumar, M. V., & Rafiq, S. (2011). Preparation of cellulose nanocrystals using an ionic liquid. *Journal of Polymers and the Environment, 19*(3), 726-731.

Manavalan, T., Manavalan, A., & Heese, K. (2015). Characterization of lignocellulolytic enzymes from white-rot fungi. *Current Microbiology, 70*(4), 485-498.

Mandal, A., & Chakrabarty, D. (2011). Isolation of nanocellulose from waste sugarcane bagasse (SCB) and its characterization. *Carbohydrate Polymers, 86*(3), 1291-1299.

Masoumi, H. R. F., Kassim, A., Basri, M., & Abdullah, D. K. (2011). Determining optimum conditions for lipase-catalyzed synthesis of triethanolamine (TEA)-based esterquat cationic surfactant by a Taguchi robust design method. *Molecules, 16*(6), 4672-4680.

Masruchin, N., Park, B.-D., Causin, V., & Um, I. C. (2015). Characteristics of TEMPO-oxidized cellulose fibril-based hydrogels induced by cationic ions and their properties. *Cellulose, 22*(3), 1993-2010.

Matsagar, B. M., & Dhepe, P. L. (2015). Brönsted acidic ionic liquid-catalyzed conversion of hemicellulose into sugars. *Catalysis Science & Technology, 5*(1), 531-539.

Maurya, D. P., Singla, A., & Negi, S. (2015). An overview of key pretreatment processes for biological conversion of lignocellulosic biomass to bioethanol. *3 Biotech, 5*(5), 597-609.

Medina, J. D. C., Woiciechowski, A., Filho, A. Z., Nigam, P. S., Ramos, L. P., & Soccol, C. R. (2016). Steam explosion pretreatment of oil palm empty fruit bunches (EFB) using autocatalytic hydrolysis: a biorefinery approach. *Bioresource Technology, 199*, 173-180.

Mihranyan, A. (2011). Cellulose from cladophorales green algae: from environmental problem to high-tech composite materials. *Journal of Applied Polymer Science, 119*(4), 2449-2460.

Missoum, K., Martoïa, F., Belgacem, M. N., & Bras, J. (2013). Effect of chemically modified nanofibrillated cellulose addition on the properties of fiber-based materials. *Industrial Crops and Products, 48*, 98-105.

Mohaiyiddin, M. S., Lin, O. H., Owi, W. T., Chan, C. H., Chia, C. H., Zakaria, S., & Akil, H. M. (2016). Characterization of nanocellulose recovery from Elaeis guineensis frond for sustainable development. *Clean Technologies and Environmental Policy*, 1-10.

Mohamad Haafiz, M. K., Eichhorn, S. J., Hassan, A., & Jawaid, M. (2013). Isolation and characterization of microcrystalline cellulose from oil palm biomass residue. *Carbohydrate Polymers, 93*(2), 628-634.

Mohamed, M., Salleh, W., Jaafar, J., Asri, S., & Ismail, A. (2015). Physicochemical properties of "green" nanocrystalline cellulose isolated from recycled newspaper. *RSC Advances, 5*(38), 29842-29849.

Mohammad, S. M., Rahman, N. A., Khalil, M. S., & Abdullah, S. R. S. (2014). An overview of biocellulose production using *Acetobacter xylinum* Culture. *Advances in Biological Research, 8*(6), 307-313.

Mohan, S., Viruthagiri, T., & Arunkumar, C. (2014). Statistical optimization of process parameters for the production of tannase by *Aspergillus flavus* under submerged fermentation. *3 Biotech, 4*(2), 159-166.

Mohkami, M., & Talaeipour, M. (2011). Investigation of the chemical structure of carboxylated and carboxymethylated fibers from waste paper via XRD and FTIR analysis. *BioResources, 6*(2), 1988-2003.

Mood, S. H., Golfeshan, A. H., Tabatabaei, M., Jouzani, G. S., Najafi, G. H., Gholami, M., & Ardjmand, M. (2013). Lignocellulosic biomass to bioethanol, a comprehensive review with a focus on pretreatment. *Renewable and Sustainable Energy Reviews, 27*, 77-93.

Moon, R. J., Martini, A., Nairn, J., Simonsen, J., & Youngblood, J. (2011). Cellulose nanomaterials review: structure, properties and nanocomposites. *Chemical Society Reviews, 40*(7), 3941-3994.

Mora-Pale, M., Meli, L., Doherty, T. V., Linhardt, R. J., & Dordick, J. S. (2011). Room temperature ionic liquids as emerging solvents for the pretreatment of lignocellulosic biomass. *Biotechnology and Bioengineering, 108*(6), 1229-1245.

Morais, J. P., Rosa Mde, F., de Souza Filho Mde, S., Nascimento, L. D., do Nascimento, D. M., & Cassales, A. R. (2013). Extraction and characterization of nanocellulose structures from raw cotton linter. *Carbohydrate Polymers, 91*(1), 229-235.

Moriana, R., Vilaplana, F., & Ek, M. (2016). Cellulose nanocrystals from forest residues as reinforcing agents for composites: a study from macro- to nano-dimensions. *Carbohydrate Polymers, 139*, 139-149.

Ng, W. P. Q., Lam, H. L., Ng, F. Y., Kamal, M., & Lim, J. H. E. (2012). Waste-to-wealth: green potential from palm biomass in Malaysia. *Journal of Cleaner Production, 34*, 57-65.

Nguyen, H. D., Mai, T. T. T., Nguyen, N. B., Dang, T. D., Le, M. L. P., & Dang, T. T. (2013). A novel method for preparing microfibrillated cellulose from bamboo fibers. *Advances in Natural Sciences: Nanoscience and Nanotechnology, 4*(1), 015016.

Ogura, K., Ninomiya, K., Takahashi, K., Ogino, C., & Kondo, A. (2014). Pretreatment of Japanese cedar by ionic liquid solutions in combination with acid and metal ion and its application to high solid loading. *Biotechnology for biofuels, 7*(1), 120.

Pacaphol, K., & Aht-Ong, D. (2017). Preparation of hemp nanofibers from agricultural waste by mechanical defibrillation in water. *Journal of Cleaner Production, 142*, 1283-1295.

Pang, C. H., Gaddipatti, S., Tucker, G., Lester, E., & Wu, T. (2014). Relationship between thermal behaviour of lignocellulosic components and properties of biomass. *Bioresource Technology, 172*, 312-320.

Park, S., Baker, J. O., Himmel, M. E., Parilla, P. A., & Johnson, D. K. (2010). Cellulose crystallinity index: measurement techniques and their impact on interpreting cellulase performance. *Biotechnology for Biofuels, 3*(1), 1.

Peng, L., Lin, L., Zhang, J., Zhuang, J., Zhang, B., & Gong, Y. (2010). Catalytic conversion of cellulose to levulinic acid by metal chlorides. *Molecules, 15*(8), 5258-5272.

Prasad, K. S., Rao, C., & Rao, D. N. (2012). Application of design of experiments to plasma arc welding process: a review. *Journal of the Brazilian Society of Mechanical Sciences and Engineering, 34*(1), 75-81.

Qing, Y., Sabo, R., Zhu, J., Agarwal, U., Cai, Z., & Wu, Y. (2013). A comparative study of cellulose nanofibrils disintegrated via multiple processing approaches. *Carbohydrate Polymers, 97*(1), 226-234.

Qua, E. H., Hornsby, P. R., Sharma, H. S. S., & Lyons, G. (2011). Preparation and characterisation of cellulose nanofibres. *Journal of Materials Science, 46*(18), 6029-6045.

Rafatullah, M., Ahmad, T., Ghazali, A., Sulaiman, O., Danish, M., & Hashim, R. (2013). Oil palm biomass as a precursor of activated carbons: a review. *Critical Reviews in Environmental Science and Technology, 43*(11), 1117-1161.

Rattaz, A., Mishra, S. P., Chabot, B., & Daneault, C. (2011). Cellulose nanofibres by sonocatalysed-TEMPO-oxidation. *Cellulose, 18*(3), 585-593.

Rebouillat, S., & Pla, F. (2013). State of the art manufacturing and engineering of nanocellulose: a review of available data and industrial applications. *Journal of Biomaterials and Nanobiotechnology, 4*(2), 165.

Rohaizu, R., & Wanrosli, W. D. (2017). Sono-assisted TEMPO oxidation of oil palm lignocellulosic biomass for isolation of nanocrystalline cellulose. *Ultrasonics Sonochemistry, 34*, 631-639.

Rojas, J., Bedoya, M., & Ciro, Y. (2015). Current trends in the production of cellulose nanoparticles and nanocomposites for biomedical applications *Cellulose–Fundamental Aspects and Current Trends* (pp. 193-228): Intech.

Rosa, M. F., Medeiros, E. S., Malmonge, J. A., Gregorski, K. S., Wood, D. F., Mattoso, L. H. C., . . . Imam, S. H. (2010). Cellulose nanowhiskers from coconut husk fibers: Effect of preparation conditions on their thermal and morphological behavior. *Carbohydrate Polymers, 81*(1), 83-92.

Rosli, N. A., Ahmad, I., & Abdullah, I. (2013). Isolation and characterization of cellulose nanocrystals from *Agave angustifolia* fibre. *BioResources, 8*(2), 1893-1908.

Sacui, I. A., Nieuwendaal, R. C., Burnett, D. J., Stranick, S. J., Jorfi, M., Weder, C., . . . Gilman, J. W. (2014). Comparison of the properties of cellulose nanocrystals and cellulose nanofibrils isolated from bacteria, tunicate, and wood processed using acid, enzymatic, mechanical, and oxidative methods. *ACS applied materials & interfaces, 6*(9), 6127-6138.

Sadeghifar, H., Filpponen, I., Clarke, S. P., Brougham, D. F., & Argyropoulos, D. S. (2011). Production of cellulose nanocrystals using hydrobromic acid and click reactions on their surface. *Journal of materials science, 46*(22), 7344-7355.

Saelee, K., Yingkamhaeng, N., Nimchua, T., & Sukyai, P. (2016). An environmentally friendly xylanase-assisted pretreatment for cellulose nanofibrils isolation from sugarcane bagasse by high-pressure homogenization. *Industrial Crops and Products, 82*, 149-160.

Satyamurthy, P., Jain, P., Balasubramanya, R. H., & Vigneshwaran, N. (2011). Preparation and characterization of cellulose nanowhiskers from cotton fibres by controlled microbial hydrolysis. *Carbohydrate Polymers, 83*(1), 122-129.

Satyamurthy, P., & Vigneshwaran, N. (2013). A novel process for synthesis of spherical nanocellulose by controlled hydrolysis of microcrystalline cellulose using anaerobic microbial consortium. *Enzyme and microbial technology, 52*(1), 20-25.

Scheller, H. V., & Ulvskov, P. (2010). Hemicelluloses. *Plant Biology, 61*(1), 263.

Segneanu, A.-E., Vlazan, P., Sfirloaga, P., Grozescu, I., Cziple, F., & Gherman, V. D. (2013). Biomass extraction methods. In *Biomass Now—Sustainable Growth and Use*. Intech.

Sheltami, R. M., Abdullah, I., Ahmad, I., Dufresne, A., & Kargarzadeh, H. (2012). Extraction of cellulose nanocrystals from mengkuang leaves (*Pandanus tectorius*). *Carbohydrate Polymers, 88*(2), 772-779.

Shen, Z., Jin, C., Pei, H., Shi, J., Liu, L., & Sun, J. (2014). Pretreatment of corn stover with acidic electrolyzed water and $FeCl_3$ leads to enhanced enzymatic hydrolysis. *Cellulose, 21*(5), 3383-3394.

Shuai, L., & Pan, X. (2012). Hydrolysis of cellulose by cellulase-mimetic solid catalyst. *Energy & Environmental Science, 5*(5), 6889-6894.

Siddiqui, N., Mills, R. H., Gardner, D. J., & Bousfield, D. (2011). Production and characterization of cellulose nanofibers from wood pulp. *Journal of Adhesion Science and Technology, 25*(6-7), 709-721.

Silva, A. C., Jorgetto, A. O., Wondracek, M. H., Saeki, M. J., Schneider, J. F., Pedrosa, V. A., . . . Castro, G. R. (2014). Characterization of corn (*Zea mays*) leaf powder and its adsorption properties regarding Cu (II) and Cd (II) from aqueous samples. *BioResources, 10*(1), 1099-1114.

Silvério, H. A., Neto, W. P. F., Dantas, N. O., & Pasquini, D. (2013). Extraction and characterization of cellulose nanocrystals from corncob for application as reinforcing agent in nanocomposites. *Industrial Crops and Products, 44*, 427-436.

Sim, S. F., Mohamed, M., Lu, N. A. L. M. I., Sarman, N. S. P., & Samsudin, S. N. S. (2012). Computer-assisted analysis of fourier transform infrared (FTIR) spectra for characterization of various treated and untreated agriculture biomass. *BioResources, 7*(4), 5367-5380.

Singh, P., Sulaiman, O., Hashim, R., Peng, L. C., & Singh, R. P. (2013). Using biomass residues from oil palm industry as a raw material for pulp and paper industry:

potential benefits and threat to the environment. *Environment, Development and Sustainability, 15*(2), 367-383.

Singha, B., Naiya, T. K., kumar Bhattacharya, A., & Das, S. K. (2011). Cr (VI) ions removal from aqueous solutions using natural adsorbents–FTIR studies. *Journal of Environmental Protection, 2*(06), 729.

Siqueira, G., Bras, J., & Dufresne, A. (2010). Cellulosic bionanocomposites: a review of preparation, properties and applications. *Polymers, 2*(4), 728-765.

Siró, I., & Plackett, D. (2010). Microfibrillated cellulose and new nanocomposite materials: a review. *Cellulose, 17*(3), 459-494.

Son, H. N., & Seo, Y. B. (2015). Physical and bio-composite properties of nanocrystalline cellulose from wood, cotton linters, cattail, and red algae. *Cellulose, 22*(3), 1789-1798.

Soni, B., & Mahmoud, B. (2015). Chemical isolation and characterization of different cellulose nanofibers from cotton stalks. *Carbohydrate Polymers, 134*, 581-589.

Spence, K. L., Venditti, R. A., Rojas, O. J., Habibi, Y., & Pawlak, J. J. (2011). A comparative study of energy consumption and physical properties of microfibrillated cellulose produced by different processing methods. *Cellulose, 18*(4), 1097-1111.

Tagusagawa, C., Takagaki, A., Iguchi, A., Takanabe, K., Kondo, J. N., Ebitani, K., . . . Domen, K. (2010). Synthesis and characterization of mesoporous Ta−W oxides as strong solid acid catalysts. *Chemistry of Materials, 22*(10), 3072-3078.

Tan, X. Y., Abd Hamid, S. B., & Lai, C. W. (2015). Preparation of high crystallinity cellulose nanocrystals (CNCs) by ionic liquid solvolysis. *Biomass and Bioenergy, 81*, 584-591.

Tang, L. R., Huang, B., Ou, W., Chen, X. R., & Chen, Y. D. (2011). Manufacture of cellulose nanocrystals by cation exchange resin-catalyzed hydrolysis of cellulose. *Bioresource Technology, 102*(23), 10973-10977.

Tang, Y., Shen, X., Zhang, J., Guo, D., Kong, F., & Zhang, N. (2015). Extraction of cellulose nano-crystals from old corrugated container fiber using phosphoric acid and enzymatic hydrolysis followed by sonication. *Carbohydrate Polymers, 125*, 360-366.

Tang, Y., Yang, S., Zhang, N., & Zhang, J. (2014). Preparation and characterization of nanocrystalline cellulose via low-intensity ultrasonic-assisted sulfuric acid hydrolysis. *Cellulose, 21*(1), 335-346.

Taokaew, S., Seetabhawang, S., Siripong, P., & Phisalaphong, M. (2013). Biosynthesis and characterization of nanocellulose-gelatin films. *Materials, 6*(3), 782-794.

Thulluri, C., Goluguri, B. R., Konakalla, R., Shetty, P. R., & Addepally, U. (2013). The effect of assorted pretreatments on cellulose of selected vegetable waste and enzymatic hydrolysis. *biomass and bioenergy, 49*, 205-213.

Tian, C., Yi, J., Wu, Y., Wu, Q., Qing, Y., & Wang, L. (2016). Preparation of highly charged cellulose nanofibrils using high-pressure homogenization coupled with strong acid hydrolysis pretreatments. *Carbohydrate Polymers, 136*, 485-492.

Tian, D., Han, Y., Lu, C., Zhang, X., & Yuan, G. (2014). Acidic ionic liquid as "quasi-homogeneous" catalyst for controllable synthesis of cellulose acetate. *Carbohydrate polymers, 113*, 83-90.

Van de Vyver, S., Geboers, J., Jacobs, P. A., & Sels, B. F. (2011). Recent advances in the catalytic conversion of cellulose. *ChemCatChem, 3*(1), 82-94.

Vieyra, H., Figueroa-López, U., Guevara-Morales, A., Vergara-Porras, B., San Martin-Martinez, E., & Aguilar-Mendez, M. Á. (2015). Optimized monitoring of production of cellulose nanowhiskers from Opuntia ficus-indica (nopal cactus). *International Journal of Polymer Science, 2015*.

Wan, C., & Li, Y. (2012). Fungal pretreatment of lignocellulosic biomass. *Biotechnology Advances, 30*(6), 1447-1457.

Wang, C., Duan, Q., Gong, W., Ye, A., Di, Z., & Miao, C. (2014). An evaluation of adaptive surrogate modeling based optimization with two benchmark problems. *Environmental Modelling & Software, 60*, 167-179.

Wang, H., Gurau, G., & Rogers, R. D. (2012). Ionic liquid processing of cellulose. *Chemical Society Reviews, 41*(4), 1519-1537.

Wang, J., Zheng, Y., & Zhang, S. (2010). The application of ionic liquids in dissolution and separation of lignocellulose. *Clean energy systems and experiences, 4*, 71-84.

Wang, N., Zhang, J., Wang, H., Li, Q., Wei, S. a., & Wang, D. (2014). Effects of metal ions on the hydrolysis of bamboo biomass in 1-butyl-3-methylimidazolium chloride with dilute acid as catalyst. *Bioresource Technology, 173*(0), 399-405.

Wang, Q., Zhao, X., & Zhu, J. (2014). Kinetics of strong acid hydrolysis of a bleached kraft pulp for producing cellulose nanocrystals (CNCs). *Industrial & Engineering Chemistry Research, 53*(27), 11007-11014.

Wang, T., Glasper, J. A., & Shanks, B. H. (2015). Kinetics of glucose dehydration catalyzed by homogeneous Lewis acidic metal salts in water. Applied Catalysis A: General, 498, 214-221.

Wang, W., Yuan, T. Q., & Cui, B. K. (2013). Fungal treatment followed by $FeCl_3$ treatment to enhance enzymatic hydrolysis of poplar wood for high sugar yields. *Biotechnology Letters, 35*(12), 2061-2067.

Wang, Y., Song, H., Peng, L., Zhang, Q., & Yao, S. (2014). Recent developments in the catalytic conversion of cellulose. *Biotechnology & Biotechnological Equipment, 28*(6), 981-988.

Wei, H., Donohoe, B., Vinzant, T., Ciesielski, P., Wang, W., Gedvilas, L., . . . Tucker, M. (2011). Elucidating the role of ferrous ion cocatalyst in enhancing dilute acid pretreatment of lignocellulosic biomass. *Biotechnology for Biofuels, 4*(1), 1-16.

Wittcoff, H. A., Reuben, B. G., & Plotkin, J. S. (2012). *Industrial organic chemicals*: John Wiley & Sons.

Xu, J., Chen, H., Kádár, Z., Thomsen, A. B., Schmidt, J. E., & Peng, H. (2011). Optimization of microwave pretreatment on wheat straw for ethanol production. *Biomass and Bioenergy, 35*(9), 3859-3864.

Xu, Q., Gao, Y., Qin, M., Wu, K., Fu, Y., & Zhao, J. (2013). Nanocrystalline cellulose from aspen kraft pulp and its application in deinked pulp. *International journal of biological macromolecules, 60*, 241-247.

Yahya, M. B., Lee, H. V., & Hamid, S. B. A. (2015). Preparation of nanocellulose via transition metal salt-catalyzed hydrolysis pathway. *BioResources, 10*(4), 7627-7639.

Yeniay, Ö. (2014). Comparative study of algorithms for response surface optimization. *Mathematical and Computational Applications, 19*(1), 93-104.

Yi, J., He, T., Jiang, Z., Li, J., & Hu, C. (2013). $AlCl_3$ catalyzed conversion of hemicellulose in corn stover. *Chinese Journal of Catalysis, 34*(11), 2146-2152.

Yu, H., Qin, Z., Liang, B., Liu, N., Zhou, Z., & Chen, L. (2013). Facile extraction of thermally stable cellulose nanocrystals with a high yield of 93% through hydrochloric acid hydrolysis under hydrothermal conditions. *Journal of Materials Chemistry A, 1*(12), 3938-3944.

Yuan, Z., Zhang, J., Jiang, A., Lv, W., Wang, Y., Geng, H., . . . Qin, M. (2015). Fabrication of cellulose self-assemblies and high-strength ordered cellulose films. *Carbohydrate Polymers, 117*, 414-421.

Zhang, D., Zhang, Q., Gao, X., & Piao, G. (2013). A nanocellulose polypyrrole composite based on tunicate cellulose. *International Journal of Polymer Science, 2013*, 6.

Zhang, H., Li, N., Pan, X., Wu, S., & Xie, J. (2016). Oxidative conversion of glucose to gluconic acid by iron(iii) chloride in water under mild conditions. *Green Chemistry, 18*(8), 2308-2312.

Zhang, Y., Li, Q., Su, J., Lin, Y., Huang, Z., Lu, Y., . . . Zhu, Y. (2015). A green and efficient technology for the degradation of cellulosic materials: structure changes and enhanced enzymatic hydrolysis of natural cellulose pretreated by synergistic interaction of mechanical activation and metal salt. *Bioresource Technology, 177*(0), 176-181.

Zhao, J., Zhang, H., Zheng, R., Lin, Z., & Huang, H. (2011). The enhancement of pretreatment and enzymatic hydrolysis of corn stover by $FeSO_4$ pretreatment. *Biochemical Engineering Journal, 56*(3), 158-164.

Zhou, Y. M. (2012). Effect of nanocellulose isolation techniques on the formation of reinforced poly(vinyl alcohol) nanocomposite films. *Express Polymer Letters, 6*(10), 794-804.

LIST OF PUBLICATIONS AND PAPERS PRESENTED

ISI-Cited Publications:

1. **You Wei Chen**, Hwei Voon Lee & Sharifah Bee Abd Hamid (2016). Preparation and Characterization of Cellulose Crystallites via Fe(III)-, Co(II)- and Ni(II)-assisted Dilute Sulfuric Acid Catalyzed Hydrolysis Process. *Journal of Nano Research*, *41*, 96–109. (Tier 4, Impact Factor = 0.564)

2. **You Wei Chen**, Hwei Voon Lee & Sharifah Bee Abd Hamid (2016). Preparation of Nanostructured Cellulose via Cr(III)-and Mn(II)-Transition Metal Salt Catalyzed Acid Hydrolysis Approach. *BioResources*, *11(3)*, 7224–7241. (Tier 1, Impact Factor = 1.425)

3. **You Wei Chen**, Hwei Voon Lee & Sharifah Bee Abd Hamid (2016). A Response Surface Methodology Study: Effects of Trivalent Cr^{3+} Metal Ion-Catalyzed Hydrolysis on Nanocellulose Crystallinity and Yield. *BioResources*, *11(2)*, 4645-4662. (Tier 1, Impact Factor = 1.425)

4. **You Wei Chen**, Hwei Voon Lee & Sharifah Bee Abd Hamid (2017). Facile Production of Nanostructured Cellulose from *Elaeis guineensis* Empty Fruit Bunch via One Pot Oxidative-Hydrolysis Isolation Approach. *Carbohydrate Polymers*, *157*, 1511–1524. (Tier 1, Impact Factor = 4.219)

5. **You Wei Chen**, Hwei Voon Lee, Joon Ching Juan & Siew Moi Phang (2016). Production of New Cellulose Nanomaterial from Red Algae Marine Biomass *Gelidium elegans*. *Carbohydrate Polymers*, *151*, 1210–1219. (Tier 1, Impact Factor = 4.219)

6. **You Wei Chen**, Thean Heng Tan, Hwei Voon Lee & Sharifah Bee Abd Hamid (2017). Easy Fabrication of Highly Thermal-Stable Cellulose Nanocrystals Using $Cr(NO_3)_3$ Catalytic Hydrolysis System: A Feasibility Study from Macro- to Nano-Dimensions. *Materials*, *10(1)*, 42. (Tier 1, Impact Factor = 2.728)

Conference proceedings:

1. **You Wei Chen**, Hwei Voon Lee & Sharifah Bee Abd Hamid (2015). Preparation and Characterization of Cellulose Nanofiber Using Acid Hydrolysis Combined with Transition Metal Ion Catalyst, presented at International Conference on Waste Management and Environment 2015 (ICWME 2015), 20–22 August 2015.

2. **You Wei Chen**, Hwei Voon Lee & Sharifah Bee Abd Hamid (2016). Catalytic Extraction of Nanocellulose from Empty Fruit Bunch (EFB) Cellulose Using Chromium (III) Metal Salt Catalyst, presented at International Symposium on Coatings & Corrosion 2016 (ISCC 2016), 16–18 May 2016.